Article:
Aad, G, Abbott, B, Abbott, DC et al. (2021) Search for new phenomena with top quark pairs in final states with one lepton, jets, and missing transverse momentum in pp collisions at √s = 13 TeV with the ATLAS detector. Journal of High Energy Physics, 2021 (4). 174. ISSN: 1126-6708

https://doi.org/10.1007/jhep04(2021)174

Published for SISSA by Springer

Received: *December 8, 2020*
Accepted: *March 12, 2021*
Published: *April 19, 2021*

Search for new phenomena with top quark pairs in final states with one lepton, jets, and missing transverse momentum in pp collisions at $\sqrt{s} = 13$ TeV with the ATLAS detector

The ATLAS collaboration

E-mail: atlas.publications@cern.ch

Abstract: A search for new phenomena with top quark pairs in final states with one isolated electron or muon, multiple jets, and large missing transverse momentum is performed. Signal regions are designed to search for two-, three-, and four-body decays of the directly pair-produced supersymmetric partner of the top quark (stop). Additional signal regions are designed specifically to search for spin-0 mediators that are produced in association with a pair of top quarks and decay into a pair of dark-matter particles. The search is performed using the Large Hadron Collider proton-proton collision dataset at a centre-of-mass energy of $\sqrt{s} = 13$ TeV recorded by the ATLAS detector from 2015 to 2018, corresponding to an integrated luminosity of 139 fb^{-1}. No significant excess above the Standard Model background is observed, and limits at 95% confidence level are set in the stop-neutralino mass plane and as a function of the mediator mass or the dark-matter particle mass. Stops are excluded up to 1200 GeV (710 GeV) in the two-body (three-body) decay scenario. In the four-body scenario stops up to 640 GeV are excluded for a stop-neutralino mass difference of 60 GeV. Scalar and pseudoscalar dark-matter mediators are excluded up to 200 GeV when the coupling strengths of the mediator to Standard Model and dark-matter particles are both equal to one and when the mass of the dark-matter particle is 1 GeV.

Keywords: Hadron-Hadron scattering (experiments), Supersymmetry

ArXiv ePrint: 2012.03799

https://doi.org/10.1007/JHEP04(2021)174

Contents

JHEP04(2021)174

1 Introduction

This paper presents a search for new phenomena in events with top quark pairs, in a final state with exactly one isolated charged lepton (electron or muon,[1] henceforth referred to as 'lepton') from the decay of an on- or off-shell W boson, jets, and a significant amount of missing transverse momentum ($\vec{p}_{\mathrm{T}}^{\,\mathrm{miss}}$), the magnitude of which is denoted by $E_{\mathrm{T}}^{\mathrm{miss}}$. This experimental signature may arise in Supersymmetry (SUSY) [1–7] or in models with a spin-0 mediator produced in association with top quarks [8, 9] and subsequently decaying into a pair of dark matter (DM) particles.

SUSY extends the Standard Model (SM) by introducing a supersymmetric partner for each SM particle, the two having identical quantum numbers except for a half-unit difference in spin. Searches for a light supersymmetric partner of the top quark, referred to as the top squark or 'stop', are of particular interest after the discovery of the Higgs boson [10, 11] at the Large Hadron Collider (LHC). Stops may largely cancel out divergent loop corrections to the Higgs boson mass [12–19], and thus, supersymmetry may provide an elegant solution to the hierarchy problem [20–23]. The superpartners of the left- and right-handed top quarks, $\tilde{t}_{\mathrm{L}}$ and $\tilde{t}_{\mathrm{R}}$, mix to form two mass eigenstates, $\tilde{t}_1$ and $\tilde{t}_2$, where $\tilde{t}_1$ is the lighter of the two. Significant mass splitting between the $\tilde{t}_1$ and $\tilde{t}_2$ particles is possible due to the large top quark Yukawa coupling. A generic R-parity-conserving[2] minimal supersymmetric extension of the SM (MSSM) [7, 12, 24–26] predicts pair production of SUSY particles and the existence of a stable lightest supersymmetric particle (LSP). The mass eigenstates from the linear superposition of charged or neutral SUSY partners of the Higgs and electroweak gauge bosons (higgsinos, winos and binos) are called charginos $\tilde{\chi}^{\pm}_{1,2}$ and neutralinos $\tilde{\chi}^{0}_{1,2,3,4}$. The lightest neutralino ($\tilde{\chi}^{0}_{1}$), assumed to be the LSP, may provide a potential dark matter (DM) candidate because it is stable and only interacts weakly with ordinary matter [27, 28]. This paper presents a search for direct pair production of $\tilde{t}_1$ particles, with significant amount of $E_{\mathrm{T}}^{\mathrm{miss}}$, from the two weakly interacting LSPs that escape detection. Scenarios with on- and off-shell production of W bosons and top quarks in the stop decays are considered, leading to two-, three- and four-body decays of the stop.

The search for a spin-0 mediator produced in association with top quarks and subsequently decaying into a pair of DM particles is motivated by SM extensions which respect the principle of minimal flavour violation resulting in the interaction strength between the spin-0 mediator and the SM quarks being proportional to the fermion masses via Yukawa-type couplings.

Dedicated searches for direct $\tilde{t}_1$ pair production were recently reported by the ATLAS [29–32] and CMS [33–40] Collaborations. Previous ATLAS and CMS searches extend the lower limit on $\tilde{t}_1$ masses at 95% confidence level to 1.2 TeV in the two-body decay scenario and up to ∼450 GeV in the three-body decay scenario. Searches for spin-0 mediators produced in association with heavy-flavour quarks and decaying into a pair of DM particles have also been reported by the ATLAS [29, 41] and CMS [42] Collaborations.

[1] Electrons and muons from τ-lepton decays are included.

[2] A multiplicative quantum number, referred to as R-parity, is introduced in SUSY models to conserve baryon and lepton number where R-parity is 1 (-1) for all SM (SUSY) particles.

JHEP04(2021)174

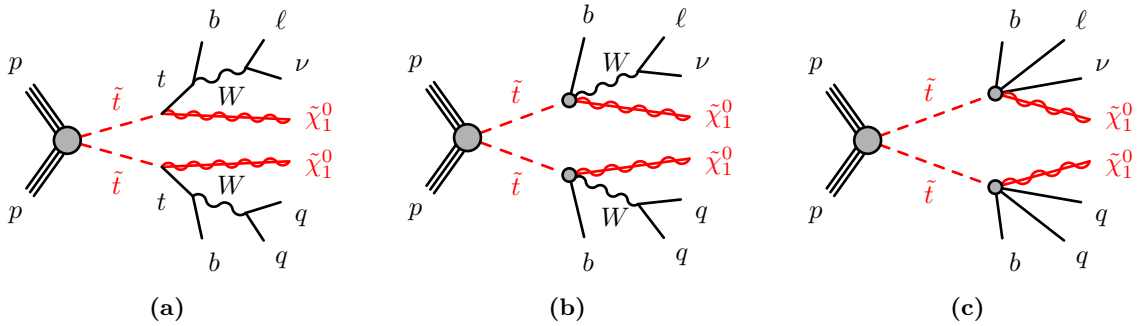

Figure 1. Diagrams illustrating the stop decay modes, which are referred to as (a) $\tilde{t}_1 \to t + \tilde{\chi}_1^0$, (b) $\tilde{t}_1 \to bW\tilde{\chi}_1^0$ and (c) $\tilde{t}_1 \to bff'\tilde{\chi}_1^0$. In these diagrams, the charge-conjugate symbols are omitted for simplicity. All the processes considered involve the production of a squark-antisquark pair.

2 Signal models and search strategy

Two classes of physics models are targeted by this search, the production of $\tilde{t}_1$ pairs in simplified SUSY models [43–45] where the only light sparticles are $\tilde{t}_1$ and $\tilde{\chi}_1^0$, and simplified benchmark models for DM production that assume the existence of a spin-0 mediator particle that can be produced in association with two top quarks [41, 46] and decays into a pair of DM particles $\chi\bar{\chi}$.

The experimental signatures of stop pair production can vary dramatically, depending on the mass-splitting between $\tilde{t}_1$ and $\tilde{\chi}_1^0$. Figure 1 illustrates the two-, three- and four-body stop decays considered in this paper. As flavour-changing neutral current processes are not considered, the dominant among the two-, three- or four-body stop decays is assumed to have a 100% branching ratio in a given $\Delta m_{\tilde{t}_1,\tilde{\chi}_1^0}$ regime. In the regime where $\Delta m_{\tilde{t}_1,\tilde{\chi}_1^0} = m(\tilde{t}_1) - m(\tilde{\chi}_1^0)$ is larger than the top quark mass m_{top}, the two-body decay $\tilde{t}_1 \to t + \tilde{\chi}_1^0$ dominates. At smaller $\Delta m_{\tilde{t}_1,\tilde{\chi}_1^0}$, the three-body decay $\tilde{t}_1 \to bW\tilde{\chi}_1^0$ dominates as long as $\Delta m_{\tilde{t}_1,\tilde{\chi}_1^0}$ is larger than the sum of the b-quark and W boson masses. At the smallest values of $\Delta m_{\tilde{t}_1,\tilde{\chi}_1^0}$ the dominant decay channel is the four-body decay $\tilde{t}_1 \to bff'\tilde{\chi}_1^0$. The stop is always assumed to decay promptly.

The searches for stops presented in this paper use several signal regions dedicated to each of the decay channels $\tilde{t}_1 \to t + \tilde{\chi}_1^0$, $\tilde{t}_1 \to bW\tilde{\chi}_1^0$ and $\tilde{t}_1 \to bff'\tilde{\chi}_1^0$. For instance, specific signal regions target the so-called compressed region where the stop undergoes a $\tilde{t}_1 \to t + \tilde{\chi}_1^0$ decay but where $\Delta m_{\tilde{t}_1,\tilde{\chi}_1^0} \approx m_{\text{top}}$. The selections are optimised for given benchmark model points, and are binned in key variables to retain sensitivity to the widest possible range of $\tilde{t}_1$ and $\tilde{\chi}_1^0$ masses.

The mediator-based DM scenarios consist of simplified models with a DM particle χ that is a SM singlet and a single spin-0 mediator that couples χ to SM fermions. Both the scenarios where the mediator is a scalar, ϕ, or a pseudoscalar, a, are considered, as illustrated in figure 2. These models have four parameters: the mass of the mediator, m_{med}, the DM mass, m_{DM}, the DM-mediator coupling, g_χ, and the coupling of the mediator to the SM fermions, g_{q}. In the models considered, the interaction strength between the mediator and

JHEP04(2021)174

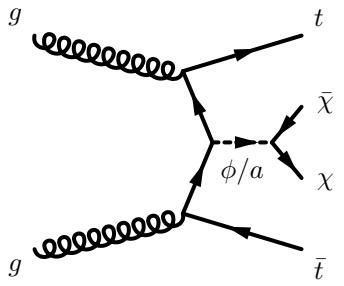

Figure 2. A representative Feynman diagram for spin-0 mediator production. The ϕ/a is the scalar/pseudoscalar mediator, which decays into a pair of dark matter (χ) particles.

JHEP04(2021)174

SM particles is proportional to the fermion masses via Yukawa-type couplings, and therefore final states involving top quarks dominate over those involving other fermions. Due to the associated production of top quarks with undetected DM particles in the same event, the mediator-based DM model predicts an excess of $t\bar{t}$ +$E_{\mathrm{T}}^{\mathrm{miss}}$ final-state events above the SM expectation. A dedicated signal region common to both the scalar and pseudoscalar models is developed. The signal region is binned in the azimuthal angle $\Delta\phi(\vec{p}_{\mathrm{T}}^{\,\mathrm{miss}}, \ell)$ between the missing transverse momentum and the leading lepton, to retain maximum sensitivity to both the scalar and pseudoscalar models and to a large range of mediator and DM particle masses.

The searches presented are based on eight dedicated analyses that target the various scenarios mentioned above. Each of these analyses corresponds to a set of event selection criteria, referred to as a signal region (SR), and is optimised to achieve three standard deviation expected sensitivity to the targeted benchmark model. Two techniques are employed to define the SRs: 'cut-and-count' and 'shape-fit' methods. The former is based on counting events in a single region of phase space, and is employed in the eight analyses. The latter is used in several SRs to improve the exclusion reach if no excess is observed in the cut-and-count signal regions, and employs SRs split into multiple bins in one or two key discriminating kinematic variables. The shape-fit method exploits the varying signal-to-background ratios in different bins to provide sensitivity to a wider range of new-particle masses than can be achieved by a single cut-and-count SR. Including these background-rich regions in the single-bin discovery SRs would significantly reduce the sensitivity to the targeted signatures.

The main background processes after the signal selections include $t\bar{t}$, $t\bar{t} + Z(\to \nu\bar{\nu})$, W+jets and the associated production of a single top quark and a W boson (Wt). Backgrounds from these SM processes are estimated by exploiting dedicated control regions (CRs) enriched in these processes. The backgrounds are normalised to data by applying a likelihood fit simultaneously to the SR and associated CRs, making the analysis more robust against potential mis-modelling in simulated events and reducing the uncertainties in the background normalisation. Before looking at the data in the signal regions, the background modelling and the normalisation procedure are tested in a series of validation regions (VRs) by applying the normalisation factors determined by a background-only fit in the CRs. A background-only fit to the CRs and SRs then provides a statistical test that

Signal scenario	Benchmark	Signal Region	Exclusion technique	Section
$\tilde{t}_1 \to t + \tilde{\chi}_1^0$	$m(\tilde{t}_1,\ \tilde{\chi}_1^0) = (800, 400)$ GeV	`tN_med`	shape-fit of $E_{\mathrm{T}}^{\mathrm{miss}}$ and m_{T}	7.1
$\tilde{t}_1 \to t + \tilde{\chi}_1^0$	$m(\tilde{t}_1,\ \tilde{\chi}_1^0) = (950, 1)$ GeV	`tN_high`	–	7.1
$\tilde{t}_1 \to t + \tilde{\chi}_1^0$	$m(\tilde{t}_1,\ \tilde{\chi}_1^0) = (225, 52)$ GeV	`tN_diag_low`	cut-and-count	7.2
$\tilde{t}_1 \to t + \tilde{\chi}_1^0$	$m(\tilde{t}_1,\ \tilde{\chi}_1^0) = (500, 327)$ GeV	`tN_diag_high`	cut-and-count	7.2
$\tilde{t}_1 \to bW\tilde{\chi}_1^0$	$m(\tilde{t}_1,\ \tilde{\chi}_1^0) = (500, 380)$ GeV	`bWN`	shape-fit in RNN score	7.3
$\tilde{t}_1 \to bff'\tilde{\chi}_1^0$	$m(\tilde{t}_1,\ \tilde{\chi}_1^0) = (450, 400)$ GeV	`bffN_btag`	shape-fit in $p_{\mathrm{T}}^{\ell}/E_{\mathrm{T}}^{\mathrm{miss}}$ and $\Delta\phi(\vec{p}_{\mathrm{T}}^{\,b\text{-jet}}, \vec{p}_{\mathrm{T}}^{\,\mathrm{miss}})$	7.4
$\tilde{t}_1 \to bff'\tilde{\chi}_1^0$	$m(\tilde{t}_1,\ \tilde{\chi}_1^0) = (450, 430)$ GeV	`bffN_softb`	shape-fit in $p_{\mathrm{T}}^{\ell}/E_{\mathrm{T}}^{\mathrm{miss}}$	7.4
Spin-0 mediator	$m(\phi/a,\ \chi) = (20, 1)$ GeV	`DM`	shape-fit in $\Delta\phi(\vec{p}_{\mathrm{T}}^{\,\mathrm{miss}}, \ell)$	7.5

Table 1. Signal scenarios, benchmark models and signal regions. For each SR, the table lists the analysis technique used for exclusion limits. The last column points to the section where the signal region is defined. For `tN_high` no exclusion technique is defined. The `tN_med` shape-fit also covers the `tN_high`-like phase space.

quantifies the existence and extent of a potential excess of events in data in the SRs. In the absence of an excess, exclusion limits are set on the associated model parameters by using the theoretical cross-sections. An overview of the signal regions and the benchmark models for optimisation is presented in table 1.

3 ATLAS detector and data collection

The ATLAS detector [47] at the LHC is a multipurpose particle detector with almost 4π coverage in solid angle around the interaction point.[3] It consists of an inner tracking detector (ID) surrounded by a superconducting solenoid providing a 2 T axial magnetic field, electromagnetic and hadronic calorimeters, and a muon spectrometer (MS), which is based on three large air-core toroidal superconducting magnets consisting of eight coils each. The ID provides charged-particle tracking in the range $|\eta| < 2.5$. During the LHC shutdown between Run 1 (2010–2012) and Run 2 (2015–2018), a new innermost layer of silicon pixels was added [48–50], which improves the track impact parameter resolution, vertex position resolution and b-tagging performance [51]. High-granularity electromagnetic and hadronic calorimeters provide energy measurements up to $|\eta| = 4.9$. The electromagnetic calorimeters, as well as the hadronic calorimeters in the endcap and forward regions, are sampling calorimeters with liquid argon as the active medium and lead, copper, or tungsten absorbers. The hadronic calorimeter in the central region of the detector is a sampling calorimeter with scintillator tiles as the active medium and steel absorbers. The MS surrounds the calorimeters and has three layers of precision tracking chambers with coverage up to $|\eta| = 2.7$ and fast detectors for triggering in the region $|\eta| < 2.4$. A two-level trigger

[3] ATLAS uses a right-handed coordinate system with its origin at the nominal interaction point (IP) in the centre of the detector and the z-axis along the beam pipe. The x-axis points from the IP to the centre of the LHC ring, and the y-axis points upwards. Cylindrical coordinates (r, ϕ) are used in the transverse plane, ϕ being the azimuthal angle around the z-axis. The pseudorapidity is defined in terms of the polar angle θ as $\eta = -\ln\tan(\theta/2)$. The transverse momentum, p_{T}, is defined in the x–y plane.

JHEP04(2021)174

Process	ME event generator	ME PDF	PS and hadronisation	UE tune	Cross-section calculation
$t\bar{t}$	Powheg-Box v2 [55]	NNPDF3.0 [56]	Pythia 8 [57]	A14 [58]	NNLO+NNLL [59–64]
Single-top					
t-channel	Powheg-Box v1	NNPDF3.0	Pythia 8	A14	NNLO+NNLL [65]
s- and Wt-channel	Powheg-Box v2	NNPDF3.0	Pythia 8	A14	NNLO+NNLL [66, 67]
V+jets ($V = W/Z$)	Sherpa 2.2.1 [68]	NNPDF3.0	Sherpa	Default	NNLO [69]
Diboson	Sherpa 2.2.1–2.2.2	NNPDF3.0	Sherpa	Default	NLO
Multiboson	Sherpa 2.2.1–2.2.2	NNPDF3.0	Sherpa	Default	NLO
$t\bar{t}+V$	MG5_aMC@NLO 2.3.3 [70]	NNPDF3.0	Pythia 8	A14	NLO [70]
SUSY signal	MadGraph 2.6.2 [70]	NNPDF2.3 [71]	Pythia 8	A14	NNLO+NNLL [72, 73]
DM signal	MadGraph 2.6.2	NNPDF3.0	Pythia 8	A14	NLO [74, 75]

Table 2. Overview of the nominal simulated samples. The cross-sections of top, single-top and SUSY samples were calculated at next-to-next-to-leading order (NNLO) with the resummation of soft gluon emission at next-to-next-to-leading-logarithm (NNLL) accuracy. The V+jets background samples were calculated at NNLO. The cross-sections of other background and DM samples were calculated at next-to-leading order (NLO).

system [52] is used to select events. The first-level trigger is hardware-based, followed by a software-based trigger system.

The results in this paper utilise the full Run 2 data sample collected from 2015 to 2018 at a centre-of-mass energy of $\sqrt{s} = 13\,\text{TeV}$. The average number of simultaneous pp interactions per bunch crossing, referred to as 'pile-up', in the recorded data is approximately 34. After the application of beam, detector and data-quality requirements, the total integrated luminosity is $139\,\text{fb}^{-1}$. The uncertainty in the combined 2015–2018 integrated luminosity is 1.7%. It is derived from the calibration of the luminosity scale using x–y beam-separation scans, following a methodology similar to that detailed in ref. [53], and using the LUCID-2 detector for the baseline luminosity measurements [54].

All events were recorded with triggers that accepted events with $E_{\text{T}}^{\text{miss}}$ above a given threshold. The $E_{\text{T}}^{\text{miss}}$ triggers relied on energy measurements in the calorimeter and on several algorithms based on cells, jets or topological clusters in addition to two methods for correcting for the effects of pile-up. The triggers were fully efficient for events passing an offline-reconstruction requirement of $E_{\text{T}}^{\text{miss}} > 230\,\text{GeV}$.

4 Simulated event samples

Samples of Monte Carlo (MC) simulated events are used for the description of the SM background processes and to model the signals. Details of the simulation samples used, including the matrix element (ME) event generator and parton distribution function (PDF) set, the parton shower (PS) and hadronisation model, the set of tuned parameters (tune) for the underlying event (UE) and the order of the cross-section calculation, are summarised in table 2.

JHEP04(2021)174

The samples produced with MadGraph5_aMC@NLO [70] and Powheg-Box [55, 76–79] used EvtGen v1.6.0 [80] for the modelling of b-hadron decays. The signal samples were all processed with a fast simulation [81], whereas all background samples were processed with the full simulation of the ATLAS detector [81] based on Geant4 [82]. All samples were produced with varying numbers of minimum-bias interactions generated by Pythia 8 with the A3 tune [83] and overlaid on the hard-scattering event to simulate the effect of multiple pp interactions in the same or nearby bunch crossings. The number of interactions per bunch crossing was reweighted to match the distribution in data.

The nominal $t\bar{t}$ sample and single-top sample cross-sections were calculated at NNLO with the resummation of soft gluon emission at NNLL accuracy and were generated with Powheg-Box (at NLO accuracy) interfaced to Pythia 8 for parton showering and hadronisation. Additional $t\bar{t}$ samples were generated with MadGraph5_aMC@NLO (at NLO accuracy)+Pythia 8 and Powheg-Box+Herwig 7 [84, 85] for modelling comparisons and the evaluation of systematic uncertainties [86]. The $t\bar{t}$ and Wt processes have identical $WWbb$ final states and can interfere. Additional $t\bar{t}$, Wt and $WWbb$ samples were generated as multi-leg processes at LO with MadGraph and used to estimate the systematic uncertainty from the interference modelling. The `tN_med` and `tN_high` regions receive significant contributions from both $t\bar{t}$ and Wt in a phase space where the interference is significant. Techniques used to model the interference such as diagram subtraction (DS) and diagram removal (DR) [87] were shown to provide predictions bracketing the data [88], but can lead to large uncertainties. Both schemes are investigated in this paper, but the DR scheme is ultimately used for the nominal Wt sample.

The W+jets and Z+jets samples were generated with Sherpa 2.2.1 [68, 89] with up to two partons at NLO and up to four partons at leading order (LO). Diboson and multiboson [90] events were generated with Sherpa 2.2.1 and 2.2.2. For dibosons, the events include up to one parton at NLO and up to three partons at LO. For triboson processes, up to two extra partons were considered at LO. The Sherpa samples used matrix elements from Comix [91] and OpenLoops [92], which were merged with the Sherpa parton shower [93] using the ME+PS@NLO prescription [94]. The W+jets and Z+jets events were further normalised to the NNLO cross-sections [69].

The $t\bar{t}+V$ samples were generated with MadGraph5_aMC@NLO (at NLO accuracy) interfaced to Pythia 8 for parton showering and hadronisation. The corresponding MC tune and generator comparisons can be found in ref. [95].

The SUSY samples were generated at LO with MadGraph 2.6.2 including up to two extra partons, and interfaced to Pythia 8 for parton showering and hadronisation. For the $\tilde{t}_1 \to t + \tilde{\chi}_1^0$ samples, the stop was decayed in Pythia 8 using only phase-space considerations and not the full ME. Since the decay products in the generated event samples did not preserve spin information, a polarisation reweighting was applied following refs. [96, 97]. A value of $\cos\theta_t = 0.553$ was assumed, corresponding to a $\tilde{t}_1$ composed mainly of $\tilde{t}_R$ (∼70%). For the $\tilde{t}_1 \to bW\tilde{\chi}_1^0$ and $\tilde{t}_1 \to bff'\tilde{\chi}_1^0$ samples the stops were decayed with MadSpin [98], interfaced to Pythia 8 for the parton showering. MadSpin emulates kinematic distributions such as the mass of the $bW^{(*)}$ system to a good approximation without calculating the full ME.

JHEP04(2021)174

The signal cross-sections for stop pair production were calculated to approximate next-to-next-to-leading order in the strong coupling constant, adding the resummation of soft gluon emission at next-to-next-to-leading-logarithm accuracy (approximate NNLO+NNLL) [73, 99–101]. The nominal cross-section and its uncertainty were derived using the PDF4LHC15_mc PDF set, following the recommendations of ref. [102]. The stop pair production cross-section varies from approximately 200 fb at $m_{\tilde{t}_1} = 600$ GeV to about 2 fb at $m_{\tilde{t}_1} = 1150$ GeV.

Signal events for the spin-0 scalar and pseudoscalar mediator models were generated at LO with up to one additional parton with MadGraph 2.6.2 interfaced to Pythia 8 for parton showering and hadronisation. In the DM sample generation the couplings of the mediator to the DM and SM particles (g_χ and g_q) were set to one. When interpreting the experimental results, a single common coupling $g = g_\chi = g_\mathrm{q}$ is always assumed. Coupling values of $g = 1$ as well as $g < 1$ are considered. The kinematics of the mediator decay were found to not depend strongly on the values of the couplings; however, the particle kinematic distributions are sensitive to the scalar or pseudoscalar nature of the mediator and to the mediator and DM particle masses. The cross-sections were computed at NLO [74, 75] and decrease significantly when the mediator is produced off-shell. The production cross-section varies from approximately 26 pb to 130 fb over a scalar mediator mass range of 10 to 200 GeV and from approximately 600 fb to 120 fb over a pseudoscalar mediator mass range of 10 to 200 GeV.

5 Event reconstruction

Events selected in the analysis must satisfy a series of beam, detector and data-quality criteria. The primary vertex, defined as the reconstructed vertex with the highest $\sum_{\text{tracks}} p_\mathrm{T}^2$, must have at least two associated tracks with $p_\mathrm{T} > 500$ MeV.

Depending on the quality and kinematic requirements imposed, reconstructed physics objects are labelled as either *baseline* or *signal*, where the latter is a subset of the former, with tighter selection criteria applied. Baseline objects are used when classifying overlapping selected objects and to compute the missing transverse momentum. Background contributions from $t\bar{t}$ and Wt production where both W bosons decay leptonically, referred to as dileptonic $t\bar{t}$ or Wt events, are suppressed by vetoing events with more than one baseline lepton. Signal objects are used to construct kinematic and discriminating variables necessary for the event selection.

Electrons are identified as energy clusters formed in the electromagnetic calorimeter matched to tracks in the ID. Baseline electrons are required to have $p_\mathrm{T} > 4.5$ GeV and $|\eta| < 2.47$, and to satisfy 'LooseAndBLayer' likelihood identification criteria that follow the methodology described in ref. [103]. Furthermore, their longitudinal impact parameter (z_0), defined as the distance along the beam direction between the primary vertex and the track's point of closest approach to the beam axis, must satisfy $|z_0 \sin\theta| < 0.5$ mm where θ is the polar angle of the track. Signal electrons must satisfy all the baseline requirements and have a transverse impact parameter (d_0) that satisfies $|d_0|/\sigma_{d_0} < 5$, where σ_{d_0} is the uncertainty in d_0. Furthermore, signal electrons are required to be isolated. The isolation is defined as the sum of the transverse energy or momentum reconstructed in a cone of

JHEP04(2021)174

size $\Delta R = \sqrt{(\Delta\eta)^2 + (\Delta\phi)^2}$ around the electron, excluding the energy of the electron itself. The isolation criteria rely on both track- and calorimeter-based information with a fixed requirement on the isolation energy divided by the electron's p_{T}. Electrons that satisfy the signal identification criteria, including the loose isolation, are called loose electrons. In addition, tight electrons must satisfy both a tight electron likelihood identification criterion and a tight isolation criterion.

Muon candidates are reconstructed from combined tracks that are formed from ID and MS tracks, or stand-alone MS tracks. Baseline muons up to $|\eta| = 2.7$ are used, and are required to have $p_{\mathrm{T}} > 4\,\mathrm{GeV}$, a longitudinal impact parameter $|z_0 \sin\theta| < 0.5$ mm, and to satisfy the 'Medium' identification criterion [104]. Signal muons must satisfy all baseline requirements and in addition have a transverse impact parameter satisfying $|d_0|/\sigma_{d_0} < 3$. Tight signal muons must satisfy tight isolation criteria, similar to those used for tight signal electrons, but with a fixed requirement on track-based isolation energy divided by the muon's p_{T}. A category of loose signal muons is also defined, which requires the 'Loose' identification criterion [104] and satisfies a looser isolation criterion.

Dedicated efficiency scale factors are derived from $Z \to \ell\bar{\ell}$ and $J/\psi \to \ell\bar{\ell}$ data samples to correct the simulations for minor mis-modelling of electron and muon identification, impact parameter and isolation selections. The p_{T} threshold of signal leptons is 25 GeV for electrons and muons in all signal regions except for signal regions dedicated to $\tilde{t}_1 \to bff'\tilde{\chi}_1^0$, where electrons with $p_{\mathrm{T}} > 4.5\,\mathrm{GeV}$ and muons with $p_{\mathrm{T}} > 4\,\mathrm{GeV}$ are used.

Jet candidates are built from topological clusters [105, 106] in the calorimeters using the anti-k_t algorithm [107] with a jet radius parameter $R = 0.4$ implemented in the FastJet package [108]. Jets are corrected for contamination from pile-up using the jet area method [109–111] and are then calibrated to account for the detector response [112, 113]. Jets in data are further calibrated according to *in situ* measurements of the jet energy scale [113]. Baseline jets are required to have $p_{\mathrm{T}} > 20\,\mathrm{GeV}$. Signal jets are required to have $|\eta| < 2.5$ and $p_{\mathrm{T}} > 25\,\mathrm{GeV}$ in all signal regions, except in the four-body signal regions, where the p_{T} threshold of signal jets is 20 GeV. Furthermore, signal jets with $p_{\mathrm{T}} < 120\,\mathrm{GeV}$ and $|\eta| < 2.5$ must satisfy track-based criteria designed to reject jets originating from pile-up [111]. Events containing a signal jet that does not satisfy specific jet-quality requirements ('jet cleaning') are rejected to suppress detector noise and non-collision backgrounds [114, 115]. The number of signal jets in an event is denoted N_{jet}. In addition to these jet candidates, the same anti-k_t algorithm is used to define larger radius (large-R) jets to provide discriminating variables for the reconstruction of top quarks, as described in section 6.

Jets identified as containing b-hadrons are referred to as b-tagged jets. Their identification is performed using the MV2c10 b-tagging algorithm, which examines quantities such as the impact parameters of associated tracks and characteristics of reconstructed secondary vertices [116, 117]. The algorithm is used at a working point that provides a 77% b-tagging efficiency in simulated $t\bar{t}$ events, and corresponds to a rejection factor of about 130 for jets originating from gluons and light-flavour quarks (light jets) and about 6 for jets induced by charm quarks. Corrections derived from data control samples are applied to account for differences between data and simulation in the efficiency and mis-tag rate of the b-tagging algorithm. The number of b-tagged jets in an event is denoted $N_{b\text{-jet}}$. Since

JHEP04(2021)174

MV2c10 is only applicable to baseline jets with $p_{\mathrm{T}} > 20\,\mathrm{GeV}$, it is not sensitive to low-p_{T} b-hadrons. The presence of low-p_{T} b-hadrons, below 20 GeV, is instead inferred using a soft b-tagging algorithm, which does not rely on the presence of a jet in the calorimeter, but requires the presence of secondary vertices [118]. This technique is used to gain sensitivity to the $\tilde{t}_1 \to bff'\tilde{\chi}_1^0$ signal in the regime with $\Delta m_{\tilde{t}_1,\tilde{\chi}_1^0}$ lower than $\sim$40 GeV. The number of secondary vertices in an event is denoted N_{SV}. Corrections derived from dedicated $t\bar{t}$ and W+jets control regions are applied to the soft b-tagging efficiencies to account for differences between data and simulation.

Jets and associated tracks are also used to identify hadronically decaying τ-leptons using the 'Loose' identification criterion described in refs. [119, 120], which has a 85% (75%) efficiency for reconstructing τ-leptons decaying into one (three) charged pions. The hadronic τ-lepton decay candidates are required to have one or three associated tracks, with total electric charge opposite to that of the signal electron or muon, $p_{\mathrm{T}} > 20\,\mathrm{GeV}$, and $|\eta| < 2.5$. The τ-lepton candidate p_{T} requirement is applied after a dedicated energy calibration [121, 122].

To avoid labelling the same detector signature as more than one object, an overlap removal procedure is applied. Given a set of baseline objects, the procedure checks for overlap based on either a shared track, ghost-matching [110], or a minimum distance ΔR_y between pairs of objects.[4] First, if a baseline lepton and a baseline jet are separated by $\Delta R_y < 0.2$, then the lepton is retained and the jet is discarded. Second, if a baseline jet and a baseline lepton are separated by $\Delta R_y < 0.4$, then the jet is retained and the lepton is discarded, to minimise the contamination from jets misidentified as leptons. For the remainder of the paper, all baseline and signal objects are those that have survived the overlap removal procedure.

The missing transverse momentum $\vec{p}_{\mathrm{T}}^{\,\mathrm{miss}}$ is reconstructed as the negative vector sum of the transverse momenta of baseline electrons, muons, jets, and a soft term built from high-quality tracks that are associated with the primary vertex but not with the baseline physics objects [123, 124]. Photons and hadronically decaying τ-leptons are not explicitly included but enter either as jets, electrons, or via the soft term.

6 Discriminating variables

The backgrounds contributing to a final state with one isolated lepton, jets and $E_{\mathrm{T}}^{\mathrm{miss}}$ are primarily semileptonic $t\bar{t}$ events with one of the W bosons decaying leptonically, and W+jets events with a leptonic decay of the W boson. Both backgrounds can be efficiently reduced by requiring the transverse mass of the event, m_{T}, to be significantly larger than the W boson mass. The transverse mass is defined as $m_{\mathrm{T}} = \sqrt{2p_{\mathrm{T}}^{\ell}E_{\mathrm{T}}^{\mathrm{miss}}[1-\cos(\Delta\phi)]}$, where $\Delta\phi$ is the azimuthal angle between the lepton and missing transverse momentum directions and p_{T}^{ℓ} is the transverse momentum of the charged lepton. Other discriminating variables used to distinguish signal from several categories of background events are described below.

[4] Rapidity $y \equiv 1/2\ln[(E+p_z)/(E-p_z)]$ is used instead of pseudorapidity (η) when computing the distance ΔR_y between objects in the overlap removal procedure.

JHEP04(2021)174

6.1 Dileptonic $t\bar{t}$ reconstruction

The m_{T2} variable [125] is a generalisation of the transverse mass, applied to signatures where two particles are not directly detected. The variable m_{T2}^{τ} [126] is a variant of m_{T2} developed to identify and remove $t\bar{t}$ events where one W boson decays into a hadronically decaying τ-lepton candidate. In this case the 'τ-jet' is used as the visible particle for one top branch and the observed electron or muon for the other top branch. For $t\bar{t}$ events where one W boson decays leptonically and the other into a hadronically decaying τ-lepton, m_{T2}^{τ} has an endpoint at the W boson mass.

Events with dileptonic decays of $t\bar{t}$ pairs, where one lepton is not identified, constitute a significant background. The lost lepton can lead to significant missing transverse momentum and m_{T2} above the W boson mass. The topness variable [127] quantifies how well an event can be reconstructed under a dileptonic top hypothesis and is defined as the logarithm of the minimum of the following quantity $\mathcal{S}$:

$$\mathcal{S}(p_{Wx}, p_{Wy}, p_{Wz}, p_{\nu z}) = \frac{[m_W^2 - (p_\ell + p_\nu)^2]^2}{a_W^4} + \frac{[m_t^2 - (p_{b1} + p_\ell + p_\nu)^2]^2}{a_t^4} + \frac{[m_t^2 - (p_{b2} + p_W)^2]^2}{a_t^4} + \frac{[4m_t^2 - (\Sigma_i p_i)^2]^2}{a_{\mathrm{CM}}^4},$$

when minimised with respect to p_W and p_ν with the constraint $\vec{p}_{\mathrm{T},\nu} + \vec{p}_{\mathrm{T,W}} = \vec{p}_{\mathrm{T}}^{\,\mathrm{miss}}$. The quantity p_W represents the four-momentum vector of the W boson for which the lepton was not reconstructed and is thus completely invisible. The quantities p_ℓ and p_ν are the lepton and neutrino four-momentum vectors from the W boson whose lepton was identified. Finally, p_{bi} refer to the two b-jets. The sum in the last term runs over the five assumed final-state particles. If the event contains two b-tagged jets, the two permutations are tested in the minimisation. If the event has a single b-tagged jet, then permutations where the second b-jet can be either of the two leading momentum untagged jets are tested during the minimisation. The values of resolution parameters a_W, a_t and a_{CM} are constants taken from ref. [127].

6.2 Reconstruction of hadronic top decays

Signal events contain one hadronic top decay $t \to q\bar{q}'b$, while such decays are absent from the dileptonic $t\bar{t}$ background. Therefore, reconstructing the hadronic top quark decay can provide additional discrimination against dileptonic $t\bar{t}$ events. A recursive reclustering jet algorithm searches for large-radius jets with radius parameter R corresponding to the radius $R(p_{\mathrm{T}}) = 2 \times m_{\mathrm{top}}/p_{\mathrm{T}}$ expected from a hadronic top quark decay $t \to q\bar{q}'b$ [29]. The algorithm is based on the anti-k_t algorithm using signal jets as inputs and with initial radius parameter $R_0 = 3.0$. If a reclustered large-radius jet is significantly narrower than the radius expected from a hadronic top quark decay of that p_{T}, it is discarded. The radius of the remaining reclustered jets is iteratively reduced until the radius approximately matches the radius expected from a hadronic top quark decay. Surviving reclustered jets constitute hadronic top candidates. If more than one hadronic top candidate is found, the candidate whose mass $m_{\mathrm{top}}^{\mathrm{reclustered}}$ is closest to m_{top} is retained.

JHEP04(2021)174

A second hadronic top quark candidate algorithm is employed that fully reconstructs the direction of both the leptonically and the hadronically decaying top quarks, denoted t_{lep} and t_{had} respectively. This algorithm is applied to events with at least four jets and one b-tagged jet. The m_{top}^{χ} variable is defined as the invariant mass of the triplet of signal jets (one of which must be b-tagged) most compatible with m_{top}, taking into account the jet momentum and energy resolution. The component of the $\vec{p}_{\text{T}}^{\,\text{miss}}$ perpendicular to t_{lep} in the $t\bar{t}$ rest frame, $E_{\text{T},\perp}^{\text{miss}}$, is small in semileptonic top quark decays since $\vec{p}_{\text{T}}^{\,\text{miss}}$ tends to align with the leptonically decaying top quark.

6.3 Backgrounds with mismeasured missing momentum

In some signal regions, additional suppression against backgrounds with mismeasured missing momentum, arising from mismeasured jets, is required. This additional rejection is provided by $H_{\text{T,sig}}^{\text{miss}} = (|\vec{H}_{\text{T}}^{\text{miss}}| - M)/\sigma_{|\vec{H}_{\text{T}}^{\text{miss}}|}$, where $\vec{H}_{\text{T}}^{\text{miss}}$ is the negative vectorial sum of the momenta of the signal jets and signal lepton [126]. The denominator is computed from the per-event jet energy uncertainties, while the lepton resolution is neglected. The offset parameter M is a characteristic scale of the background processes and is fixed at 100 GeV.

6.4 Variables for compressed $\tilde{t}_1 \to t + \tilde{\chi}_1^0$

To discriminate stop pair production from SM $t\bar{t}$ production, in the phase space dominated by the decay $\tilde{t}_1 \to t + \tilde{\chi}_1^0$ in the compressed regime $\Delta m_{\tilde{t}_1,\tilde{\chi}_1^0} \approx m_{\text{top}}$, events are reconstructed according to both the stop and semileptonic $t\bar{t}$ hypotheses. These techniques are employed in the `tN_diag_low` and `tN_diag_high` SRs.

The reconstruction of the event under the semileptonic $t\bar{t}$ hypothesis starts by searching for the hadronically decaying top quark candidate through the minimisation of the loss function

$$L_t = \frac{(m_W^{\text{cand}} - m_W)^2}{m_W} + \frac{(m_{t_{\text{had}}}^{\text{cand}} - m_{\text{top}})^2}{m_{\text{top}}}$$

with m_W and m_{top} being the experimentally known W boson and top quark masses. The W boson candidate mass m_W^{cand} is either the mass of a single large anti-k_t jet with radius 1.0 or 1.2 or the invariant mass of two anti-k_t jets with radius 0.4. The hadronically decaying top quark candidate t_{had} is either one of the large-R jets or the W boson candidate plus a b-tagged jet. The jet permutation with the minimum loss function is considered as the candidate for the hadronic top. The visible part of the leptonically decaying top quark candidate ($t_{\text{lep}^{\text{vis}}}$) four-momentum vector is determined by adding the four-momentum vectors of the remaining highest-p_{T} b-tagged jet and the signal lepton.

The reconstruction of the event under the stop hypothesis relies on the collinear approximation [128, 129], in which the top quark and the neutralino from the stop decay are collinear. This approximation is valid for compressed $\tilde{t}_1 \to t + \tilde{\chi}_1^0$ models ($\Delta m_{\tilde{t}_1,\tilde{\chi}_1^0} \approx m_{\text{top}}$), where the requirement of a high-p_{T} initial-state radiation (ISR) jet in the event forces the momentum of the $\tilde{t}_1$ to be much larger than the sum of the top and $\tilde{\chi}_1^0$ masses.

With this approximation and a given value of the parameter $\alpha = m_{\tilde{\chi}_1^0}/m_{\tilde{t}_1}$, the four-momentum vector $p^{\mu}(\alpha)$ of the neutrino can be calculated from the missing transverse energy and the measured momenta of the hadronic and visible leptonic top quark candidates

JHEP04(2021)174

under the assumption that the longitudinal neutrino momentum p_z is zero. The resulting $p^\mu(\alpha)$ is then used to compute the leptonically decaying W boson's transverse mass m_{T}^{α} and the difference in m_{T} between the calculation under the hypothesis of a $t\bar{t}$ event and under the signal hypothesis, $\Delta m_{\mathrm{T}}^{\alpha} = m_{\mathrm{T}} - m_{\mathrm{T}}^{\alpha}$.

The `tN_diag_low` SR is optimised to probe the previously unexcluded region around the point with a stop mass of 200 GeV and neutralino mass of 27 GeV [29] which corresponds to $\alpha = 0.135$. Therefore this region uses the variable $\Delta m_{\mathrm{T}}^{\alpha}$ with α fixed to 0.135. For other compressed regions, which are targeted by the `tN_diag_high` SR, α can be determined dynamically by minimising the loss function

$$L_\alpha = \frac{[m(\ell+\nu) - m_W]^2}{m_W} + \frac{[m(t_{\mathrm{lep}^{\mathrm{vis}}} + \nu) - m_{\mathrm{top}}]^2}{m_{\mathrm{top}}}$$

where $m(\ell+\nu)$ is the invariant mass of the lepton and the neutrino, and $m(t_{\mathrm{lep}^{\mathrm{vis}}} + \nu)$ is the invariant mass of the leptonic top candidate and the neutrino. Using the approximation $\alpha = m_{\tilde{\chi}_1^0}/(m_{\tilde{\chi}_1^0} + m_{t_{\mathrm{had}}})$ and the measured value of $m_{t_{\mathrm{had}}}^{\mathrm{cand}}$, the values of $\Delta m_{\mathrm{T}}^{\alpha}$ and the mass of the $\tilde{\chi}_1^0$ at the minimum of the loss function can be determined. These variables are labelled $\Delta m_{\mathrm{T}}^{\mathrm{dyn}}$ and $m_{\tilde{\chi}_1^0}^{\mathrm{dyn}}$ respectively.

Although the neutrino momentum under the collinear approximation is fully known for a given value of α, there is an ambiguity as to how the remaining missing transverse momentum is split between the two neutralinos. To resolve this, the following loss function, which compares the reconstructed leptonic and hadronic $\tilde{t}_1$ masses with a given $\tilde{t}_1$ mass hypothesis, $m_{\tilde{t}_1}$, is defined and used in the `tN_diag_low` SR:

$$L_{\tilde{t}_1} = \frac{\left(m_{\tilde{t}_1}^{\mathrm{had}} - m_{\tilde{t}_1}\right)^2}{m_{\tilde{t}_1}} + \frac{\left(m_{\tilde{t}_1}^{\mathrm{lep}} - m_{\tilde{t}_1}\right)^2}{m_{\tilde{t}_1}}$$

A minimisation of this loss function, again under the assumption that $\alpha = 0.135$, is performed with respect to the angles between each neutralino momentum vector and each of the two top quarks. The mass $m_{\tilde{t}_1}^{\mathrm{lep}}$, which denotes the leptonic $\tilde{t}_1$ mass at the minimum of this loss function, takes lower and more peaked values for compressed $\tilde{t}_1 \to t + \tilde{\chi}_1^0$ models than for the SM top quark backgrounds. Finally, the ratio x_1 of the hadronic top quark momentum to the parent stop momentum is also used to discriminate between the stop signal and the background. Since it is computed as a projection, x_1 can take negative values for background processes, or if the collinear assumption does not hold.

7 Signal regions

A preselection that exploits the basic characteristics of the signals is applied: the presence of a signal lepton, b-tagged jets and missing transverse momentum. The preselection is designed to have very high efficiency for the signal and to remove the most trivial backgrounds. To cover signals with both high-momentum decay products such as in $\tilde{t}_1 \to t + \tilde{\chi}_1^0$ and low-momentum decay products such as in $\tilde{t}_1 \to bff'\tilde{\chi}_1^0$, 'soft-lepton' and 'hard-lepton' preselections are defined and are presented in table 3. All regions require $E_{\mathrm{T}}^{\mathrm{miss}} > 230$ GeV

JHEP04(2021)174

Selection		**hard-lepton**	**soft-lepton**
Trigger		$E_{\mathrm{T}}^{\mathrm{miss}}$ trigger	
Data quality		jet cleaning, primary vertex	
Second-lepton veto		no additional baseline leptons	
Number of leptons, tightness		= 1 'loose' lepton	= 1 'tight' lepton
Lepton p_{T}	[GeV]	> 25	> 4 (4.5) for μ (e)
Number of jets (jet p_{T})		≥ 4 (> 25 GeV)	≥ 1 (> 200 GeV) or ≥ 2 (> 20 GeV)
$E_{\mathrm{T}}^{\mathrm{miss}}$	[GeV]	> 230	
$\Delta\phi(j_{1,2}, \vec{p}_{\mathrm{T}}^{\,\mathrm{miss}})$	[rad]	> 0.4	
$N_{b\text{-jet}}$		≥ 1	–
m_{T}	[GeV]	> 30	–
m_{T2}^{τ}	[GeV]	> 80	–

Table 3. Preselection criteria used for the hard-lepton signal regions (left) and the soft-lepton signal regions (right).

to ensure that the trigger was fully efficient. To reject multijet events with mismeasured jet momenta, a minimum azimuthal angular distance is required between the missing transverse momentum direction and the two leading jets, $\Delta\phi(j_{1,2}, \vec{p}_{\mathrm{T}}^{\,\mathrm{miss}}) > 0.4$.

The signal regions are then optimised using simulated event samples to maximise the expected Z significance [130, 131] for the benchmark signals.[5] A set of benchmark signal models, selected to cover the various stop and spin-0 mediator models, is used for optimisation. The optimisation is performed using an iterative algorithm, considering all discriminating variables and accounting for statistical and systematic errors in the evaluation of the discovery significance. An overview of the signal regions and the benchmark models for optimisation is presented in table 1. The SRs are not designed to be orthogonal. The final exclusion limits are obtained by selecting at each point of the model parameter space the SR with the best expected sensitivity.

7.1 $\tilde{t}_1 \to t + \tilde{\chi}_1^0$

Two signal regions, `tN_med` and `tN_high`, are designed for models with $\Delta m_{\tilde{t}_1,\tilde{\chi}_1^0}$ significantly larger than m_{top}, and rely on large missing momentum and energetic jets. Selections on m_{T}, $H_{\mathrm{T,sig}}^{\mathrm{miss}}$, $E_{\mathrm{T},\perp}^{\mathrm{miss}}$ and topness are dictated by the need to suppress the three main backgrounds, namely W+jets, $t\bar{t}$, and $t\bar{t} + V$. The presence of a hadronic top quark candidate with $m_{\mathrm{top}}^{\mathrm{reclustered}} > 150\,\mathrm{GeV}$ is required primarily to ensure orthogonality with the control regions.

[5] Significance Z of observing n events for a prediction of $b \pm \sigma$ is defined as

$$Z = \sqrt{2\left\{n \ln\left[\frac{n(b+\sigma^2)}{b^2+n\sigma^2}\right] - \frac{b^2}{\sigma^2}\ln\left[1+\frac{\sigma^2(n-b)}{b(b+\sigma^2)}\right]\right\}} \quad \text{when } n \geq b, \text{ or}$$

$$Z = -\sqrt{2\left\{n \ln\left[\frac{n(b+\sigma^2)}{b^2+n\sigma^2}\right] - \frac{b^2}{\sigma^2}\ln\left[1+\frac{\sigma^2(n-b)}{b(b+\sigma^2)}\right]\right\}} \quad \text{when } n < b.$$

JHEP04(2021)174

Selection		tN_med	tN_high
Preselection		hard-lepton preselection	
N_{jet}, $N_{b\text{-jet}}$		$\geq (4, 1)$	$\geq (4, 1)$
Jet p_{T}	[GeV]	$> (100, 90, 70, 50)$	$> (120, 50, 50, 25)$
$E_{\text{T}}^{\text{miss}}$	[GeV]	> 230	> 520
$E_{\text{T},\perp}^{\text{miss}}$	[GeV]	> 400	–
$H_{\text{T,sig}}^{\text{miss}}$		> 16	> 25
m_{T}	[GeV]	> 220	> 380
Topness		> 9	> 8
$m_{\text{top}}^{\text{reclustered}}$	[GeV]	> 150	
$\Delta R(b, \ell)$		< 2.8	< 2.6
Exclusion technique		Based on shape-fit in $E_{\text{T}}^{\text{miss}}$ and m_{T} in tN_med	
Bin boundaries	[GeV]	$E_{\text{T}}^{\text{miss}} \in [230, 400]$, $m_{\text{T}} > 220$	
		$E_{\text{T}}^{\text{miss}} \in [400, 500]$, $m_{\text{T}} > 220$	
		$E_{\text{T}}^{\text{miss}} \in [500, 600]$, $m_{\text{T}} \in [220, 380]$	
		$E_{\text{T}}^{\text{miss}} \in [500, 600]$, $m_{\text{T}} > 380$	
		$E_{\text{T}}^{\text{miss}} > 600$, $m_{\text{T}} \in [220, 380]$	
		$E_{\text{T}}^{\text{miss}} > 600$, $m_{\text{T}} > 380$	

Table 4. Event selections defining the signal regions tN_med and tN_high.

The tN_med and tN_high definitions are given in table 4. A common exclusion region is defined by performing a two-variable shape-fit on the tN_med signal region, if no excess is observed in the single-bin discovery signal regions. The binning is designed to maximise the excluded parameter space in the $m_{\tilde{t}_1}$–$m_{\tilde{\chi}_1^0}$ plane. The two variables chosen for the binning are the two discriminating variables that best distinguish between tN_med and tN_high, namely $E_{\text{T}}^{\text{miss}}$ and m_{T}. The resulting six bins are given in table 4.

7.2 Compressed $\tilde{t}_1 \to t + \tilde{\chi}_1^0$

The kinematics of the decay $\tilde{t}_1 \to t + \tilde{\chi}_1^0$ in the region where $\Delta m_{\tilde{t}_1,\tilde{\chi}_1^0} \approx m_{\text{top}}$ differ significantly from the two signal regions defined above, and the stop signal is kinematically very similar to the dominant $t\bar{t}$ background. This region of parameter space is referred to as the diagonal region. Two dedicated signal regions, tN_diag_low and tN_diag_high, are designed to target scenarios on the diagonal for low-mass and high-mass stops respectively. The sensitivity of the tN_diag_low SR is such that it is expected to be able to exclude scenarios with $\Delta m_{\tilde{t}_1,\tilde{\chi}_1^0} = m_{\text{top}}$ and $m(\tilde{t}_1)$ between 200 and 250 GeV. Both the tN_diag_low and tN_diag_high signal regions rely on the presence of a high-p_{T} ISR jet, which serves to boost the di-stop system. The signal region definitions are shown in table 5 and are used both for exclusion and for discovery.

JHEP04(2021)174

Selection		tN_diag_low	tN_diag_high
Preselection		hard-lepton preselection without τ-lepton veto	
N_{jet}, $N_{b\text{-jet}}$		$> (4, 1)$	
Jet p_{T}	[GeV]	$> (400, 40, 40, 40)$	
m_{T}	[GeV]	> 150	> 110
$E_{\text{T}}^{\text{miss}}$	[GeV]	–	> 400
m_{T2}	[GeV]	–	< 360
$\Delta m_{\text{T}}^{\alpha}$	[GeV]	> 40	–
$\Delta m_{\text{T}}^{\text{dyn}}$	[GeV]	–	> 60
$m_{\tilde{t}_1}^{\text{lep}}$	[GeV]	< 600	–
$m_{\tilde{\chi}_1^0}^{\text{dyn}}$	[GeV]	> 5	[220, 595]
x_1		–	> -0.2
Exclusion technique		cut-and-count	

Table 5. Event selections defining the signal regions `tN_diag_low` and `tN_diag_high`.

7.3 $\tilde{t}_1 \to bW\tilde{\chi}_1^0$

The signal region for the decay $\tilde{t}_1 \to bW\tilde{\chi}_1^0$ is labelled `bWN` and defined using an optimised two-step machine learning (ML) approach, applied to events preselected according to the hard-lepton preselection criteria and additionally satisfying $m_{\text{T}} > 110\,\text{GeV}$. The background mostly consists of $t\bar{t}$, which has strong similarities to the signal in this region of phase space. For this reason the ML technique is selected. The jet multiplicity in signal events varies significantly due to the potential presence of ISR jets and fluctuations in the number of low-energy jets reconstructed from the hadronically decaying W boson. To deal with the variable number of signal jets, the first step of the ML procedure is to use a recurrent neural network (RNN) that has the ability to extract information from sequences of variable length [132]. The RNN uses a long short-term memory (LSTM) algorithm [133] and takes the four-momentum vectors of the jets as inputs. The LSTM output becomes the input of the second step, made up of a shallow neutral network (NN) with a single hidden layer and an output corresponding to the signal probability. The RNN and NN are trained simultaneously in one step. The NN uses the following discriminating variables as input: output of the RNN, $E_{\text{T}}^{\text{miss}}$, m_{T}, the azimuthal ϕ angle of $\vec{p}_{\text{T}}^{\,\text{miss}}$, the azimuthal angle $\Delta\phi(\vec{p}_{\text{T}}^{\,\text{miss}}, \ell)$ between the lepton and $\vec{p}_{\text{T}}^{\,\text{miss}}$, the invariant mass $m_{\ell\text{b}}$ of the lepton and the b-tagged jet, the transverse momentum of the b-tagged jet, the lepton four-momentum vector, N_{jet} and $N_{b\text{-jet}}$.

Before training, the hard-lepton preselection and the additional selection $m_{\text{T}} > 110\,\text{GeV}$ are applied. The size of the training sample is a crucial aspect for the performance of any ML method. Generating fully simulated signal samples with adequate sample sizes after the hard-lepton preselection and $m_{\text{T}} > 110\,\text{GeV}$ is computationally expensive. To overcome this difficulty, signal events without detector simulation were used for the training to enhance the number of signal events by two orders of magnitude. Fully simulated SM background

JHEP04(2021)174

Selection		bWN	bWN-TCR	bWN-TVR
Preselection		hard-lepton preselection		
N_{jet}, $N_{b\text{-jet}}$		$\geq (4, 1)$		
Jet p_{T}	[GeV]	$> (25, 25, 25, 25)$		
m_{T}	[GeV]	> 110	> 150	> 150
NN_{bWN}		> 0.9	$\in [0.4, 0.6]$	$\in [0.60, 0.65]$
Exclusion technique		shape-fit in NN_{bWN}		
Bin boundaries		$\{0.65, 0.7, 0.75, 0.8, 0.82, 0.84, 0.86, 0.88, 0.90, 0.92, 1.0\}$ and $m_{\text{T}} > 150\,\text{GeV}$ if $\text{NN}_{\text{bWN}} < 0.8$		

Table 6. Event selections defining the signal region bWN, along with its CR and VR.

events were available in sufficiently large numbers to be used directly for the training. For the signal, the generated events are 'smeared' using a dedicated procedure to emulate the effects of detector simulation and reconstruction. Parameterisations for reconstruction and identification efficiencies are obtained from dedicated ATLAS measurements and applied to jets, leptons and b-tagged jet identification. Particle-level electron, muon and jet four-momentum vectors are smeared according to their respective p_{T}, η and identification working point. The $E_{\text{T}}^{\text{miss}}$ is recomputed from all smeared objects. The kinematic distributions of all input variables after smearing are found to have fair agreement with distributions after full event reconstruction. The output score of the ML classifier, denoted NN_{bWN}, shows good agreement between smeared samples and fully simulated samples after full event reconstruction. The classifier output also shows a good agreement between simulation and data. The smeared samples are used only for the training, while signal and background predictions are obtained with the samples described in section 4.

The discovery signal region is defined by selecting events with $\text{NN}_{\text{bWN}} > 0.9$. The exclusion limits are obtained by performing a shape-fit using ten bins in NN_{bWN}, with bin boundaries $\{0.65, 0.7, 0.75, 0.8, 0.82, 0.84,\ 0.86, 0.88, 0.90, 0.92, 1.0\}$. The $t\bar{t}$ background in the first three bins is reduced by applying an additional selection, namely $m_{\text{T}} > 150\,\text{GeV}$. The selections that define the bWN signal region are presented in table 6.

7.4 $\tilde{t}_1 \to bff'\tilde{\chi}_1^0$

The four-body decay $\tilde{t}_1 \to bff'\tilde{\chi}_1^0$ occurs when $\Delta m_{\tilde{t}_1,\tilde{\chi}_1^0}$ is smaller than the W boson mass. In this scenario, the decay products have low momenta and often fall below the standard jet and lepton reconstruction p_{T} thresholds. It is therefore necessary to apply a soft-lepton preselection and require the presence of a high-momentum ISR jet, with $p_{\text{T}} > 200\,\text{GeV}$, to boost the momenta of the final-state particles. A first four-body signal region, labelled as bffN_btag, is optimised by requiring the presence of at least one b-tagged jet. The background in the bffN_btag signal region mostly consists of $t\bar{t}$ events. Because the b-tagged jets are required to have $p_{\text{T}} > 20\,\text{GeV}$, bffN_btag is not sensitive to $\Delta m_{\tilde{t}_1,\tilde{\chi}_1^0}$ below $\sim$40 GeV. For this reason a second signal region, labelled as bffN_softb, is defined. This

JHEP04(2021)174

Selection		bffN_softb	bffN_btag
Preselection		soft-lepton preselection	
N_{jet}		≥ 1	≥ 2
Jet p_{T}	[GeV]	> 200	
$N_{b\text{-jet}}$		$=0$	≥ 1
b-jet p_{T}	[GeV]	–	< 50
N_{SV}		≥ 1	–
m_{T}	[GeV]	> 90	
$E_{\text{T}}^{\text{miss}}$	[GeV]	> 250	–
$\Delta\phi(\vec{p}_{\text{T}}^{\,\text{miss}}, \ell)$	[rad]	< 2.0	–
C_{T2}	[GeV]	–	> 400
$\Delta\phi(p_{\text{T}}^{b\text{-jet}}, \vec{p}_{\text{T}}^{\,\text{miss}})$	[rad]	–	< 1.5
$p_{\text{T}}^{\ell}/E_{\text{T}}^{\text{miss}}$		< 0.04	< 0.05
Exclusion technique		shape-fit in $p_{\text{T}}^{\ell}/E_{\text{T}}^{\text{miss}}$	shape-fit in $p_{\text{T}}^{\ell}/E_{\text{T}}^{\text{miss}}$ and $\Delta\phi(p_{\text{T}}^{b\text{-jet}}, \vec{p}_{\text{T}}^{\,\text{miss}})$
Bin boundaries in $p_{\text{T}}^{\ell}/E_{\text{T}}^{\text{miss}}$		$\{0, 0.015, 0.025, 0.04, 0.06, 0.08\}$	$\{0, 0.03, 0.06, 0.1\}$
Bin boundaries in $\Delta\phi(p_{\text{T}}^{b\text{-jet}}, \vec{p}_{\text{T}}^{\,\text{miss}})$	[rad]		$\{0, 0.8, 1.5\}$

Table 7. Event selections defining the signal regions `bffN_softb` and `bffN_btag`.

region does not rely on b-tagged jets but instead requires a soft b-tag identified by the presence of a secondary vertex. The dominant background processes in this region are $t\bar{t}$ and W+jets. The `bffN_btag` signal region also exploits the correlation between the ISR jet p_{T} and $E_{\text{T}}^{\text{miss}}$ by cutting on the C_{T2} variable defined by $C_{\text{T2}} = \min(E_{\text{T}}^{\text{miss}}, p_{\text{T}}^{\text{ISR}} - 25\,\text{GeV})$. The key variable used at the last stage of the selection is the ratio of the lepton's transverse momentum to the missing transverse momentum, $p_{\text{T}}^{\ell}/E_{\text{T}}^{\text{miss}}$, which has small values for the $\tilde{t}_1 \to bff'\tilde{\chi}_1^0$ signal and large values for the backgrounds. The exact definitions of the four-body signal regions are given in table 7. For exclusion limits, the last selection, namely on $p_{\text{T}}^{\ell}/E_{\text{T}}^{\text{miss}}$, is replaced by a shape-fit. In the `bffN_softb`, the shape-fit is performed in five bins of the variable $p_{\text{T}}^{\ell}/E_{\text{T}}^{\text{miss}}$ with bin boundaries $\{0, 0.015, 0.025, 0.04, 0.06, 0.08\}$. In the `bffN_btag` signal region the shape-fit is performed in two variables, namely three bins in $p_{\text{T}}^{\ell}/E_{\text{T}}^{\text{miss}}$ with bin boundaries $\{0, 0.03, 0.06, 0.1\}$ and two bins in $\Delta\phi(p_{\text{T}}^{b\text{-jet}}, \vec{p}_{\text{T}}^{\,\text{miss}})$ with bin boundaries $\{0, 0.8, 1.5\}$.

7.5 Dark matter

The dominant background to the search for spin-0 mediator models is the $t\bar{t} + V$ process. The optimisation of this signal region favours a selection with at least two b-tagged jets and a leading b-tagged jet with $p_{\text{T}} > 80\,\text{GeV}$. The distribution of $\Delta\phi(\vec{p}_{\text{T}}^{\,\text{miss}}, \ell)$ differentiates the scalar and pseudoscalar models from each other and also from the background. The resulting `DM_scalar` and `DM_pseudoscalar` signal region definitions are given in table 8. In addition to the selection criteria optimised for discovery described above, the exclusion sensitivity is maximised by relying on a shape-fit in the region `DM_scalar` with the binning in $\Delta\phi(\vec{p}_{\text{T}}^{\,\text{miss}}, \ell)$ given in table 8.

JHEP04(2021)174

Selection		DM_scalar	DM_pseudoscalar
Preselection		hard-lepton preselection	
N_{jet}, $N_{b\text{-jet}}$		$\geq (4, 2)$	
Jet p_{T}	[GeV]	$> (80, 60, 30, 25)$	
b-tagged jet p_{T}	[GeV]	$> (80, 25)$	
$E_{\text{T}}^{\text{miss}}$	[GeV]	> 230	
$H_{\text{T,sig}}^{\text{miss}}$		> 15	
m_{T}	[GeV]	> 180	
Topness		> 8	
$m_{\text{top}}^{\text{reclustered}}$	[GeV]	> 150	
$\Delta\phi(\text{jet}_i, \vec{p}_{\text{T}}^{\,\text{miss}})$, $i \in [1, 4]$	[rad]	> 0.9	
$\Delta\phi(\vec{p}_{\text{T}}^{\,\text{miss}}, \ell)$	[rad]	> 1.1	> 1.5
Exclusion technique		Based on shape-fit in $\Delta\phi(\vec{p}_{\text{T}}^{\,\text{miss}}, \ell)$	
Bin boundaries in $\Delta\phi(\vec{p}_{\text{T}}^{\,\text{miss}}, \ell)$		$\{1.1, 1.5, 2.0, 2.5, \pi\}$	

Table 8. Event selections defining the DM signal regions.

8 Backgrounds

Data can be used to constrain the normalisation of the most significant background processes. To this end, control regions (CRs) are defined by minimally modifying the SR selections to suppress the signal while enhancing the fraction of the targeted background process. The CRs are then incorporated into a simultaneous likelihood fit to constrain the background process normalisations in the signal region. The ratio of the number of background events of a given process in the SR to those in a CR is estimated in MC background samples but is allowed to deviate from that ratio within dedicated MC modelling systematic uncertainties. Less significant background processes, such as diboson production and Z+jets, are estimated directly from MC simulation since they typically represent only a few percent of the signal region yields. CRs are defined to normalise $t\bar{t}$ (TCR), W+jets (WCR), single-top (STCR) and $t\bar{t} + Z$ (TZCR). Whether a control region is defined for a given background and signal region depends on the relative contribution of the process to the SR yield.

To validate the background estimates from the CRs, validation regions (VRs) are introduced for $t\bar{t}$ (TVR) and W+jets (WVR). The VRs are disjoint from both the SRs and CRs. The TZCR is designed to be as close as possible to the signal region in order to obtain the most precise estimate of the large $t\bar{t} + Z$ background, and thus does not leave space between the SR and the CR to introduce a VR for this process. Background normalisations, referred to as normalisation factors (NF), determined in the CRs are applied to the VRs and compared with the data. The VRs are not included in the final simultaneous fit, but provide a statistically independent test of the background estimates in background-dominated regions.

JHEP04(2021)174

Signal Region	Signal Scenario	TCR	WCR	STCR	TZCR	TVR	WVR
tN_med	$\tilde{t}_1 \to t + \tilde{\chi}_1^0$	✓	✓	✓	✓	✓	✓
tN_high	$\tilde{t}_1 \to t + \tilde{\chi}_1^0$	✓	✓	✓	✓	✓	✓
tN_diag_low	$\tilde{t}_1 \to t + \tilde{\chi}_1^0$	✓	–	–	–	✓	–
tN_diag_high	$\tilde{t}_1 \to t + \tilde{\chi}_1^0$	✓	–	–	–	✓	–
bWN	$\tilde{t}_1 \to bW\tilde{\chi}_1^0$	✓	–	–	–	✓	–
bffN_btag	$\tilde{t}_1 \to bff'\tilde{\chi}_1^0$	✓	✓	–	–	✓	✓
bffN_softb	$\tilde{t}_1 \to bff'\tilde{\chi}_1^0$	✓	✓	–	–	✓	✓
DM	spin-0 mediator	✓	–	–	✓	✓	–

Table 9. Summary of the control and validation regions used (✓) for each signal region.

The CRs and VRs are designed to minimise potential contamination from signal processes. The signal contamination is generally well below 10%, but in some TCRs and TVRs, for models close to the previously excluded region of parameter space, it can reach approximately 15%. The signal contributions to the CRs are not included in the background-only fits but are taken into account in the exclusion fits described in section 11. The CRs and VRs used for each SR are summarised in table 9. If a process is not normalised via a control region then it is estimated directly from MC simulation and theoretical cross-sections.

8.1 Control and validation regions for $\tilde{t}_1 \to t + \tilde{\chi}_1^0$ and spin-0 mediator signals

The dominant background process in the tN_med, tN_high and DM signal regions is $t\bar{t} + Z$, and therefore each of these SRs uses a dedicated TZCR. The TZCRs aim at capturing $t\bar{t} + Z$ events where the Z boson decays into two electrons or muons, and thus is kinematically similar to the $t\bar{t} + Z$ background in the signal regions where the Z boson decays into a pair of neutrinos. This CR is built by selecting events with three leptons (electrons or muons), one pair of which must be of opposite charge and same flavour with an invariant mass within 10 GeV of the Z boson mass. The exact definitions of the TZCRs follow the definitions of the tN_med, tN_high and DM SRs in terms of the number of jets, b-tagged jets and jet p_{T} thresholds. A modified missing momentum variable, $\tilde{E}_{\mathrm{T}}^{\mathrm{miss}}$, is defined, where the leptons associated with the Z boson decay are considered invisible. The $\tilde{E}_{\mathrm{T}}^{\mathrm{miss}}$ is the magnitude of the vector with components $\vec{\tilde{p}}_{\mathrm{x,y}}^{\mathrm{miss}}$ derived from the x, y components $\vec{p}_{\mathrm{x,y}}^{\mathrm{miss}}$ of $\vec{p}_{\mathrm{T}}^{\,\mathrm{miss}}$ introduced in section 5. The components $\vec{\tilde{p}}_{\mathrm{x,y}}^{\mathrm{miss}}$ are obtained as follows: $\vec{\tilde{p}}_{\mathrm{x,y}}^{\mathrm{miss}} = \vec{p}_{\mathrm{x,y}}^{\mathrm{miss}} + \vec{p}_{\mathrm{x,y}}^{\,l2} + \vec{p}_{\mathrm{x,y}}^{\,l3}$, where $\vec{p}_{\mathrm{x,y}}^{\,l2}$ and $\vec{p}_{\mathrm{x,y}}^{\,l3}$ are the x, y components of the momenta of the leptons that make up the Z boson candidate. The TZCRs require $\tilde{E}_{\mathrm{T}}^{\mathrm{miss}} > 230$ GeV. The remaining SR selections are not applied to the TZCRs, in order to retain a large enough event sample.

The W+jets and dileptonic $t\bar{t}$ processes are significant in tN_med and tN_high, and therefore dedicated CRs, WCR and TCR, are employed. The DM signal region also employs a TCR but does not require a WCR due to the smaller size of the W+jets background. These CRs have the same requirements on the number of jets, the number of b-tagged

JHEP04(2021)174

jets and the jet p_{T} thresholds as listed in tables 4 and 8 for their respective signal regions. Table 10 presents the definitions of the TCRs, WCRs and VRs, by showing which selections differ from the `tN_med` and `tN_high` SRs definitions. Neither W+jets nor dileptonic $t\bar{t}$ processes yield hadronic top decays, so a veto on the presence of a hadronic reclustered top candidate is used to ensure orthogonality with the signal regions. The number of events in TCR and WCR is increased by relaxing several selections compared with the SR selections. The $H_{\mathrm{T,sig}}^{\mathrm{miss}}$ selection is lowered to 10 for both `tN_med` and `tN_high`, and to 13 for `DM`. In addition, $E_{\mathrm{T},\perp}^{\mathrm{miss}}$ is lowered to 300 GeV for `tN_med`, while $E_{\mathrm{T}}^{\mathrm{miss}}$ is lowered to 450 GeV for `tN_high`. In the `DM` signal region the requirement on $\Delta\phi(\mathrm{jet}_i, \vec{p}_{\mathrm{T}}^{\,\mathrm{miss}})$ is lowered to 0.6.

The topness and m_{T} selections are used to differentiate between WCR and TCR. In the WCR, m_{T} is required to be in the range 30–90 GeV, compatible with the presence of a semileptonic W decay, but incompatible with dileptonic $t\bar{t}$ because of the topness selection. In the TCR, the topness selection of the SR is inverted, thus selecting events compatible with dileptonic $t\bar{t}$, while $m_{\mathrm{T}} > 120$ GeV is required, as larger values are favoured by the presence of two leptonically decaying W bosons. The TCR dedicated to the `DM` signal region has the same m_{T} selection as its signal region, $m_{\mathrm{T}} > 180$ GeV. The purity of the WCR is further improved by using only positively charged leptons, exploiting the lepton charge asymmetry in W+jets events from pp collisions.

To validate the dileptonic $t\bar{t}$ background normalisation, a TVR dominated by $t\bar{t}$ production is designed. The TVRs for `tN_med` and `tN_high` have the same selections as the corresponding TCR, except for the veto on the presence of a hadronic reclustered top quark candidate, which is replaced by a selection requiring the presence of such a hadronic top quark, with a mass $m_{\mathrm{top}}^{\mathrm{reclustered}} > 150$ GeV.

The validation of the W+jets background for `tN_high` is performed with a WVR with the same selection as `tN_high` but requiring the presence of a hadronic reclustered top candidate with $m_{\mathrm{top}}^{\mathrm{reclustered}} > 150$ GeV and $H_{\mathrm{T,sig}}^{\mathrm{miss}} > 25$, in order to be closer to the SR. The WVR for `tN_med` is defined starting from the WCR selections, but replacing several selections with those used in its SR: $E_{\mathrm{T}}^{\mathrm{miss}} > 400$ GeV, $H_{\mathrm{T,sig}}^{\mathrm{miss}} > 16$ and the presence of a hadronic top quark, with a mass $m_{\mathrm{top}}^{\mathrm{reclustered}} > 150$ GeV.

The `DM` SR contains only a small fraction of W+jets events due to the requirement of two b-tagged jets, and therefore only a TVR is considered. It is constructed from the `DM` SR definition, but with the topness selection inverted, and to increase the number of events and limit signal contamination, the selection on $\Delta\phi(\mathrm{jet}_i, \vec{p}_{\mathrm{T}}^{\,\mathrm{miss}})$ is relaxed to 0.6.

The `tN_med` and `tN_high` definitions permit the construction of a STCR with enough data events for comparison with the DS- and DR-based MC predictions. The STCR is defined with selections close to those of the WCR, but requires a second b-tagged jet, $30 < m_{\mathrm{T}} < 120$ GeV and the distance $\Delta R(b_1, b_2)$ between the two b-tagged jets to be larger than 1.4. To ensure orthogonality with the WCR, events with two b-tagged jets inside the WCR must have $\Delta R(b_1, b_2) < 1.4$. It is found that the DS and DR scheme predictions bracket the observed number of events in the STCR data, with a large discrepancy between the two predictions. The largest discrepancy is observed in the STCR associated with the `tN_med` SR. The data-to-prediction ratio in the STCR is $0.1^{+0.3}_{-0.1}$ with the DR scheme and 1.5 ± 1.3 with the DS scheme.

JHEP04(2021)174

Selection		tN_med	tN_med-TCR (-TVR)	tN_med-WCR (-WVR)	tN_med-STCR
$m_{\text{top}}^{\text{reclustered}}$	[GeV]	> 150	veto (> 150)	veto (> 150)	veto
$H_{\text{T,sig}}^{\text{miss}}$		> 16	> 10	> 10 (> 16)	> 10
$E_{\text{T},\perp}^{\text{miss}}$	[GeV]	> 400	> 300	> 300 (> 400)	350
m_{T}	[GeV]	> 220	> 120	$\in [30, 90]$	$\in [30, 120]$
Topness		> 9	< 9	> 9	> 10
$\Delta R(b, \ell)$		< 2.8	–	–	–
$\Delta R(b_1, b_2)$		–	–	< 1.4	> 1.4
Lepton charge		–	–	> 0	–
$N_{b\text{-jet}}$		≥ 1	≥ 1	≥ 1	≥ 2
Selection		tN_high	tN_high-TCR (-TVR)	tN_high-WCR (-WVR)	tN_high-STCR
$m_{\text{top}}^{\text{reclustered}}$	[GeV]	> 150	veto (> 150)	veto (> 150)	veto
$H_{\text{T,sig}}^{\text{miss}}$		> 25	> 10	>10 (> 25)	> 10
$E_{\text{T}}^{\text{miss}}$	[GeV]	> 520	> 450	> 450	> 450
m_{T}	[GeV]	> 380	> 120	$\in [30, 90]$	$\in [30, 120]$
Topness		> 8	< 8	> 8	> 10
$\Delta R(b, \ell)$		< 2.6	–	–	–
$\Delta R(b_1, b_2)$		–	–	< 1.4	> 1.4
Lepton charge		–	–	> 0	–
$N_{b\text{-jet}}$		≥ 1	≥ 1	≥ 1	≥ 2
Selection		DM	DM-TCR (-TVR)		
$m_{\text{top}}^{\text{reclustered}}$	[GeV]	> 150	veto (> 150)		
$H_{\text{T,sig}}^{\text{miss}}$		> 15	> 13 (> 15)		
Topness		> 8	< 8		
$\Delta\phi(\text{jet}_i, \vec{p}_{\text{T}}^{\text{miss}})$	[rad]	> 0.9	> 0.6		

Table 10. Event selections defining the CRs and VRs in tN_med, tN_high and DM relative to their respective signal regions. Only variables for which the selection criteria in the CRs or VRs differ from those in the SRs are listed.

The availability of the STCR allows the normalisation of the single-top background to be constrained from data. The fit to the STCR is performed with both the DS and DR MC schemes, and the resulting two predictions for single-top in the STCR and in the SRs are compatible within uncertainties. Therefore, once the STCR is used to constrain the single-top normalisation, the choice of the DS or DR scheme is found to have a negligible impact on the single-top prediction in the SR. In accordance with ref. [88], the DR scheme is used for the default Wt sample.

Figures 3, 4 and 5 compare data and prediction in CRs and VRs for several variables used in the $\tilde{t}_1 \to t + \tilde{\chi}_1^0$ and DM SRs. Good agreement is observed between data and prediction, within uncertainties.

JHEP04(2021)174

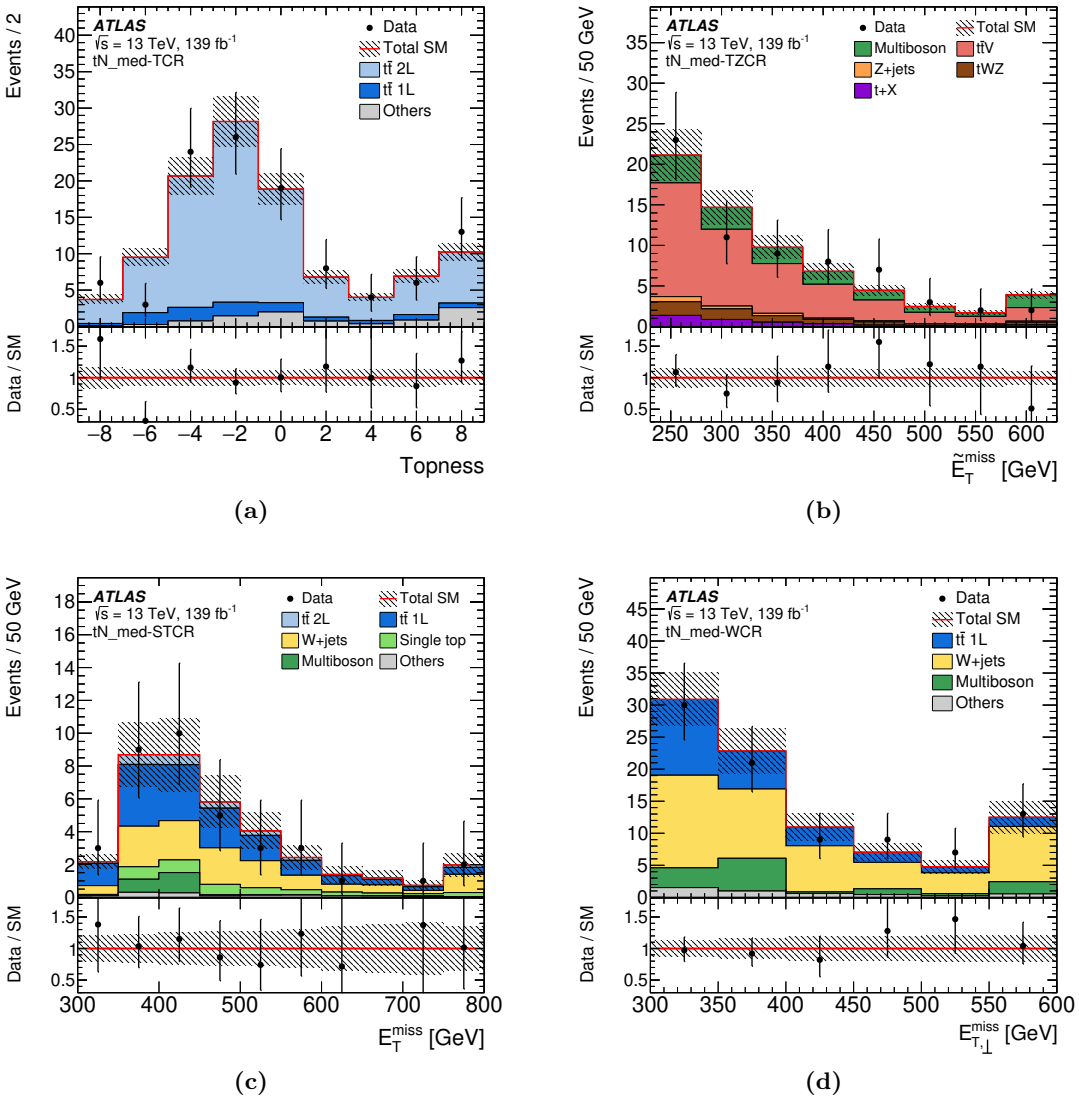

Figure 3. Selected kinematic distributions in `tN_med` CRs: (a) topness in the TCR, (b) $\tilde{E}_{\mathrm{T}}^{\mathrm{miss}}$ in the TZCR, (c) $E_{\mathrm{T}}^{\mathrm{miss}}$ in the STCR, (d) $E_{\mathrm{T},\perp}^{\mathrm{miss}}$ in the WCR. The distributions shown are post-fit, i.e. each background is scaled by a normalisation factor obtained from a background-only likelihood fit to the CRs (see table 14). The hatched area around the total SM prediction and the hatched band in the Data/SM ratio include all statistical and systematic uncertainties. The last (first) bin contains overflows (underflows).

JHEP04(2021)174

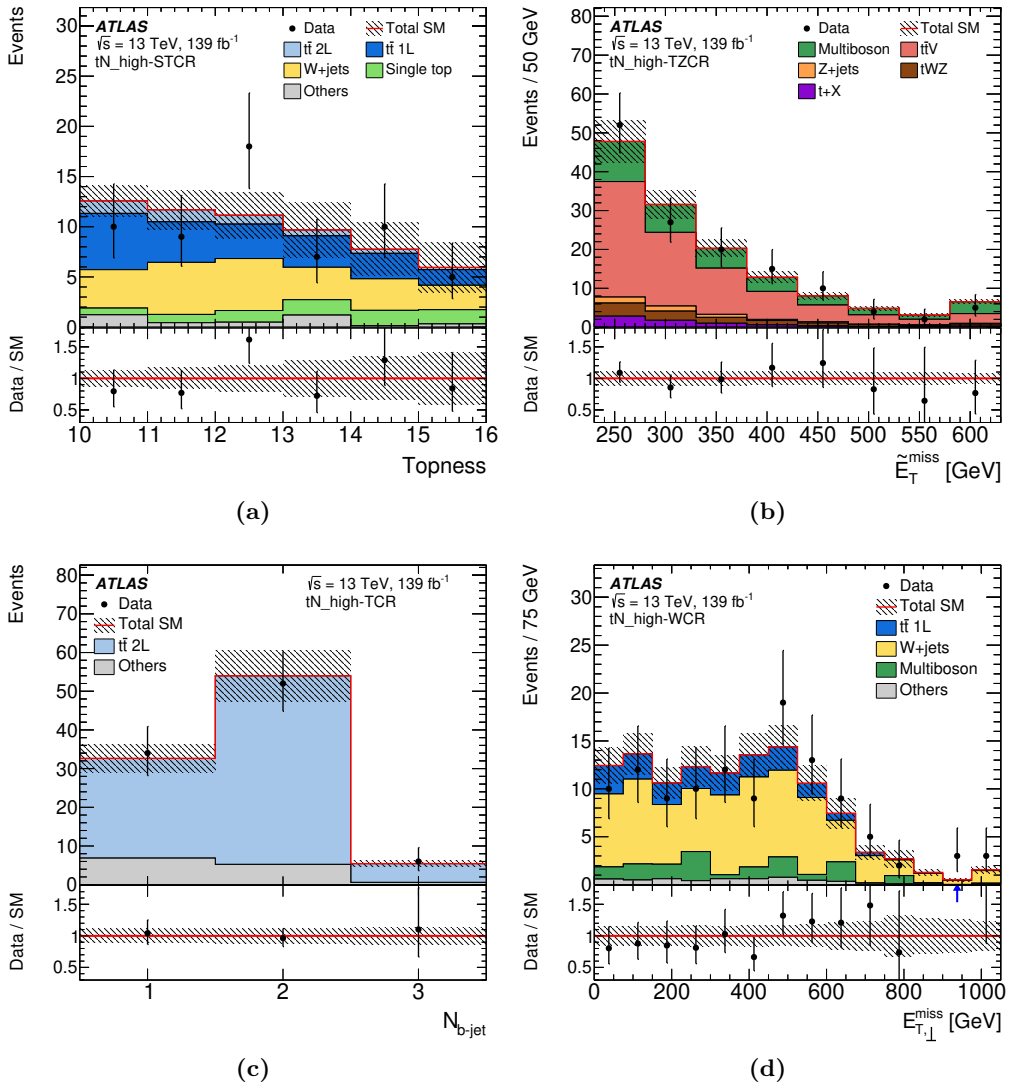

Figure 4. Selected kinematic distributions in `tN_high` CRs: (a) topness in the STCR, (b) $\tilde{E}_{\mathrm{T}}^{\mathrm{miss}}$ in the TZCR, (c) $N_{b\text{-jet}}$ in the TCR, (d) $E_{\mathrm{T},\perp}^{\mathrm{miss}}$ in the WCR. The distributions shown are post-fit, i.e. each background is scaled by a normalisation factor obtained from a background-only likelihood fit to the CRs (see table 14). The hatched area around the total SM prediction and the hatched band in the Data/SM ratio include all statistical and systematic uncertainties. The last (first) bin contains overflows (underflows).

JHEP04(2021)174

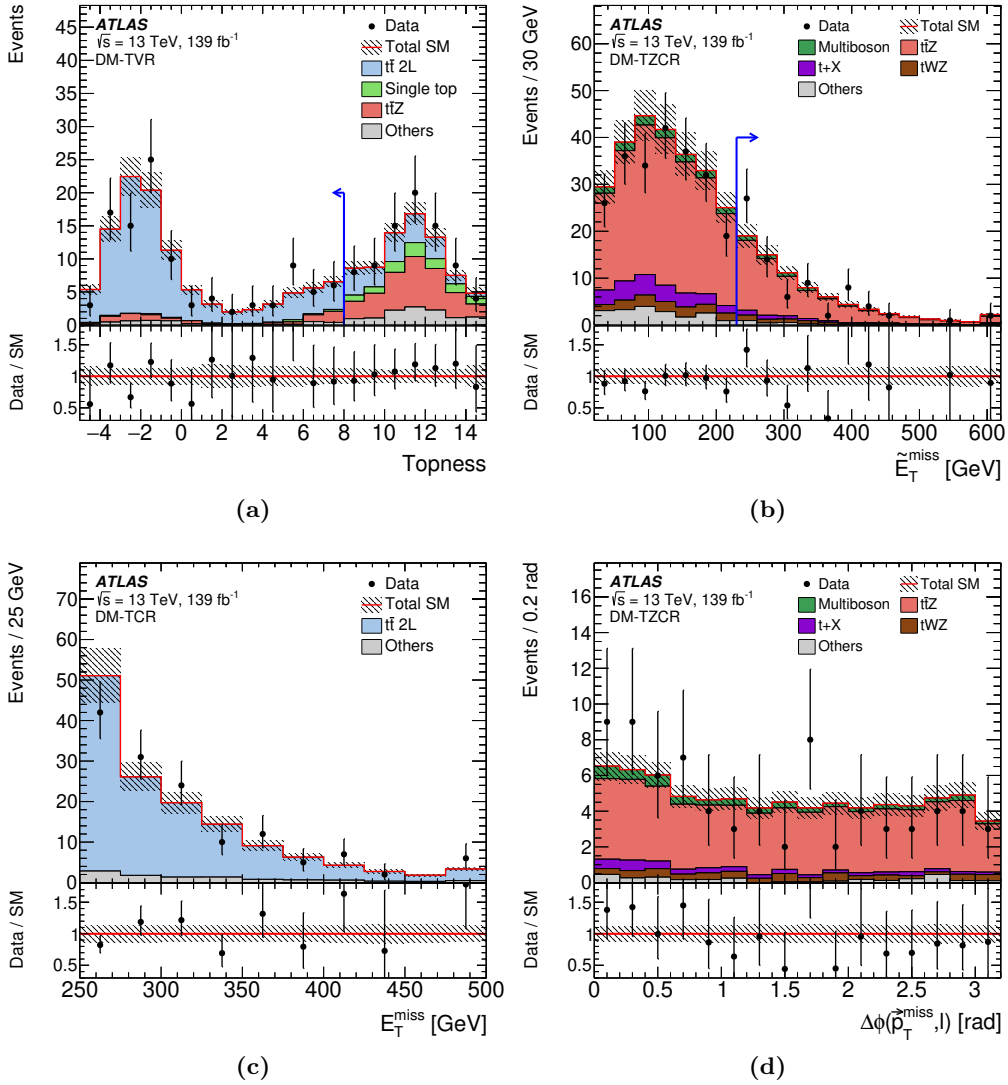

Figure 5. Selected kinematic distributions in DM CRs and VRs: (a) topness in the TVR before applying the topness selection, (b) $\tilde{E}_{\mathrm{T}}^{\mathrm{miss}}$ in the TZCR before applying the $\tilde{E}_{\mathrm{T}}^{\mathrm{miss}}$ selection, (c) $E_{\mathrm{T}}^{\mathrm{miss}}$ in the TCR, (d) $\Delta\phi(\vec{p}_{\mathrm{T}}^{\,\mathrm{miss}}, \ell)$ in the TZCR. For distributions where the requirement on the displayed variable is removed an arrow indicates the final selection on that variable. The distributions shown are post-fit, i.e. each background is scaled by a normalisation factor obtained from a background-only likelihood fit to the CRs (see table 14). The hatched area around the total SM prediction and the hatched band in the Data/SM ratio include all statistical and systematic uncertainties. The last (first) bin contains overflows (underflows).

JHEP04(2021)174

Selection		tN_diag_low	tN_diag_low-TCR	tN_diag_low-TVR
Leading jet p_{T}	[GeV]	> 400	[200, 360]	> 400
m_{T}	[GeV]	> 150	> 110	
$\Delta m_{\mathrm{T}}^{\alpha}$	[GeV]	> 40	< 0	
$m_{\tilde{t}_1}^{\mathrm{lep}}$	[GeV]	< 600	–	
Selection		tN_diag_high	tN_diag_high-TCR	tN_diag_high-TVR
Leading jet p_{T}	[GeV]	> 400	[200, 440]	> 440
$E_{\mathrm{T}}^{\mathrm{miss}}$	[GeV]	> 400	> 350	
m_{T2}	[GeV]	< 360	–	
$\Delta m_{\mathrm{T}}^{\mathrm{dyn}}$	[GeV]	> 60	< 30	
$m_{\tilde{\chi}_1^0}^{\mathrm{dyn}}$	[GeV]	[220, 595]	–	

Table 11. Event selections defining the tN_diag_low and tN_diag_high TCR and TVR relative to their respective signal regions.

8.2 Control and validation regions for compressed $\tilde{t}_1 \to t + \tilde{\chi}_1^0$

The definitions of the control and validation regions for the compressed two-body decays rely on dedicated discriminating variables introduced in section 6.4. The dominant background process in both tN_diag_low and tN_diag_high is $t\bar{t}$ production. Each of these regions has its own dedicated TCR. The TCRs build upon the same N_{jet}, $N_{b\text{-jet}}$, m_{T} and hard-lepton preselection as the SRs. In both TCRs the selection on the p_{T} of the leading jet is lower than in the SR, and is chosen to be in the range 200–360 GeV for tN_diag_low and in the range 200–440 GeV for tN_diag_high. In the TCR associated with tN_diag_low, $\Delta m_{\mathrm{T}}^{\alpha}$ is required to be below zero to avoid signal contamination. In addition, to increase the number of events, the selection on $m_{\tilde{t}_1}^{\mathrm{lep}}$ is removed and the selection on m_{T} is lowered to 110 GeV. The TCR associated with tN_diag_high requires $\Delta m_{\mathrm{T}}^{\mathrm{dyn}}$ below 30 GeV to ensure orthogonality with the SR and limit signal contamination. To increase the number of events in the TCR associated with tN_diag_high, the $E_{\mathrm{T}}^{\mathrm{miss}}$ selection is lowered to 350 GeV and selections on $m_{\tilde{\chi}_1^0}^{\mathrm{dyn}}$ and m_{T2} are removed.

The top background normalisation in the two-body compressed region is validated using one VR for each of the regions tN_diag_low and tN_diag_high. The TVR corresponding to tN_diag_low is identical to the TCR except for the leading jet p_{T}, required to be above 400 GeV. The TVR associated with tN_diag_high is identical to the TCR, but requires the leading jet p_{T} to be larger than 440 GeV. Table 11 summarises the definitions of the TCR and TVR for tN_diag_low and tN_diag_high relative to the SR definitions.

Figure 6 compares data and prediction in CRs and VRs for several variables used in the tN_diag_low and tN_diag_high SRs. Good agreement is observed between data and prediction, within uncertainties.

JHEP04(2021)174

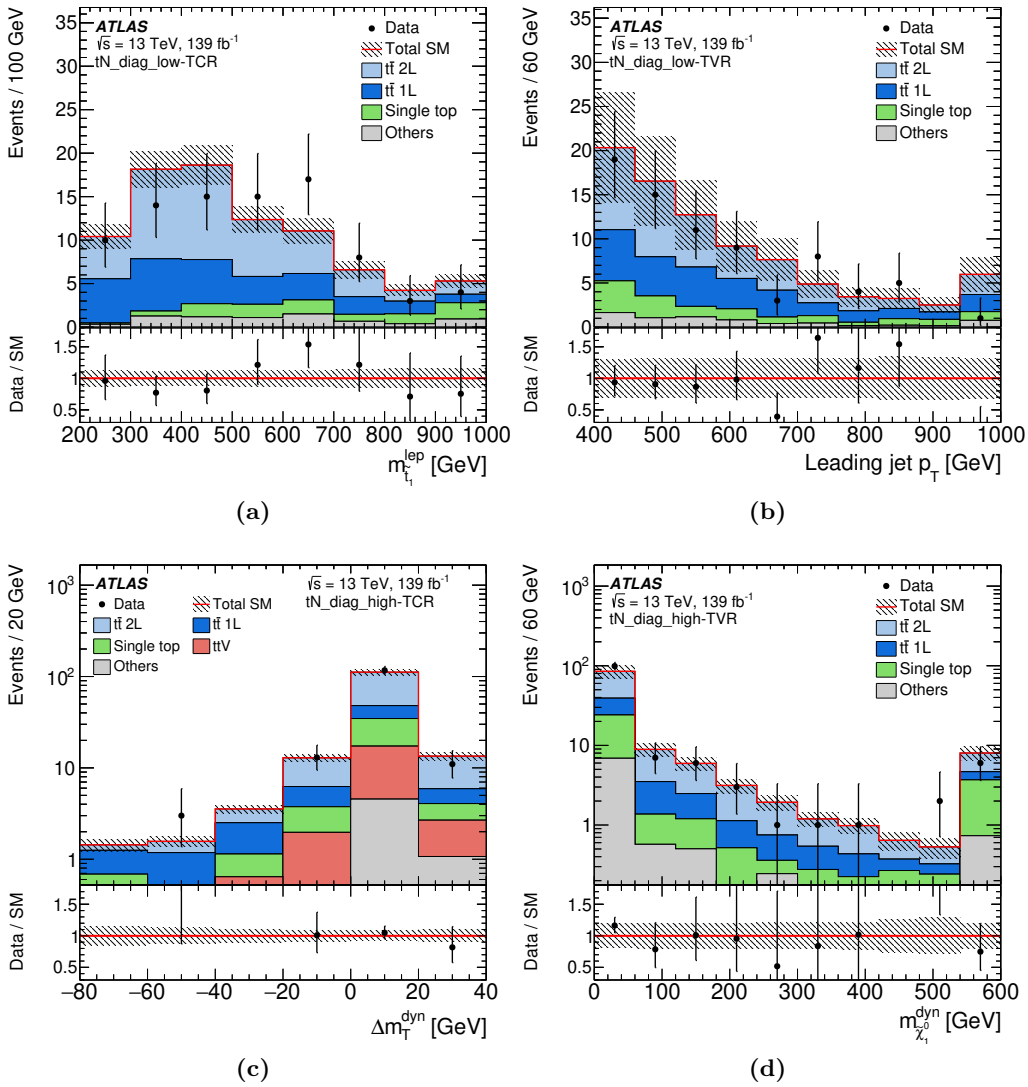

Figure 6. Selected kinematic distributions in `tN_diag_low` and `tN_diag_high` TCRs and TVRs: (a) $m_{\tilde{t}_1}^{\mathrm{lep}}$ in the `tN_diag_low` TCR, (b) leading jet p_{T} in the `tN_diag_low` TVR, (c) $\Delta m_{\mathrm{T}}^{\mathrm{dyn}}$ in the `tN_diag_high` TCR, (d) $m_{\tilde{\chi}_1^0}^{\mathrm{dyn}}$ in the `tN_diag_high` TVR. The distributions shown are post-fit, i.e. each background is scaled by a normalisation factor obtained from a background-only likelihood fit to the CRs (see table 14). The hatched area around the total SM prediction and the hatched band in the Data/SM ratio include all statistical and systematic uncertainties. The last (first) bin contains overflows (underflows).

JHEP04(2021)174

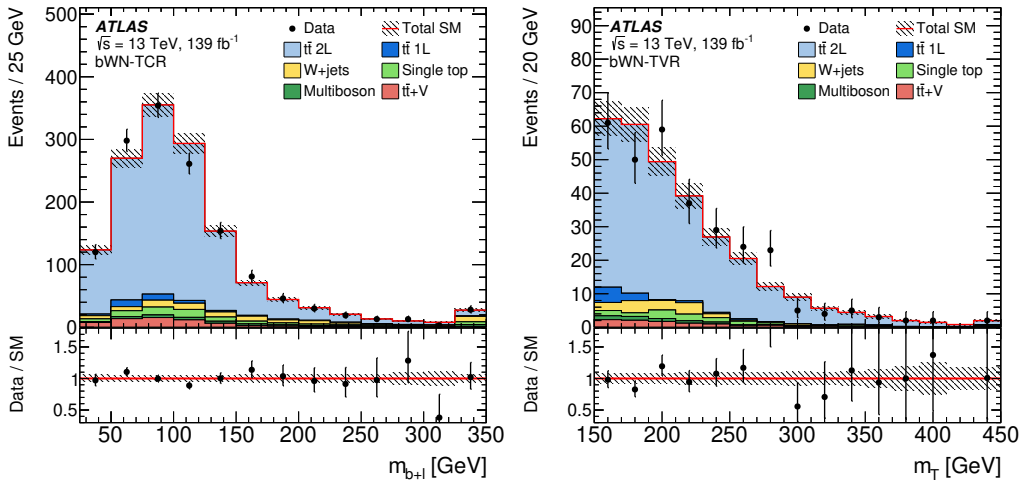

(a) (b)

Figure 7. Selected distributions in the `bWN` CR and VR: (a) $m_{\mathrm{b}+\ell}$ in the TCR, (b) m_{T} in the TVR. The distributions shown are post-fit, i.e. each background is scaled by a normalisation factor obtained from a background-only likelihood fit to the CRs (see table 14). The hatched area around the total SM prediction and the hatched band in the Data/SM ratio include all statistical and systematic uncertainties. The last (first) bin contains overflows (underflows).

8.3 Control and validation regions for $\tilde{t}_1 \to bW\tilde{\chi}_1^0$

More than 80% of the `bWN` SR yield consists of dileptonic $t\bar{t}$ events, while other background components range between 2% and 5% of the SR yield. Therefore, the $\tilde{t}_1 \to bW\tilde{\chi}_1^0$ SR requires only a TCR. In addition to the hard-lepton preselection, the `bWN` SR requires $\mathrm{NN}_{\mathrm{bWN}} > 0.9$ and $m_{\mathrm{T}} > 100\,\mathrm{GeV}$. To prevent overlap with the signal region, the TCR requires a lower interval of the output score, namely $\mathrm{NN}_{\mathrm{bWN}} \in [0.4, 0.6]$. To preserve the same background composition as the signal region, the selection on m_{T} is tightened to 150 GeV.

The TVR for the $\tilde{t}_1 \to bW\tilde{\chi}_1^0$ signal is designed by selecting $\mathrm{NN}_{\mathrm{bWN}} \in [0.6, 0.65]$, in between the $\mathrm{NN}_{\mathrm{bWN}}$ ranges used for the CR and the SR. In addition, $m_{\mathrm{T}} > 150\,\mathrm{GeV}$ is required to enhance the contribution of semileptonic $t\bar{t}$ events, representative of the background in the SR. The selections that define the TCR and TVR for `bWN` are summarised in table 6. Figure 7 compares data and prediction in the CR and VR associated with `bWN`. Good agreement is observed between data and prediction, within uncertainties.

8.4 Control and validation regions for $\tilde{t}_1 \to bff'\tilde{\chi}_1^0$

In the signal region `bffN_softb` the largest background is W+jets followed by approximately equal amounts of dileptonic and semileptonic $t\bar{t}$. A W+jets control region, WCR, is built upon the same selections as the SR, but to enhance the fraction of W+jets events, $p_{\mathrm{T}}^{\ell}/E_{\mathrm{T}}^{\mathrm{miss}}$ is required to be in the interval [0.16, 0.32] while the lepton charge is required to be positive. A $t\bar{t}$ control region, TCR, is designed to have approximately equal amounts of the two types of $t\bar{t}$ backgrounds. The TCR builds on the same selections as `bffN_softb`, but it requires

JHEP04(2021)174

Selection		`bffN_softb`	`bffN_softb`-TCR (-TVR)	`bffN_softb`-WCR (-WVR)
$N_{b\text{-jet}}$		$= 0$	≥ 1	$=0$
Lepton charge		–	< 0	> 0
$p_{\mathrm{T}}^{\ell}/E_{\mathrm{T}}^{\mathrm{miss}}$		< 0.04	$\in [0.12, 0.25]$ ($\in [0.08, 0.12]$)	$\in [0.16, 0.32]$ ($\in [0.08, 0.16]$)
Selection		`bffN_btag`	`bffN_btag`-TCR (-TVR)	`bffN_btag`-WCR (-WVR)
b-jet p_{T}	[GeV]	< 50	> 100 ($\in [50, 100]$)	–
m_{T}	[GeV]	> 90	> 110	>90
$p_{\mathrm{T}}^{\ell}/E_{\mathrm{T}}^{\mathrm{miss}}$		< 0.05	> 0.05	> 0.05
$\Delta\phi(p_{\mathrm{T}}^{b\text{-jet}}, \vec{p}_{\mathrm{T}}^{\,\mathrm{miss}})$	[rad]	< 1.5	< 1.5	> 2.3 ($\in [1.5, 2.3]$)
Lepton charge		–	–	> 0

Table 12. Event selections defining the CRs and VRs in `bffN_softb` and `bffN_btag` relative to their respective signal regions.

the presence of at least one b-tagged jet in order to increase the fraction of $t\bar{t}$ and to ensure orthogonality with the `bffN_softb` SR. The TCR also requires $p_{\mathrm{T}}^{\ell}/E_{\mathrm{T}}^{\mathrm{miss}}$ to be in the interval [0.12, 0.25] and that the lepton charge be negative for orthogonality with the WCR.

The validation region TVR associated with `bffN_softb` is defined with the same selections as the TCR, except for the ratio $p_{\mathrm{T}}^{\ell}/E_{\mathrm{T}}^{\mathrm{miss}}$, which is required to be in the interval [0.08, 0.12]. The WVR for `bffN_softb` has the same selections as the WCR, except $p_{\mathrm{T}}^{\ell}/E_{\mathrm{T}}^{\mathrm{miss}}$ is required to be in the interval [0.08, 0.16]. Table 12 shows the selection differences between the `bffN_softb` SR and the associated CRs and VRs.

The soft b-tagging efficiency and mis-tag rate depend on the track multiplicity, kinematics of the b-hadrons, and the b-hadron fragmentation. Two highly populated soft b-tagging regions enriched in $t\bar{t}$ and W+jets are defined, where it is found that the track multiplicity differs between data and MC simulations. In each region a weight is defined as a function of the track multiplicity to reweight the MC simulation to the data. After reweighting, good agreement is found between the data and the simulation in a range of secondary vertex variables such as vertex mass, vertex momentum, vertex distance to the primary vertex and vertex track multiplicity. The 'after-to-before-reweighting' ratios of efficiencies and mis-tag rates define scale factors that are derived separately for Sherpa and Pythia 8. The largest discrepancy after reweighting is found in the W+jets region and is of the order of 20%. A corresponding 20% systematic uncertainty in the soft b-tagging scale factors is introduced.

In the signal region `bffN_btag`, the dominant background process is dileptonic $t\bar{t}$, representing almost half of all background events, followed by W+jets. To ensure orthogonality with the SR and limit signal contamination, the TCR control region has the same selections as the SR, but requires the leading b-tagged jet p_{T} to be above 100 GeV, $m_{\mathrm{T}} > 110$ GeV and $p_{\mathrm{T}}^{\ell}/E_{\mathrm{T}}^{\mathrm{miss}} > 0.05$. Compared with the SR, the WCR removes the upper bound on the leading b-tagged jet p_{T}, requires $\Delta\phi(p_{\mathrm{T}}^{b\text{-jet}}, \vec{p}_{\mathrm{T}}^{\,\mathrm{miss}}) > 2.3$, $p_{\mathrm{T}}^{\ell}/E_{\mathrm{T}}^{\mathrm{miss}} > 0.05$ and a positive lepton charge.

The TVR associated with the `bffN_btag` signal region has the same selections as TCR but the b-tagged jet p_{T} is required to be in the interval [50, 100] GeV, and is thus between

JHEP04(2021)174

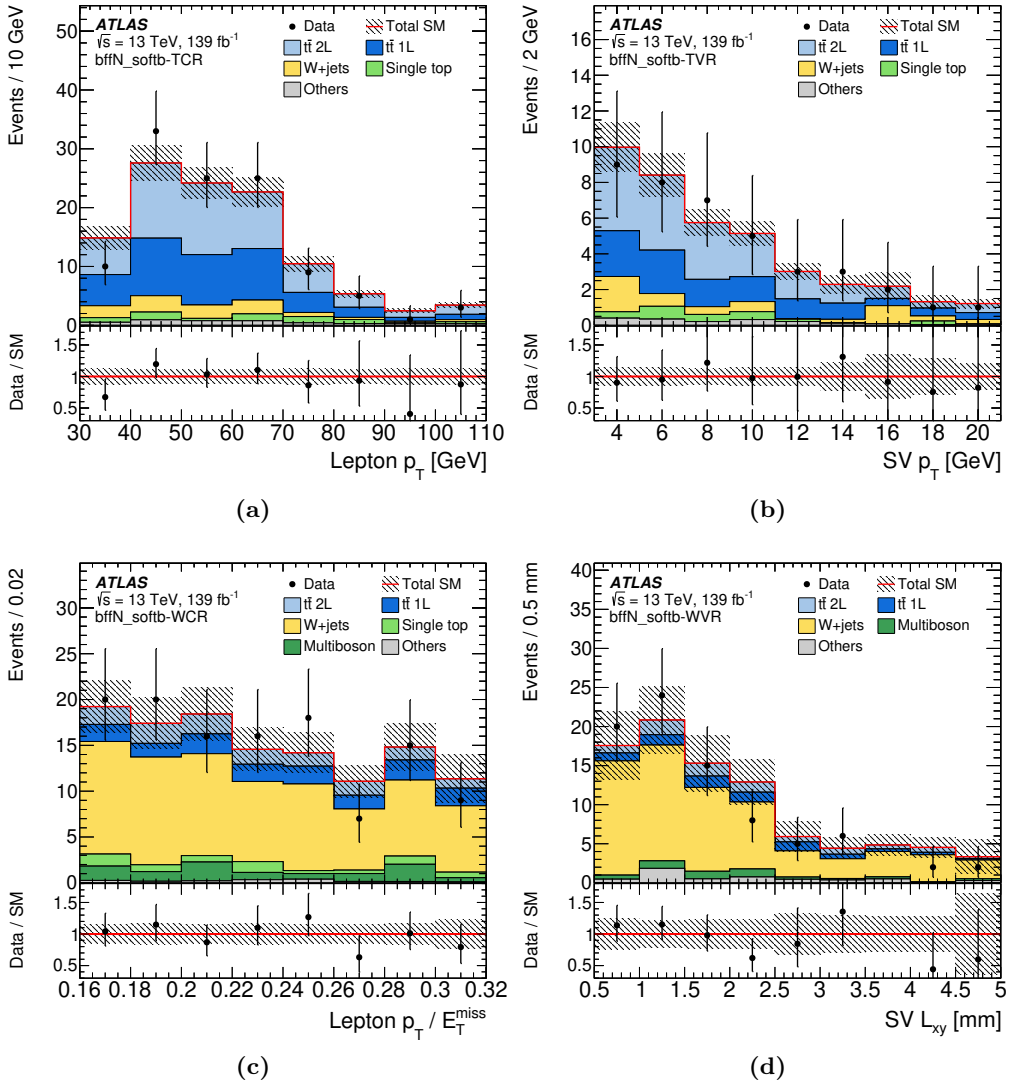

Figure 8. Selected kinematic distributions in `bffN_softb` CRs and VRs: (a) lepton p_{T} in the TCR, (b) transverse component of the total track momentum attached to the secondary vertex, SV p_{T}, in the TVR, (c) $p_{\mathrm{T}}^{\ell}/E_{\mathrm{T}}^{\mathrm{miss}}$ in the WCR, (d) distance from the primary vertex to the secondary vertex in the transverse plane, SV L_{xy}, in the WVR. The distributions shown are post-fit, i.e. each background is scaled by a normalisation factor obtained from a background-only likelihood fit to the CRs (see table 14). The hatched area around the total SM prediction and the hatched band in the Data/SM ratio include all statistical and systematic uncertainties. The last (first) bin contains overflows (underflows).

the signal region and control region. The WVR has the same selections as the WCR except for the angle $\Delta\phi(p_{\mathrm{T}}^{b\text{-jet}}, \vec{p}_{\mathrm{T}}^{\,\mathrm{miss}})$, which is required to be in the intermediate range between the WCR and the SR, namely the interval [1.5, 2.3].

Figures 8 and 9 compare data and predictions in the `bffN_softb` and `bffN_btag` CRs and VRs. Good agreement is observed between data and prediction, within uncertainties.

JHEP04(2021)174

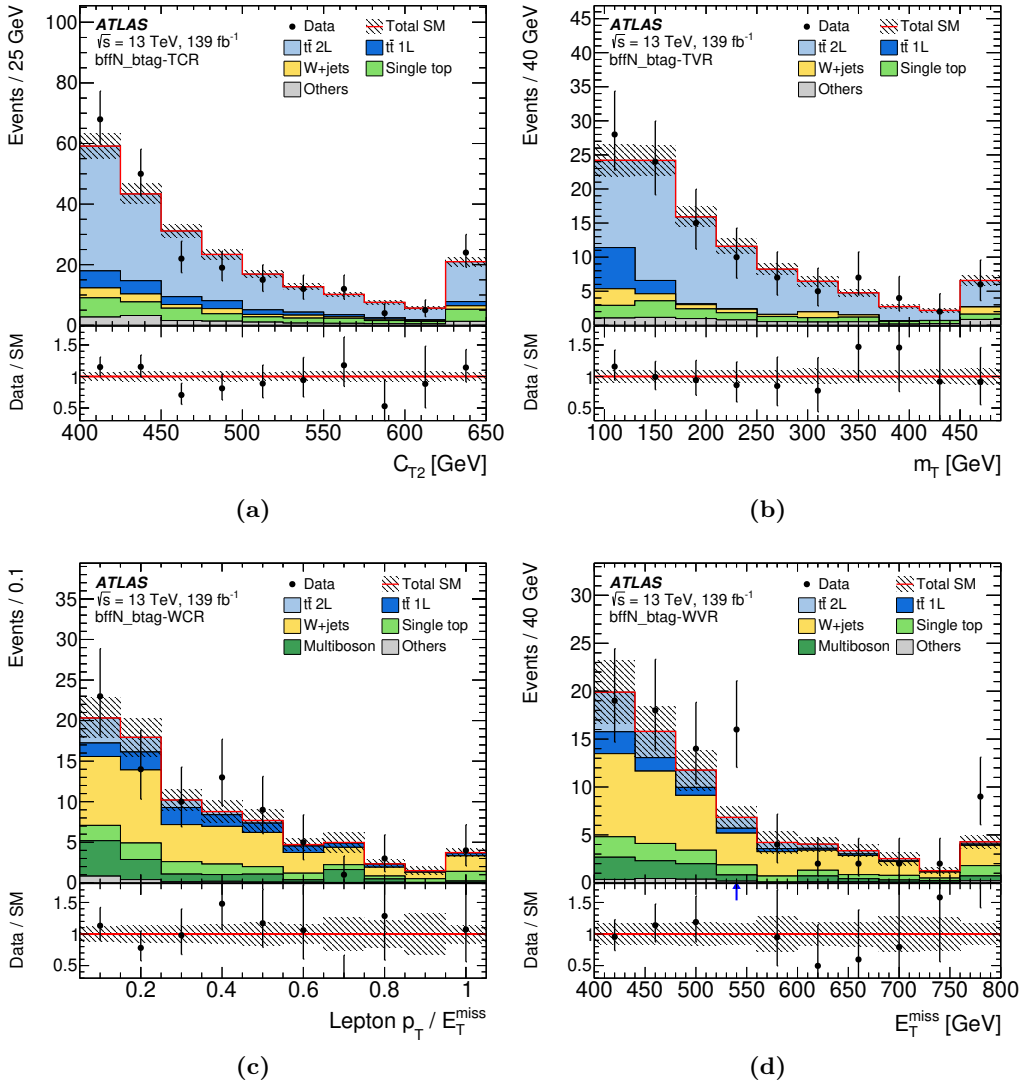

Figure 9. Selected kinematic distributions in `bffN_btag` CRs and VRs: (a) C_{T2} in the TCR, (b) m_{T} in the TVR, (c) $p_{\mathrm{T}}^{\ell}/E_{\mathrm{T}}^{\mathrm{miss}}$ in the WCR, (d) $E_{\mathrm{T}}^{\mathrm{miss}}$ in the WVR. The distributions shown are post-fit, i.e. each background is scaled by a normalisation factor obtained from a background-only likelihood fit to the CRs (see table 14). The hatched area around the total SM prediction and the hatched band in the Data/SM ratio include all statistical and systematic uncertainties. The last (first) bin contains overflows (underflows).

9 Systematic uncertainties

The systematic uncertainties in the background estimates arise from multiple experimental and theoretical sources and can enter the SR background yield either via direct predictions from theoretical cross-sections or from uncertainties in the extrapolation from CRs to SRs. The sources of systematic uncertainties are grouped into categories whose labels are defined in parentheses in the paragraphs below. Their effect on the background predictions in the SRs is summarised in table 13. The systematic uncertainties are included as nuisance parameters constrained by Gaussian probability distributions and profiled in the likelihood fits.

JHEP04(2021)174

Experimental uncertainties arise from imperfect knowledge of the jet energy scale (*JES*), jet energy resolution (*JER*) [113], scale and resolution of the $E_{\mathrm{T}}^{\mathrm{miss}}$ soft term (E_T^{miss} *experimental*) [123], as well as the modelling of the b-tagging or soft b-tagging efficiencies and mis-tag rates [117] (*b-tagging experimental*). Other experimental uncertainties arise from the modelling of the lepton energy scales, energy resolutions, reconstruction and identification efficiencies (*Leptons experimental*). There is also an experimental uncertainty arising from the reweighting of the simulation as a function of the number of interactions per bunch crossing in data and the additional cuts applied to jets to ensure they arise from the hard-scatter primary vertex (*Pile-up*).

Backgrounds such as dibosons and Z+jets, derived directly from a MC prediction and a theoretical cross-section, have theoretical systematic uncertainties (*Theory*) arising from theoretical cross-section calculations, including those related to parton distribution functions and factorisation and normalisation scales. The systematic uncertainty on the integrated luminosity is also included in this category. As shown in table 9, the single-top, $t\bar{t}+Z$ and W+jets backgrounds are also predicted directly from MC simulations for some SRs, in which case the theory uncertainties apply also to those processes.

When the yield from a background such as $t\bar{t}$, single-top, $t\bar{t}+V$ or W+jets is normalised using a CR, modelling uncertainties affect the extrapolation from the control to the signal region, but not the overall normalisation. In each of these cases, the background has a normalisation systematic uncertainty (*Normalisation*) from the fit, arising from the statistical power of the CR for the given background and a modelling uncertainty (*Modelling*) that affects the extrapolation factor from the CR to the SR.

The uncertainties in the modelling of the $t\bar{t}$ background include effects related to the MC event generator, the hadronisation modelling and the amount of initial- and final-state radiation [86]. The MC generator uncertainty is estimated by taking the full difference in event yields between Powheg-Box v2+Pythia 8 and MadGraph5_aMC@NLO v2.6.0 +Pythia 8. Events generated with Powheg-Box v2 are showered and subsequently hadronised with either Pythia 8 or Herwig 7.0 in order to estimate the effect from modelling of the hadronisation. The systematic uncertainty from the amount of initial- and final-state radiation is derived by comparing Powheg-Box results obtained with different shower radiation, NLO radiation and modified factorisation and renormalisation scales.

The single-top Wt process modelling uncertainty is derived from the size of the interference between $t\bar{t}$ and Wt using the $t\bar{t}$, Wt and $WWbb$ samples generated with MadGraph. It is obtained by comparing Wt with the difference between $WWbb$ and $t\bar{t}$. The Wt sample generated with MadGraph is found to be in good agreement with the nominal samples generated with Powheg-Box v2+Pythia 8. For the `tN_med` and `tN_high` SRs where STCR is used, the Wt modelling uncertainty enters via the ratio of the number of Wt events in the signal region to the number in the STCR. Given the potentially large modelling uncertainty in the interference between $t\bar{t}$ and Wt, the modelling uncertainty is also evaluated for the `DM` SR by comparing the predicted single-top yield from Wt with the difference between $WWbb$ and $t\bar{t}$.

The modelling uncertainties considered for $t\bar{t}+Z$ are the renormalisation and factorisation scales, and the amount of initial- and final-state radiation, obtained by

JHEP04(2021)174

SR Uncertainty [%]	tN_med	tN_high	tN_diag_low	tN_diag_high	bWN	bffN_btag	bffN_softb	DM
$t\bar{t}$ normalisation	4.4	2.7	12.3	15.8	7.8	6.6	3.7	3.0
$t\bar{t}+Z$ normalisation	9.0	6.8	–	–	–	–	–	8.5
W+jets normalisation	3.0	4.8	–	–	–	5.5	11.1	–
Wt normalisation	2.8	3.4	–	–	–	–	–	–
$t\bar{t}$ modelling	3.0	9.1	18.4	29.3	17.6	3.1	3.3	4.1
$t\bar{t}+Z$ modelling	7.7	7.1	–	–	–	–	–	7.4
W+jets modelling	2.3	3.8	–	–	–	4.3	9.7	–
Wt modelling	0.5	0.8	–	–	–	–	–	6.4
JER	10.9	5.1	4.1	5.0	6.1	1.8	7.6	6.5
$E_{\mathrm{T}}^{\mathrm{miss}}$ experimental	0.7	0.4	1.0	0.2	0.9	2.4	3.4	0.1
b-tagging experimental	1.7	3.6	1.3	0.9	1.6	1.9	3.2	3.1
JES	6.0	2.5	4.7	4.1	2.7	6.1	11.7	2.4
Leptons experimental	1.0	1.6	1.3	0.3	0.1	2.3	4.9	0.6
Pile-up	1.1	1.2	1.2	0.3	0.8	1.0	2.1	1.1
Theory	0.9	1.3	1.4	0.5	4.8	3.8	3.7	0.7
MC statistics	4.1	6.6	5.8	3.5	3.1	4.9	17.2	3.2
Total	19	17	24	33	20	12	27	15

Table 13. Summary of the dominant systematic uncertainties as a percentage of the total predicted background yields in the SRs, obtained from the background-only fits described in section 10.

considering the variation of the same parameters used for the $t\bar{t}$ initial- and final-state radiation systematic uncertainties. The W+jets modelling uncertainties include generator modelling, derived by considering an alternative W+jets sample generated with MadGraph as well as modified factorisation, renormalisation, resummation and parton matching scales.

Most of the SRs are binned in one or two variables in order to enhance sensitivity to a wider range of models for exclusion limits. In this situation the normalisation factors to go from the CR to the SR are rederived specifically for each bin of the SR. The modelling systematic uncertainties are also rederived following the scheme above but applied to the normalisation factor from the CR to each specific bin of the SR.

The SUSY signal cross-section uncertainty is taken from an envelope of cross-section predictions using different PDF sets and factorisation and renormalisation scales as described in ref. [134]. The uncertainty in the DM production cross-section is derived from the scale variations and PDF choices. Dedicated uncertainties in the SUSY and DM signal acceptance due to the modelling of additional radiation, factorisation, renormalisation and parton matching scales are considered. The total systematic uncertainty for the SUSY models varies between 9% and 35%, increasing at higher stop mass and at lower values of $\Delta m_{\tilde{t}_1,\tilde{\chi}_1^0}$. For the spin-0 mediator signals the total systematic uncertainty is between 15% and 18%.

JHEP04(2021)174

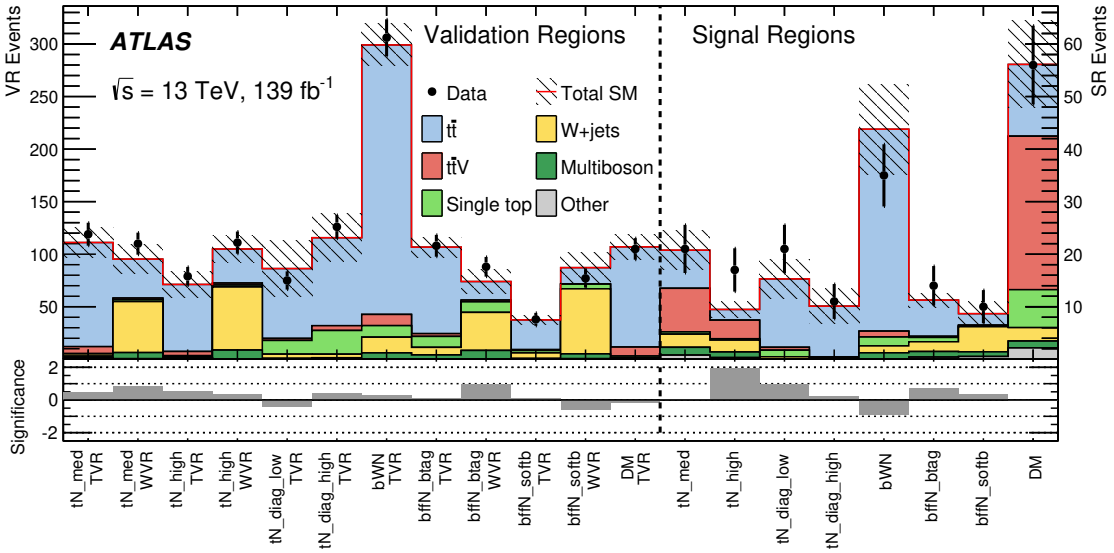

Figure 10. The upper panel shows the comparison between the observed data (n_{obs}) and the predicted SM background (n_{exp}) in all VRs and SRs. The background predictions are obtained using the background-only fit, and the hatched area around the SM prediction includes all uncertainties. The bottom panel shows the Z significance of the observed number of events given the SM expectation.

10 Results

To determine the SM background yields in the SRs, a background-only likelihood fit is performed for each analysis. The fit does not use the signal region data, but only the dedicated CRs to normalise the backgrounds.

The number of observed events and the predicted number of SM background events from the background-only fits in all VRs and SRs are shown in figure 10 together with the Z significance of the observation. The SRs are not mutually exclusive and are therefore not statistically independent. In all SRs, the distributions indicate good agreement between the data and the SM background estimate. The largest excess over the background-only hypothesis is 1.9σ observed in the `tN_high` SR.

The number of observed events together with the predicted number of SM background events in all SRs are summarised in table 14, showing the breakdown of the various backgrounds that contribute to the SRs. The table also lists the results for the fit parameters that control the normalisation of the main backgrounds (normalisation factors, NFs),[6] together with the associated fit uncertainties including the theoretical modelling uncertainties. To quantify the level of agreement of the SM background-only hypothesis with the observations in the SRs, a profile-likelihood-ratio test [135] is performed. The resulting p-values (p_0) are also presented in the table together with the Z significances. For SRs with an observed number of events below the SM prediction, the p_0 values are capped at 0.5. Model-independent upper limits on beyond-the-SM contributions are derived for

[6]The $t\bar{t}$ NFs in the `tN_diag_low`, `bffN_btag`, and `bffN_softb` SRs are applied to semileptonic and dileptonic $t\bar{t}$ events while all other SRs apply the $t\bar{t}$ NFs to the dileptonic component only.

JHEP04(2021)174

	tN_med	tN_high	tN_diag_low	tN_diag_high	bWN	bffN_btag	bffN_softb	DM
Observed	21	17	21	11	35	14	10	56
Total SM	21 ± 4	9.5 ± 1.6	15 ± 4	10.1 ± 3.4	44 ± 9	11.3 ± 1.4	8.7 ± 2.3	56 ± 8
$t\bar{t}$	7.2 ± 1.2	2.0 ± 1.0	13.0 ± 2.8	9.6 ± 2.6	38 ± 9	6.9 ± 1.1	2.2 ± 0.6	14 ± 4
$t\bar{t}V$	8.3 ± 2.5	3.5 ± 1.0	0.55 ± 0.17	0.12 ± 0.04	1.1 ± 1.1	0.21 ± 0.12	0.06 ± 0.04	29 ± 6
Single top	$0.4^{+0.6}_{-0.4}$	$0.27^{+0.34}_{-0.27}$	1.24 ± 0.27	0.26 ± 0.06	1.7 ± 1.7	0.8 ± 0.5	0.22 ± 0.08	7 ± 4
W+jets	2.5 ± 2.3	2.3 ± 1.0	0.41 ± 0.13	0.080 ± 0.020	1.3 ± 0.6	1.9 ± 0.8	4.8 ± 2.1	2.56 ± 0.24
Multiboson	1.49 ± 0.21	1.06 ± 0.16	0.070 ± 0.020	0.020 ± 0.010	1.22 ± 0.30	1.07 ± 0.35	0.89 ± 0.32	1.31 ± 0.18
Other	0.78 ± 0.06	0.320 ± 0.024	–	–	–	0.40 ± 0.13	0.52 ± 0.19	2.15 ± 0.16
$t\bar{t}$ NF	$0.98^{+0.14}_{-0.12}$	0.90 ± 0.12	$0.88^{+0.13}_{-0.12}$	$0.73^{+0.14}_{-0.13}$	1.06 ± 0.10	$0.80^{+0.09}_{-0.08}$	0.68 ± 0.10	$1.12^{+0.15}_{-0.13}$
$t\bar{t}V$ NF	$0.95^{+0.22}_{-0.20}$	0.92 ± 0.17	–	–	–	–	–	$1.18^{+0.20}_{-0.18}$
Single top NF	$0.11^{+0.26}_{-0.11}$	$0.12^{+0.22}_{-0.12}$	–	–	–	–	–	–
W+jets NF	$0.96^{+0.25}_{-0.23}$	0.86 ± 0.17	–	–	–	0.83 ± 0.28	$1.04^{+0.22}_{-0.20}$	-
p_0 (Z)	0.49 (0.03)	0.01 (2.20)	0.17 (0.95)	0.31 (0.50)	0.50 (0.00)	0.20 (0.84)	0.26 (0.64)	0.50 (0.00)
$N^{\text{limit}}_{\text{non-SM}}$ exp.	$12.4^{+5.4}_{-2.6}$	$9.8^{+2.8}_{-1.8}$	$14.1^{+4.8}_{-3.3}$	$9.7^{+3.7}_{-2.1}$	$21.8^{+7.6}_{-7.9}$	$8.6^{+3.6}_{-1.2}$	$8.9^{+3.8}_{-2.0}$	$27.4^{+7.6}_{-5.0}$
$N^{\text{limit}}_{\text{non-SM}}$ obs.	12.9	16.2	17.7	10.9	15.3	11.7	10.5	28.2

Table 14. The number of observed events in the various SRs together with the expected numbers of background events and their uncertainties as predicted by the background-only fits, the normalisation factors for the background predictions obtained in the fit, the probabilities (represented by p_0 and Z values) that the observed numbers of events are compatible with the background-only hypothesis, and the expected ($N^{\text{limit}}_{\text{non-SM}}$ exp.) and observed ($N^{\text{limit}}_{\text{non-SM}}$ obs.) 95% CL upper limits on the number of beyond-SM events.

each SR. A generic signal model is assumed that contributes only to the SR and for which neither experimental nor theoretical systematic uncertainties except for the luminosity uncertainty are considered. All limits are calculated using the CL_s prescription [136]. The NFs are compatible with unity in most cases. One exception is for the single-top NFs in the `tN_med` and `tN_high` SRs. The single-top NFs are significantly below unity when using the DR scheme for the treatment of the interference between the Wt and $t\bar{t}$ processes. When changing to the DS scheme, the NFs become larger than unity but the predicted number of single-top events in the signal regions after the fit does not change significantly. This is explained by the fact that the DS and DR schemes give the same SR to STCR event yield ratio, within uncertainties. The $t\bar{t}$ NFs in `tN_diag_high`, `bffN_btag` and `bffN_softb` are below unity, which could potentially point to some mismodelling in this extreme region of phase-space. But good agreement is seen in the $t\bar{t}$ VRs, giving confidence in the $t\bar{t}$ background estimates.

Figures 11 and 12 show comparisons between the observed data and the SM background prediction with all SR selections applied except the requirement on the plotted variable. The expected distributions from representative signal benchmark models are overlaid.

JHEP04(2021)174

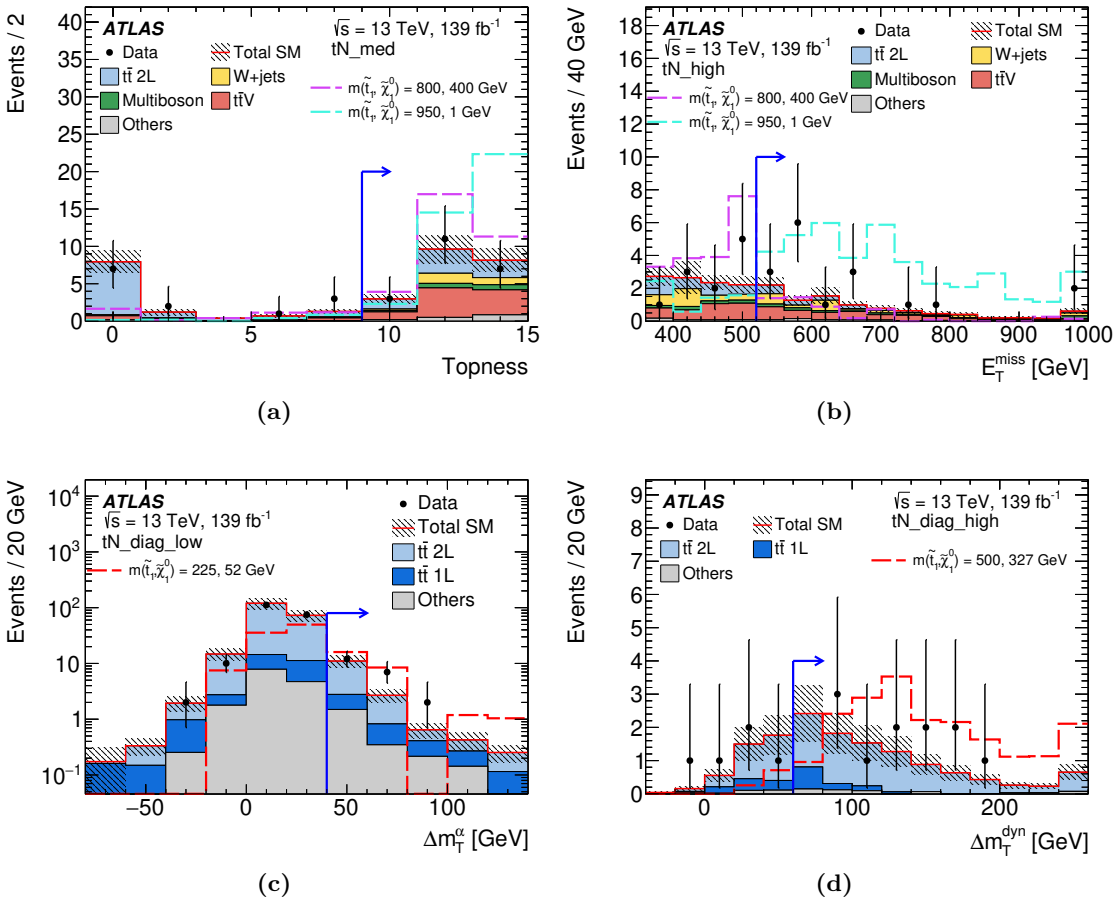

Figure 11. Kinematic distributions in the (a) `tN_med`, (b) `tN_high`, (c) `tN_diag_low` and (d) `tN_diag_high` SRs. The full event selection in the corresponding signal region is applied, except for the requirement (indicated by an arrow) that is imposed on the variable being plotted. The distributions shown are post-fit, i.e. each background is scaled by a normalisation factor obtained from a background-only likelihood fit to the CRs (see table 14). In addition to the background prediction, a signal model is shown on each plot. The hatched area around the total SM prediction includes statistical and experimental uncertainties. The last (first) bin contains overflows (underflows).

11 Interpretations

No significant excess is observed, and exclusion limits based on profile-likelihood fits are set for the stop pair production models and the spin-0 mediator models. Exclusion limits at 95% confidence level (CL) are obtained by selecting the signal region with the lowest expected CL_s value for each signal model and the exclusion contours are derived by interpolating in the CL_s value. The signal uncertainties and potential signal contributions to all regions are taken into account, and all uncertainties except those in the theoretical signal cross-section are included in the fit. In all exclusion plots, the $\pm 1\sigma_{\text{exp}}$ uncertainty band indicates how much the expected limit is affected by the systematic and statistical uncertainties included in the fit. The $\pm 1\sigma_{\text{theory}}^{\text{SUSY}}$ uncertainty lines around the observed limit illustrate the change

JHEP04(2021)174

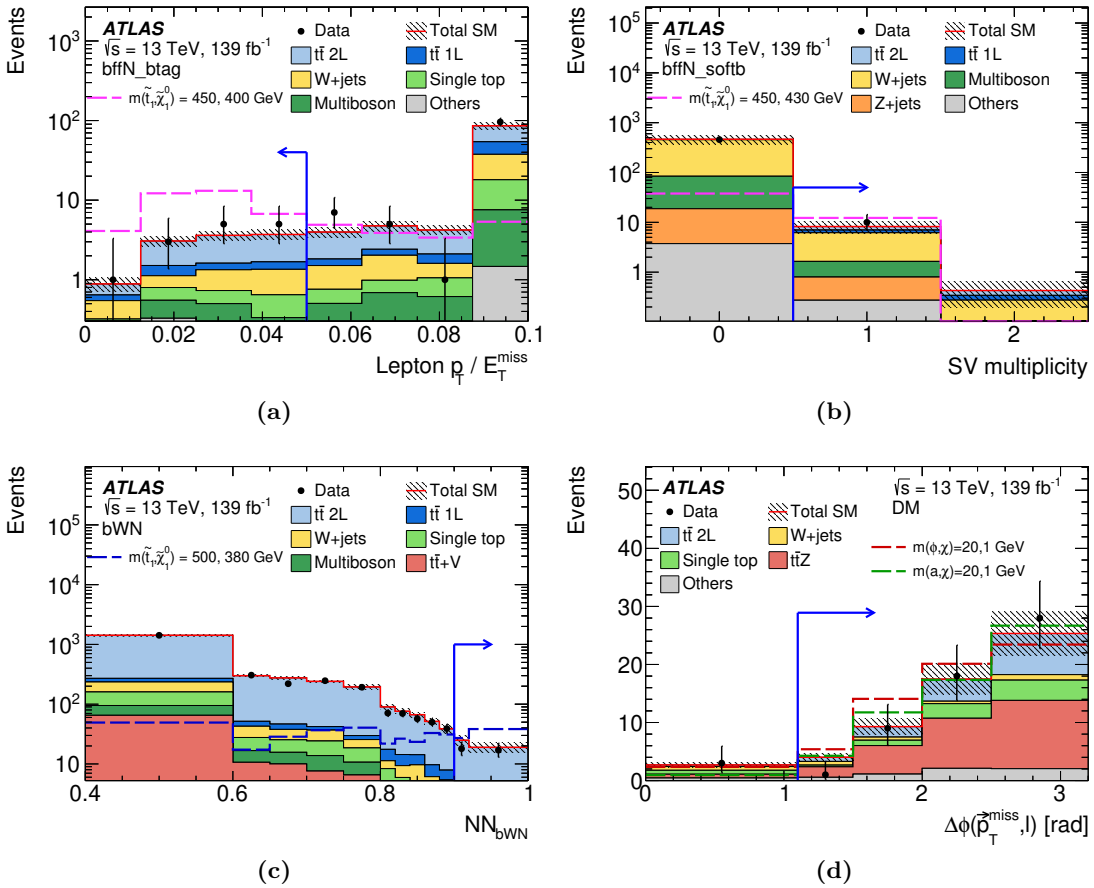

Figure 12. Kinematic distributions in the (a) `bffN_btag`, (b) `bffN_softb`, (c) `bWN` and (d) `DM` SRs. The full event selection in the corresponding signal region is applied, except for the requirement (indicated by an arrow) that is imposed on the variable being plotted. In the `DM` SR, the signal is normalised under the assumption of the coupling strength g=1.0. The distributions shown are post-fit, i.e. each background is scaled by a normalisation factor obtained from a background-only likelihood fit to the CRs (see table 14). In addition to the background prediction, a signal model is shown on each plot. The hatched area around the total SM prediction includes statistical and experimental uncertainties. The last (first) bin contains overflows (underflows).

in the observed limit as the nominal signal cross-section is scaled up and down by the theoretical cross-section uncertainty.

Figures 13 and 14 show the expected and observed exclusion contours as a function of the stop mass, the neutralino mass and the mass difference between the stop and the neutralino, for the $\tilde{t}_1 \to t + \tilde{\chi}_1^0$, $\tilde{t}_1 \to bW\tilde{\chi}_1^0$ and $\tilde{t}_1 \to bff'\tilde{\chi}_1^0$ scenarios. In models with a massless neutralino, stop masses up to 1200 GeV are excluded at 95% CL. In the diagonal region, where the mass difference between the stop and the neutralino coincides with the mass of the top quark, stop masses up to 600 GeV are excluded, which covers the previously unexcluded diagonal region between 210 GeV and 250 GeV in stop mass. In the three-body (four-body) region, stop masses up to 710 GeV (640 GeV) are excluded for a neutralino mass

JHEP04(2021)174

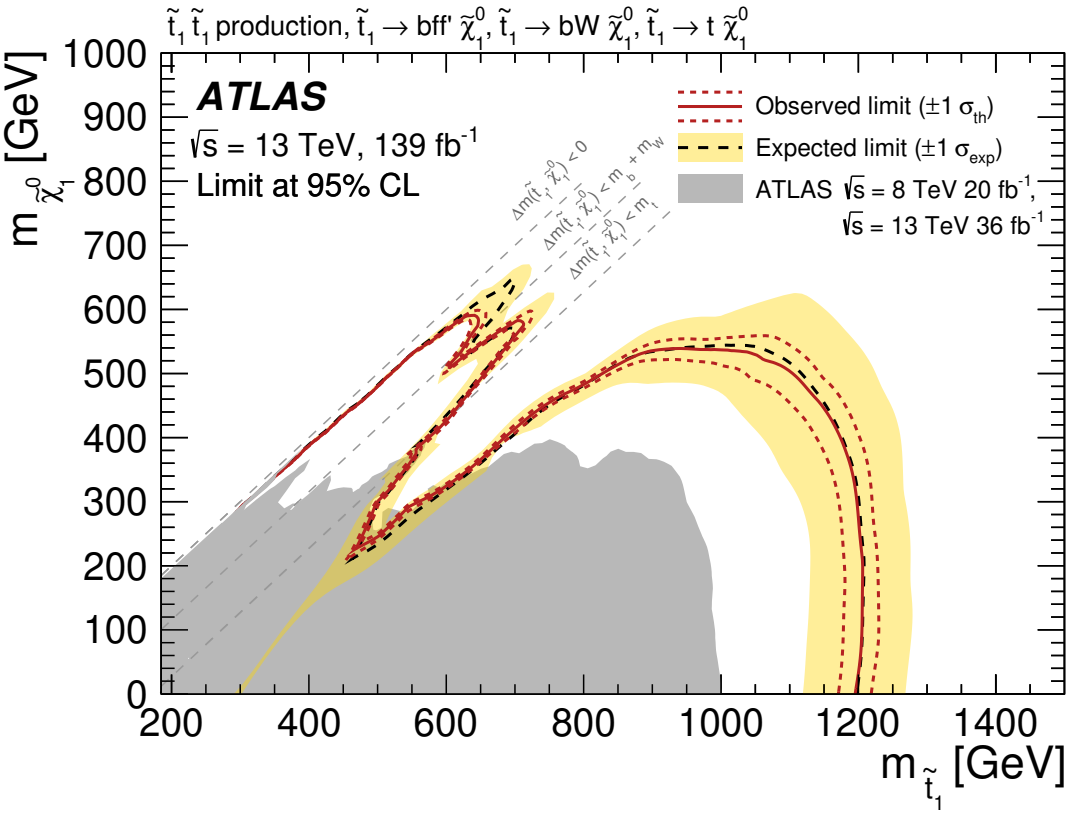

Figure 13. Expected and observed 95% CL excluded regions in the plane of $m_{\tilde{\chi}_1^0}$ and $m_{\tilde{t}_1}$ for direct stop pair production assuming either a $\tilde{t}_1 \to t + \tilde{\chi}_1^0$, $\tilde{t}_1 \to bW\tilde{\chi}_1^0$ or $\tilde{t}_1 \to bff'\tilde{\chi}_1^0$ decay with a branching ratio of 100%. The excluded regions from previous publications [29–31, 137] are shown by the shaded area and include additional topologies. The diagonal dashed lines indicate the kinematical border of the stop decay modes.

of approximately 580 GeV. The small excess observed in `tN_high` does not appear because the exclusion limits are obtained from the shape-fit in the `tN_med` signal region (table 4). The $E_{\mathrm{T},\perp}^{\mathrm{miss}}$ requirement applied in `tN_med` but not in `tN_high` removes most of the excess. The shape-fit is designed to have better expected sensitivity than the single-bin SRs over the whole $\tilde{t}_1 \to t + \tilde{\chi}_1^0$ parameter space.

Figure 15 shows the upper limit on the ratio of the production cross-section for the spin-0 mediator model to the theoretical cross-section. Limits are shown under the hypothesis of a scalar or pseudoscalar mediator for a fixed DM candidate mass. Scalar and pseudoscalar mediator masses up to approximately 200 GeV are excluded at 95% CL, assuming a 1 GeV dark-matter particle mass and a common coupling of $g = 1$ to SM and dark-matter particles. With the common coupling reduced to $g = 0.8$, mediator masses up to approximately 100 GeV are excluded. Models with a mediator mass of 10 GeV and a dark-matter particle mass of 1 GeV are excluded down to a coupling of approximately $g = 0.7$.

JHEP04(2021)174

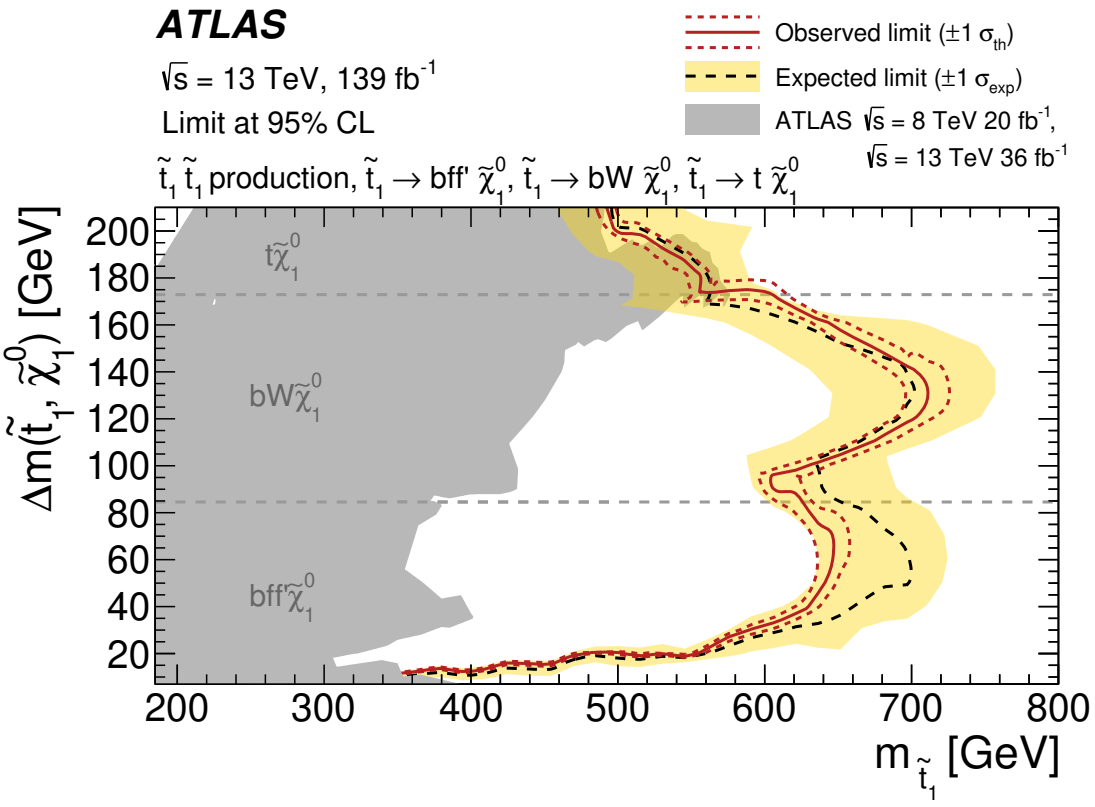

Figure 14. Expected and observed 95% CL excluded regions in the plane of $\Delta(m_{\tilde{t}_1}, m_{\tilde{\chi}_1^0})$ and $m_{\tilde{t}_1}$ for direct stop pair production assuming either a $\tilde{t}_1 \to t + \tilde{\chi}_1^0$, $\tilde{t}_1 \to bW\tilde{\chi}_1^0$ or $\tilde{t}_1 \to bff'\tilde{\chi}_1^0$ decay with a branching ratio of 100%. The excluded regions from previous publications [29–31, 137] are shown by the shaded area and include additional topologies. The horizontal dashed lines indicate the kinematical border of the stop decay modes.

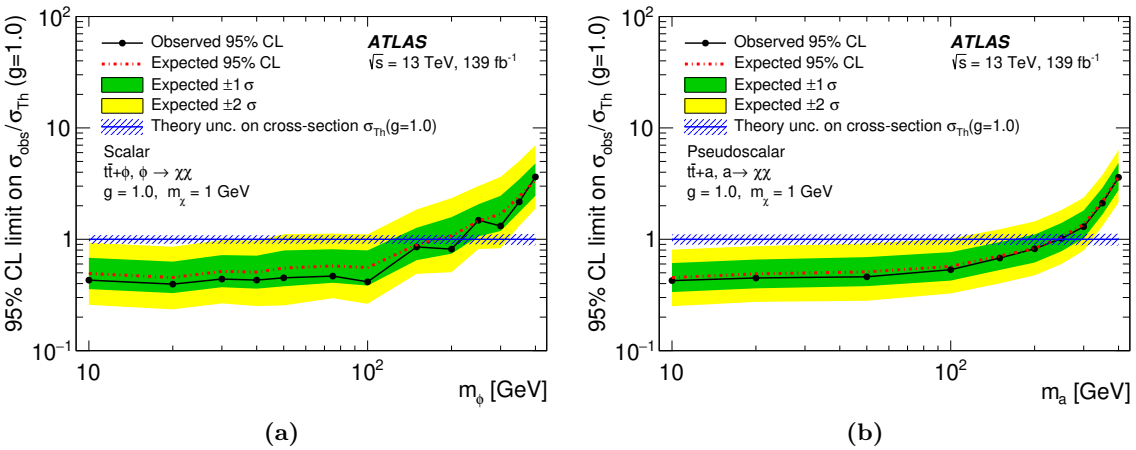

(a) (b)

Figure 15. Upper limit on the ratio of the production cross-section for the spin-0 mediator model to the theoretical cross-section under the hypothesis of (a) a scalar or (b) a pseudoscalar mediator. The limit is shown as a function of the mediator mass for a fixed mass of the DM candidate of 1 GeV. The coupling of the mediator to SM and DM particles is assumed to be $g = 1$.

JHEP04(2021)174

12 Conclusion

This paper presents searches for direct stop pair production covering various regions of SUSY phase space and searches for a spin-0 mediator decaying into pair-produced dark-matter particles. The searches use the final state with one isolated lepton, jets, and $E_{\mathrm{T}}^{\mathrm{miss}}$.

The analysis uses 139 fb^{-1} of pp collision data collected with the ATLAS detector at the LHC at a centre-of-mass energy of $\sqrt{s} = 13\,\mathrm{TeV}$. The largest excess over the background-only hypothesis is 1.9σ in the `tN_high` signal region. As no significant deviation from the Standard Model expectation is observed, exclusion limits at 95% confidence level are derived for the models considered. Stops are excluded up to 1200 GeV (710 GeV) in the two-body (three-body) decay scenario, extended from about 1000 GeV (400–600 GeV) in previous results. The introduction of ML techniques contributes to the significantly improved sensitivity in the challenging three-body decay scenario. In the four-body scenario, the exclusion of stops is extended from about 400 GeV in earlier results to up to 640 GeV for a stop-neutralino mass difference of 60 GeV. The introduction of the soft b-tagging algorithm contributes to the significantly improved sensitivity at small mass differences between the stop and the lightest neutralino. Scalar and pseudoscalar dark-matter mediators are excluded up to 200 GeV for a common coupling of $g = 1$ to Standard Model and dark-matter particles, from 100 GeV in earlier results. The introduction of a shape-fit in the DM signal region contributes to this improvement.

Acknowledgments

We thank CERN for the very successful operation of the LHC, as well as the support staff from our institutions without whom ATLAS could not be operated efficiently.

We acknowledge the support of ANPCyT, Argentina; YerPhI, Armenia; ARC, Australia; BMWFW and FWF, Austria; ANAS, Azerbaijan; SSTC, Belarus; CNPq and FAPESP, Brazil; NSERC, NRC and CFI, Canada; CERN; ANID, Chile; CAS, MOST and NSFC, China; COLCIENCIAS, Colombia; MSMT CR, MPO CR and VSC CR, Czech Republic; DNRF and DNSRC, Denmark; IN2P3-CNRS and CEA-DRF/IRFU, France; SRNSFG, Georgia; BMBF, HGF and MPG, Germany; GSRT, Greece; RGC and Hong Kong SAR, China; ISF and Benoziyo Center, Israel; INFN, Italy; MEXT and JSPS, Japan; CNRST, Morocco; NWO, Netherlands; RCN, Norway; MNiSW and NCN, Poland; FCT, Portugal; MNE/IFA, Romania; MES of Russia and NRC KI, Russia Federation; JINR; MESTD, Serbia; MSSR, Slovakia; ARRS and MIZŠ, Slovenia; DST/NRF, South Africa; MICINN, Spain; SRC and Wallenberg Foundation, Sweden; SERI, SNSF and Cantons of Bern and Geneva, Switzerland; MOST, Taiwan; TAEK, Turkey; STFC, United Kingdom; DOE and NSF, United States of America. In addition, individual groups and members have received support from BCKDF, CANARIE, Compute Canada and CRC, Canada; ERC, ERDF, Horizon 2020, Marie Skłodowska-Curie Actions and COST, European Union; Investissements d'Avenir Labex, Investissements d'Avenir Idex and ANR, France; DFG and AvH Foundation, Germany; Herakleitos, Thales and Aristeia programmes co-financed by EU-ESF and the Greek NSRF, Greece; BSF-NSF and GIF, Israel; La Caixa Banking Foundation, CERCA

JHEP04(2021)174

Programme Generalitat de Catalunya and PROMETEO and GenT Programmes Generalitat Valenciana, Spain; Göran Gustafssons Stiftelse, Sweden; The Royal Society and Leverhulme Trust, United Kingdom.

The crucial computing support from all WLCG partners is acknowledged gratefully, in particular from CERN, the ATLAS Tier-1 facilities at TRIUMF (Canada), NDGF (Denmark, Norway, Sweden), CC-IN2P3 (France), KIT/GridKA (Germany), INFN-CNAF (Italy), NL-T1 (Netherlands), PIC (Spain), ASGC (Taiwan), RAL (U.K.) and BNL (U.S.A.), the Tier-2 facilities worldwide and large non-WLCG resource providers. Major contributors of computing resources are listed in ref. [138].

JHEP04(2021)174

References

[1] Y.A. Golfand and E.P. Likhtman, *Extension of the Algebra of Poincaré Group Generators and Violation of p Invariance*, *JETP Lett.* **13** (1971) 323 [INSPIRE].

[2] D.V. Volkov and V.P. Akulov, *Is the Neutrino a Goldstone Particle?*, *Phys. Lett. B* **46** (1973) 109 [INSPIRE].

[3] J. Wess and B. Zumino, *Supergauge Transformations in Four-Dimensions*, *Nucl. Phys. B* **70** (1974) 39 [INSPIRE].

[4] J. Wess and B. Zumino, *Supergauge Invariant Extension of Quantum Electrodynamics*, *Nucl. Phys. B* **78** (1974) 1 [INSPIRE].

[5] S. Ferrara and B. Zumino, *Supergauge invariant Yang-Mills theories*, *Nucl. Phys. B* **79** (1974) 413.

[6] A. Salam and J.A. Strathdee, *Supersymmetry and Nonabelian Gauges*, *Phys. Lett. B* **51** (1974) 353 [INSPIRE].

[7] G.R. Farrar and P. Fayet, *Phenomenology of the Production, Decay, and Detection of New Hadronic States Associated with Supersymmetry*, *Phys. Lett. B* **76** (1978) 575 [INSPIRE].

[8] G. D'Ambrosio, G.F. Giudice, G. Isidori and A. Strumia, *Minimal flavor violation: An Effective field theory approach*, *Nucl. Phys. B* **645** (2002) 155 [hep-ph/0207036] [INSPIRE].

[9] G. Isidori and D.M. Straub, *Minimal Flavour Violation and Beyond*, *Eur. Phys. J. C* **72** (2012) 2103 [arXiv:1202.0464] [INSPIRE].

[10] ATLAS collaboration, *Observation of a new particle in the search for the Standard Model Higgs boson with the ATLAS detector at the LHC*, *Phys. Lett. B* **716** (2012) 1 [arXiv:1207.7214] [INSPIRE].

[11] CMS collaboration, *Observation of a New Boson at a Mass of* 125 *GeV with the CMS Experiment at the LHC*, *Phys. Lett. B* **716** (2012) 30 [arXiv:1207.7235] [INSPIRE].

[12] S. Dimopoulos and H. Georgi, *Softly broken supersymmetry and* SU(5), *Nucl. Phys. B* **193** (1981) 150.

[13] E. Witten, *Dynamical Breaking of Supersymmetry*, *Nucl. Phys. B* **188** (1981) 513 [INSPIRE].

[14] M. Dine, W. Fischler and M. Srednicki, *Supersymmetric Technicolor*, *Nucl. Phys. B* **189** (1981) 575 [INSPIRE].

[15] S. Dimopoulos and S. Raby, *Supercolor*, *Nucl. Phys. B* **192** (1981) 353 [INSPIRE].

[16] N. Sakai, *Naturalness in Supersymmetric Guts*, *Z. Phys. C* **11** (1981) 153 [INSPIRE].

[17] R.K. Kaul and P. Majumdar, *Cancellation of Quadratically Divergent Mass Corrections in Globally Supersymmetric Spontaneously Broken Gauge Theories*, *Nucl. Phys. B* **199** (1982) 36 [INSPIRE].

[18] R. Barbieri and G.F. Giudice, *Upper Bounds on Supersymmetric Particle Masses*, *Nucl. Phys. B* **306** (1988) 63 [INSPIRE].

[19] B. de Carlos and J.A. Casas, *One loop analysis of the electroweak breaking in supersymmetric models and the fine tuning problem*, *Phys. Lett. B* **309** (1993) 320 [hep-ph/9303291] [INSPIRE].

[20] S. Weinberg, *Implications of Dynamical Symmetry Breaking*, *Phys. Rev. D* **13** (1976) 974 [INSPIRE].

[21] E. Gildener, *Gauge Symmetry Hierarchies*, *Phys. Rev. D* **14** (1976) 1667 [INSPIRE].

[22] S. Weinberg, *Implications of dynamical symmetry breaking: An addendum*, *Phys. Rev. D* **19** (1979) 1277. [INSPIRE].

[23] L. Susskind, *Dynamics of Spontaneous Symmetry Breaking in the Weinberg-Salam Theory*, *Phys. Rev. D* **20** (1979) 2619 [INSPIRE].

[24] P. Fayet, *Supersymmetry and Weak, Electromagnetic and Strong Interactions*, *Phys. Lett. B* **64** (1976) 159 [INSPIRE].

[25] P. Fayet, *Spontaneously Broken Supersymmetric Theories of Weak, Electromagnetic and Strong Interactions*, *Phys. Lett. B* **69** (1977) 489 [INSPIRE].

[26] P. Fayet, *Relations Between the Masses of the Superpartners of Leptons and Quarks, the Goldstino Couplings and the Neutral Currents*, *Phys. Lett. B* **84** (1979) 416 [INSPIRE].

[27] H. Goldberg, *Constraint on the Photino Mass from Cosmology*, *Phys. Rev. Lett.* **50** (1983) 1419 [*Erratum ibid.* **103** (2009) 099905] [INSPIRE].

[28] J.R. Ellis, J.S. Hagelin, D.V. Nanopoulos, K.A. Olive and M. Srednicki, *Supersymmetric Relics from the Big Bang*, *Nucl. Phys. B* **238** (1984) 453 [INSPIRE].

[29] ATLAS collaboration, *Search for top-squark pair production in final states with one lepton, jets, and missing transverse momentum using* $36\,fb^{-1}$ *of* $\sqrt{s} = 13$ *TeV pp collision data with the ATLAS detector*, *JHEP* **06** (2018) 108 [arXiv:1711.11520] [INSPIRE].

[30] ATLAS collaboration, *Search for a scalar partner of the top quark in the jets plus missing transverse momentum final state at* $\sqrt{s} = 13$ *TeV with the ATLAS detector*, *JHEP* **12** (2017) 085 [arXiv:1709.04183] [INSPIRE].

[31] ATLAS collaboration, *Search for direct top squark pair production in final states with two leptons in* $\sqrt{s} = 13$ *TeV pp collisions with the ATLAS detector*, *Eur. Phys. J. C* **77** (2017) 898 [arXiv:1708.03247] [INSPIRE].

[32] ATLAS collaboration, *ATLAS Run 1 searches for direct pair production of third-generation squarks at the Large Hadron Collider*, *Eur. Phys. J. C* **75** (2015) 510 [*Erratum ibid.* **76** (2016) 153] [arXiv:1506.08616] [INSPIRE].

JHEP04(2021)174

[33] CMS collaboration, *Searches for physics beyond the standard model with the M_{T2} variable in hadronic final states with and without disappearing tracks in proton-proton collisions at $\sqrt{s} = 13$ TeV*, *Eur. Phys. J. C* **80** (2020) 3 [arXiv:1909.03460] [INSPIRE].

[34] CMS collaboration, *Search for direct production of supersymmetric partners of the top quark in the all-jets final state in proton-proton collisions at $\sqrt{s} = 13$ TeV*, *JHEP* **10** (2017) 005 [arXiv:1707.03316] [INSPIRE].

[35] CMS collaboration, *Search for top squark pair production in pp collisions at $\sqrt{s} = 13$ TeV using single lepton events*, *JHEP* **10** (2017) 019 [arXiv:1706.04402] [INSPIRE].

[36] CMS collaboration, *Search for top squarks and dark matter particles in opposite-charge dilepton final states at $\sqrt{s} = 13$ TeV*, *Phys. Rev. D* **97** (2018) 032009 [arXiv:1711.00752] [INSPIRE].

[37] CMS collaboration, *Searches for pair production of third-generation squarks in $\sqrt{s} = 13$ TeV pp collisions*, *Eur. Phys. J. C* **77** (2017) 327 [arXiv:1612.03877] [INSPIRE].

[38] CMS collaboration, *A search for new phenomena in pp collisions at $\sqrt{s} = 13$ TeV in final states with missing transverse momentum and at least one jet using the α_T variable*, *Eur. Phys. J. C* **77** (2017) 294 [arXiv:1611.00338] [INSPIRE].

[39] CMS collaboration, *Inclusive search for supersymmetry using razor variables in pp collisions at $\sqrt{s} = 13$ TeV*, *Phys. Rev. D* **95** (2017) 012003 [arXiv:1609.07658] [INSPIRE].

[40] CMS collaboration, *Search for direct top squark pair production in events with one lepton, jets, and missing transverse momentum at 13 TeV with the CMS experiment*, *JHEP* **05** (2020) 032 [arXiv:1912.08887] [INSPIRE].

[41] ATLAS collaboration, *Search for dark matter produced in association with bottom or top quarks in $\sqrt{s} = 13$ TeV pp collisions with the ATLAS detector*, *Eur. Phys. J. C* **78** (2018) 18 [arXiv:1710.11412] [INSPIRE].

[42] CMS collaboration, *Search for dark matter produced in association with heavy-flavor quark pairs in proton-proton collisions at $\sqrt{s} = 13$ TeV*, *Eur. Phys. J. C* **77** (2017) 845 [arXiv:1706.02581] [INSPIRE].

[43] J. Alwall, M.-P. Le, M. Lisanti and J.G. Wacker, *Searching for Directly Decaying Gluinos at the Tevatron*, *Phys. Lett. B* **666** (2008) 34 [arXiv:0803.0019] [INSPIRE].

[44] J. Alwall, P. Schuster and N. Toro, *Simplified Models for a First Characterization of New Physics at the LHC*, *Phys. Rev. D* **79** (2009) 075020 [arXiv:0810.3921] [INSPIRE].

[45] LHC New Physics Working Group collaboration, *Simplified Models for LHC New Physics Searches*, *J. Phys. G* **39** (2012) 105005 [arXiv:1105.2838] [INSPIRE].

[46] D. Abercrombie et al., *Dark Matter Benchmark Models for Early LHC Run-2 Searches: Report of the ATLAS/CMS Dark Matter Forum*, *Phys. Dark Univ.* **27** (2020) 100371 [arXiv:1507.00966] [INSPIRE].

[47] ATLAS collaboration, *The ATLAS Experiment at the CERN Large Hadron Collider*, 2008 *JINST* **3** S08003 [INSPIRE].

[48] ATLAS collaboration, *Atlas Insertable B-Layer Technical Design Report*, ATLAS-TDR-19 (2010).

[49] ATLAS collaboration, *ATLAS Insertable B-Layer Technical Design Report Addendum*, ATLAS-TDR-19-ADD-1 (2012).

JHEP04(2021)174

[50] ATLAS IBL collaboration, *Production and Integration of the ATLAS Insertable B-Layer*, 2018 *JINST* **13** T05008 [arXiv:1803.00844] [INSPIRE].

[51] ATLAS collaboration, *Optimisation of the ATLAS b-tagging performance for the 2016 LHC Run*, ATL-PHYS-PUB-2016-012 (2016).

[52] ATLAS collaboration, *Performance of the ATLAS Trigger System in 2015*, *Eur. Phys. J. C* **77** (2017) 317 [arXiv:1611.09661] [INSPIRE].

[53] ATLAS collaboration, *Luminosity determination in pp collisions at $\sqrt{s} = 8$ TeV using the ATLAS detector at the LHC*, *Eur. Phys. J. C* **76** (2016) 653 [arXiv:1608.03953] [INSPIRE].

[54] G. Avoni et al., *The new LUCID-2 detector for luminosity measurement and monitoring in ATLAS*, 2018 *JINST* **13** P07017 [INSPIRE].

[55] S. Alioli, P. Nason, C. Oleari and E. Re, *A general framework for implementing NLO calculations in shower Monte Carlo programs: the POWHEG BOX*, *JHEP* **06** (2010) 043 [arXiv:1002.2581] [INSPIRE].

[56] NNPDF collaboration, *Parton distributions for the LHC Run II*, *JHEP* **04** (2015) 040 [arXiv:1410.8849] [INSPIRE].

[57] T. Sjöstrand, S. Mrenna and P.Z. Skands, *A Brief Introduction to PYTHIA 8.1*, *Comput. Phys. Commun.* **178** (2008) 852 [arXiv:0710.3820] [INSPIRE].

[58] *ATLAS PYTHIA 8 tunes to 7 TeV data*, ATL-PHYS-PUB-2014-021 (2014).

[59] M. Czakon, P. Fiedler and A. Mitov, *Total Top-Quark Pair-Production Cross Section at Hadron Colliders Through $O(\alpha_S^4)$*, *Phys. Rev. Lett.* **110** (2013) 252004 [arXiv:1303.6254] [INSPIRE].

[60] M. Czakon and A. Mitov, *NNLO corrections to top pair production at hadron colliders: the quark-gluon reaction*, *JHEP* **01** (2013) 080 [arXiv:1210.6832] [INSPIRE].

[61] M. Czakon and A. Mitov, *NNLO corrections to top-pair production at hadron colliders: the all-fermionic scattering channels*, *JHEP* **12** (2012) 054 [arXiv:1207.0236] [INSPIRE].

[62] P. Bärnreuther, M. Czakon and A. Mitov, *Percent Level Precision Physics at the Tevatron: First Genuine NNLO QCD Corrections to $q\bar{q} \to t\bar{t} + X$*, *Phys. Rev. Lett.* **109** (2012) 132001 [arXiv:1204.5201] [INSPIRE].

[63] M. Cacciari, M. Czakon, M. Mangano, A. Mitov and P. Nason, *Top-pair production at hadron colliders with next-to-next-to-leading logarithmic soft-gluon resummation*, *Phys. Lett. B* **710** (2012) 612 [arXiv:1111.5869] [INSPIRE].

[64] M. Czakon and A. Mitov, *Top++: A Program for the Calculation of the Top-Pair Cross-Section at Hadron Colliders*, *Comput. Phys. Commun.* **185** (2014) 2930 [arXiv:1112.5675] [INSPIRE].

[65] N. Kidonakis, *Next-to-next-to-leading-order collinear and soft gluon corrections for t-channel single top quark production*, *Phys. Rev. D* **83** (2011) 091503 [arXiv:1103.2792] [INSPIRE].

[66] N. Kidonakis, *Two-loop soft anomalous dimensions for single top quark associated production with a W^- or H^-*, *Phys. Rev. D* **82** (2010) 054018 [arXiv:1005.4451] [INSPIRE].

[67] N. Kidonakis, *NNLL resummation for s-channel single top quark production*, *Phys. Rev. D* **81** (2010) 054028 [arXiv:1001.5034] [INSPIRE].

[68] T. Gleisberg et al., *Event generation with SHERPA 1.1*, *JHEP* **02** (2009) 007 [arXiv:0811.4622] [INSPIRE].

[69] S. Catani, L. Cieri, G. Ferrera, D. de Florian and M. Grazzini, *Vector boson production at hadron colliders: a fully exclusive QCD calculation at NNLO*, *Phys. Rev. Lett.* **103** (2009) 082001 [arXiv:0903.2120] [INSPIRE].

[70] J. Alwall et al., *The automated computation of tree-level and next-to-leading order differential cross sections, and their matching to parton shower simulations*, *JHEP* **07** (2014) 079 [arXiv:1405.0301] [INSPIRE].

[71] R.D. Ball et al., *Parton distributions with LHC data*, *Nucl. Phys. B* **867** (2013) 244 [arXiv:1207.1303] [INSPIRE].

[72] M. Beneke, M. Czakon, P. Falgari, A. Mitov and C. Schwinn, *Threshold expansion of the $gg(q\bar{q}) \to \overline{QQ} + X$ cross section at $O(\alpha_s^4)$*, *Phys. Lett. B* **690** (2010) 483 [*Erratum ibid.* **778** (2018) 464] [arXiv:0911.5166] [INSPIRE].

[73] W. Beenakker, C. Borschensky, M. Krämer, A. Kulesza and E. Laenen, *NNLL-fast: predictions for coloured supersymmetric particle production at the LHC with threshold and Coulomb resummation*, *JHEP* **12** (2016) 133 [arXiv:1607.07741] [INSPIRE].

[74] O. Mattelaer and E. Vryonidou, *Dark matter production through loop-induced processes at the LHC: the s-channel mediator case*, *Eur. Phys. J. C* **75** (2015) 436 [arXiv:1508.00564] [INSPIRE].

[75] M. Backović, M. Krämer, F. Maltoni, A. Martini, K. Mawatari and M. Pellen, *Higher-order QCD predictions for dark matter production at the LHC in simplified models with s-channel mediators*, *Eur. Phys. J. C* **75** (2015) 482 [arXiv:1508.05327] [INSPIRE].

[76] E. Re, *Single-top Wt-channel production matched with parton showers using the POWHEG method*, *Eur. Phys. J. C* **71** (2011) 1547 [arXiv:1009.2450] [INSPIRE].

[77] S. Frixione, P. Nason and G. Ridolfi, *A Positive-weight next-to-leading-order Monte Carlo for heavy flavour hadroproduction*, *JHEP* **09** (2007) 126 [arXiv:0707.3088] [INSPIRE].

[78] R. Frederix, E. Re and P. Torrielli, *Single-top t-channel hadroproduction in the four-flavour scheme with POWHEG and aMC@NLO*, *JHEP* **09** (2012) 130 [arXiv:1207.5391] [INSPIRE].

[79] S. Alioli, P. Nason, C. Oleari and E. Re, *NLO single-top production matched with shower in POWHEG: s- and t-channel contributions*, *JHEP* **09** (2009) 111 [*Erratum ibid.* **02** (2010) 011] [arXiv:0907.4076] [INSPIRE].

[80] D.J. Lange, *The EvtGen particle decay simulation package*, *Nucl. Instrum. Meth. A* **462** (2001) 152 [INSPIRE].

[81] ATLAS collaboration, *The ATLAS Simulation Infrastructure*, *Eur. Phys. J. C* **70** (2010) 823 [arXiv:1005.4568] [INSPIRE].

[82] GEANT4 collaboration, *GEANT4: a simulation toolkit*, *Nucl. Instrum. Meth. A* **506** (2003) 250 [INSPIRE].

[83] ATLAS collaboration, *The PYTHIA 8 A3 tune description of ATLAS minimum bias and inelastic measurements incorporating the Donnachie-Landshoff diffractive model*, ATL-PHYS-PUB-2016-017 (2016).

[84] M. Bahr et al., *HERWIG++ Physics and Manual*, *Eur. Phys. J. C* **58** (2008) 639 [arXiv:0803.0883] [INSPIRE].

[85] J. Bellm et al., *HERWIG 7.0/HERWIG++ 3.0 release note*, *Eur. Phys. J. C* **76** (2016) 196 [arXiv:1512.01178] [INSPIRE].

[86] ATLAS collaboration, *Studies on top-quark Monte Carlo modelling with Sherpa and MG5_aMC@NLO*, ATL-PHYS-PUB-2017-007 (2017).

[87] S. Frixione, E. Laenen, P. Motylinski, B.R. Webber and C.D. White, *Single-top hadroproduction in association with a W boson*, *JHEP* **07** (2008) 029 [arXiv:0805.3067] [INSPIRE].

[88] ATLAS collaboration, *Probing the quantum interference between singly and doubly resonant top-quark production in pp collisions at* $\sqrt{s} = 13$ *TeV with the ATLAS detector*, *Phys. Rev. Lett.* **121** (2018) 152002 [arXiv:1806.04667] [INSPIRE].

[89] ATLAS collaboration, *ATLAS simulation of boson plus jets processes in Run 2*, ATL-PHYS-PUB-2017-006 (2017).

[90] ATLAS collaboration, *Multi-Boson Simulation for* 13 *TeV ATLAS Analyses*, ATL-PHYS-PUB-2017-005 (2017).

[91] T. Gleisberg and S. Höche, *Comix, a new matrix element generator*, *JHEP* **12** (2008) 039 [arXiv:0808.3674] [INSPIRE].

[92] F. Cascioli, P. Maierhofer and S. Pozzorini, *Scattering Amplitudes with Open Loops*, *Phys. Rev. Lett.* **108** (2012) 111601 [arXiv:1111.5206] [INSPIRE].

[93] S. Schumann and F. Krauss, *A Parton shower algorithm based on Catani-Seymour dipole factorisation*, *JHEP* **03** (2008) 038 [arXiv:0709.1027] [INSPIRE].

[94] S. Höche, F. Krauss, M. Schönherr and F. Siegert, *QCD matrix elements + parton showers: The NLO case*, *JHEP* **04** (2013) 027 [arXiv:1207.5030] [INSPIRE].

[95] *Modelling of the* $t\bar{t}H$ *and* $t\bar{t}V$ $(V = W, Z)$ *processes for* $\sqrt{s} = 13$ *TeV ATLAS analyses*, ATL-PHYS-PUB-2016-005 (2016).

[96] I. Low, *Polarized charginos (and top quarks) in scalar top quark decays*, *Phys. Rev. D* **88** (2013) 095018 [arXiv:1304.0491] [INSPIRE].

[97] M. Perelstein and A. Weiler, *Polarized Tops from Stop Decays at the LHC*, *JHEP* **03** (2009) 141 [arXiv:0811.1024] [INSPIRE].

[98] P. Artoisenet, R. Frederix, O. Mattelaer and R. Rietkerk, *Automatic spin-entangled decays of heavy resonances in Monte Carlo simulations*, *JHEP* **03** (2013) 015 [arXiv:1212.3460] [INSPIRE].

[99] W. Beenakker, M. Krämer, T. Plehn, M. Spira and P.M. Zerwas, *Stop production at hadron colliders*, *Nucl. Phys. B* **515** (1998) 3 [hep-ph/9710451] [INSPIRE].

[100] W. Beenakker, S. Brensing, M. Krämer, A. Kulesza, E. Laenen and I. Niessen, *Supersymmetric top and bottom squark production at hadron colliders*, *JHEP* **08** (2010) 098 [arXiv:1006.4771] [INSPIRE].

[101] W. Beenakker, C. Borschensky, R. Heger, M. Krämer, A. Kulesza and E. Laenen, *NNLL resummation for stop pair-production at the LHC*, *JHEP* **05** (2016) 153 [arXiv:1601.02954] [INSPIRE].

[102] J. Butterworth et al., *PDF4LHC recommendations for LHC Run II*, *J. Phys. G* **43** (2016) 023001 [arXiv:1510.03865] [INSPIRE].

[103] ATLAS collaboration, *Electron reconstruction and identification in the ATLAS experiment using the 2015 and 2016 LHC proton-proton collision data at* $\sqrt{s} = 13$ *TeV*, *Eur. Phys. J. C* **79** (2019) 639 [arXiv:1902.04655] [INSPIRE].

JHEP04(2021)174

[104] ATLAS collaboration, *Muon reconstruction performance of the ATLAS detector in proton-proton collision data at $\sqrt{s} = 13$ TeV*, *Eur. Phys. J. C* **76** (2016) 292 [arXiv:1603.05598] [INSPIRE].

[105] ATLAS collaboration, *Topological cell clustering in the ATLAS calorimeters and its performance in LHC Run 1*, *Eur. Phys. J. C* **77** (2017) 490 [arXiv:1603.02934] [INSPIRE].

[106] ATLAS collaboration, *Jet energy measurement with the ATLAS detector in proton-proton collisions at $\sqrt{s} = 7$ TeV*, *Eur. Phys. J. C* **73** (2013) 2304 [arXiv:1112.6426] [INSPIRE].

[107] M. Cacciari, G.P. Salam and G. Soyez, *The anti-k_t jet clustering algorithm*, *JHEP* **04** (2008) 063 [arXiv:0802.1189] [INSPIRE].

[108] M. Cacciari, G.P. Salam and G. Soyez, *FastJet User Manual*, *Eur. Phys. J. C* **72** (2012) 1896 [arXiv:1111.6097] [INSPIRE].

[109] M. Cacciari and G.P. Salam, *Pileup subtraction using jet areas*, *Phys. Lett. B* **659** (2008) 119 [arXiv:0707.1378] [INSPIRE].

[110] M. Cacciari, G.P. Salam and G. Soyez, *The Catchment Area of Jets*, *JHEP* **04** (2008) 005 [arXiv:0802.1188] [INSPIRE].

[111] ATLAS collaboration, *Performance of pile-up mitigation techniques for jets in pp collisions at $\sqrt{s} = 8$ TeV using the ATLAS detector*, *Eur. Phys. J. C* **76** (2016) 581 [arXiv:1510.03823] [INSPIRE].

[112] ATLAS collaboration, *Jet energy measurement and its systematic uncertainty in proton-proton collisions at $\sqrt{s} = 7$ TeV with the ATLAS detector*, *Eur. Phys. J. C* **75** (2015) 17 [arXiv:1406.0076] [INSPIRE].

[113] ATLAS collaboration, *Jet energy scale measurements and their systematic uncertainties in proton-proton collisions at $\sqrt{s} = 13$ TeV with the ATLAS detector*, *Phys. Rev. D* **96** (2017) 072002 [arXiv:1703.09665] [INSPIRE].

[114] ATLAS collaboration, *Characterisation and mitigation of beam-induced backgrounds observed in the ATLAS detector during the 2011 proton-proton run*, 2013 *JINST* **8** P07004 [arXiv:1303.0223] [INSPIRE].

[115] *Selection of jets produced in 13TeV proton-proton collisions with the ATLAS detector*, ATLAS-CONF-2015-029 (2015).

[116] ATLAS collaboration, *Performance of b-Jet Identification in the ATLAS Experiment*, 2016 *JINST* **11** P04008 [arXiv:1512.01094] [INSPIRE].

[117] ATLAS collaboration, *ATLAS b-jet identification performance and efficiency measurement with $t\bar{t}$ events in pp collisions at $\sqrt{s} = 13$ TeV*, *Eur. Phys. J. C* **79** (2019) 970 [arXiv:1907.05120] [INSPIRE].

[118] ATLAS collaboration, *Soft b-hadron tagging for compressed SUSY scenarios*, ATLAS-CONF-2019-027 (2019).

[119] ATLAS collaboration, *Measurement of the tau lepton reconstruction and identification performance in the ATLAS experiment using pp collisions at $\sqrt{s} = 13$ TeV*, ATLAS-CONF-2017-029 (2017).

[120] ATLAS collaboration, *Reconstruction of hadronic decay products of tau leptons with the ATLAS experiment*, *Eur. Phys. J. C* **76** (2016) 295 [arXiv:1512.05955] [INSPIRE].

JHEP04(2021)174

[121] ATLAS collaboration, *Modelling $Z \to \tau\tau$ processes in ATLAS with τ-embedded $Z \to \mu\mu$ data*, 2015 *JINST* **10** P09018 [arXiv:1506.05623] [INSPIRE].

[122] ATLAS collaboration, *Identification and energy calibration of hadronically decaying tau leptons with the ATLAS experiment in pp collisions at $\sqrt{s} = 8$ TeV*, *Eur. Phys. J. C* **75** (2015) 303 [arXiv:1412.7086] [INSPIRE].

[123] ATLAS collaboration, *Performance of missing transverse momentum reconstruction with the ATLAS detector using proton-proton collisions at $\sqrt{s} = 13$ TeV*, *Eur. Phys. J. C* **78** (2018) 903 [arXiv:1802.08168] [INSPIRE].

[124] ATLAS collaboration, *E_T^{miss} performance in the ATLAS detector using 2015-2016 LHC p-p collisions*, ATLAS-CONF-2018-023 (2018).

[125] C.G. Lester and D.J. Summers, *Measuring masses of semiinvisibly decaying particles pair produced at hadron colliders*, *Phys. Lett. B* **463** (1999) 99 [hep-ph/9906349] [INSPIRE].

[126] ATLAS collaboration, *Search for top squark pair production in final states with one isolated lepton, jets, and missing transverse momentum in $\sqrt{s} = 8$ TeV pp collisions with the ATLAS detector*, *JHEP* **11** (2014) 118 [arXiv:1407.0583] [INSPIRE].

[127] M.L. Graesser and J. Shelton, *Hunting Mixed Top Squark Decays*, *Phys. Rev. Lett.* **111** (2013) 121802 [arXiv:1212.4495] [INSPIRE].

[128] H. An and L.-T. Wang, *Opening up the compressed region of top squark searches at 13 TeV LHC*, *Phys. Rev. Lett.* **115** (2015) 181602 [arXiv:1506.00653] [INSPIRE].

[129] S. Macaluso, M. Park, D. Shih and B. Tweedie, *Revealing Compressed Stops Using High-Momentum Recoils*, *JHEP* **03** (2016) 151 [arXiv:1506.07885] [INSPIRE].

[130] R.D. Cousins, J.T. Linnemann and J. Tucker, *Evaluation of three methods for calculating statistical significance when incorporating a systematic uncertainty into a test of the background-only hypothesis for a Poisson process*, *Nucl. Instrum. Meth. A* **595** (2008) 480 [physics/0702156] [INSPIRE].

[131] T.P. Li and Y.Q. Ma, *Analysis methods for results in gamma-ray astronomy*, *Astrophys. J.* **272** (1983) 317 [INSPIRE].

[132] I. Goodfellow, Y. Bengio and A. Courville, *Deep Learning*, MIT Press (2016) [ISBN: 9780262035613].

[133] S. Hochreiter and J. Schmidhuber, *Long short-term memory*, *Neural Comput.* **9** (1997) 1735.

[134] C. Borschensky et al., *Squark and gluino production cross sections in pp collisions at $\sqrt{s} = 13, 14, 33$ and 100 TeV*, *Eur. Phys. J. C* **74** (2014) 3174 [arXiv:1407.5066] [INSPIRE].

[135] G. Cowan, K. Cranmer, E. Gross and O. Vitells, *Asymptotic formulae for likelihood-based tests of new physics*, *Eur. Phys. J. C* **71** (2011) 1554 [*Erratum ibid.* **73** (2013) 2501] [arXiv:1007.1727] [INSPIRE].

[136] A.L. Read, *Presentation of search results: The CL_s technique*, *J. Phys. G* **28** (2002) 2693 [INSPIRE].

[137] ATLAS collaboration, *Search for dark matter and other new phenomena in events with an energetic jet and large missing transverse momentum using the ATLAS detector*, *JHEP* **01** (2018) 126 [arXiv:1711.03301] [INSPIRE].

[138] ATLAS collaboration, *ATLAS Computing Acknowledgements*, ATL-SOFT-PUB-2020-001 (2020).

JHEP04(2021)174

The ATLAS collaboration

G. Aad[102], B. Abbott[128], D.C. Abbott[103], A. Abed Abud[36], K. Abeling[53], D.K. Abhayasinghe[94], S.H. Abidi[167], O.S. AbouZeid[40], N.L. Abraham[156], H. Abramowicz[161], H. Abreu[160], Y. Abulaiti[6], B.S. Acharya[67a,67b,n], B. Achkar[53], L. Adam[100], C. Adam Bourdarios[5], L. Adamczyk[84a], L. Adamek[167], J. Adelman[121], M. Adersberger[114], A. Adiguzel[12c,ae], S. Adorni[54], T. Adye[143], A.A. Affolder[145], Y. Afik[160], C. Agapopoulou[65], M.N. Agaras[38], A. Aggarwal[119], C. Agheorghiesei[27c], J.A. Aguilar-Saavedra[139f,139a,ad], A. Ahmad[36], F. Ahmadov[80], W.S. Ahmed[104], X. Ai[18], G. Aielli[74a,74b], S. Akatsuka[86], T.P.A. Åkesson[97], E. Akilli[54], A.V. Akimov[111], K. Al Khoury[65], G.L. Alberghi[23b,23a], J. Albert[176], M.J. Alconada Verzini[161], S. Alderweireldt[36], M. Aleksa[36], I.N. Aleksandrov[80], C. Alexa[27b], T. Alexopoulos[10], A. Alfonsi[120], F. Alfonsi[23b,23a], M. Alhroob[128], B. Ali[141], S. Ali[158], M. Aliev[166], G. Alimonti[69a], C. Allaire[36], B.M.M. Allbrooke[156], B.W. Allen[131], P.P. Allport[21], A. Aloisio[70a,70b], F. Alonso[89], C. Alpigiani[148], E. Alunno Camelia[74a,74b], M. Alvarez Estevez[99], M.G. Alviggi[70a,70b], Y. Amaral Coutinho[81b], A. Ambler[104], L. Ambroz[134], C. Amelung[26], D. Amidei[106], S.P. Amor Dos Santos[139a], S. Amoroso[46], C.S. Amrouche[54], F. An[79], C. Anastopoulos[149], N. Andari[144], T. Andeen[11], J.K. Anders[20], S.Y. Andrean[45a,45b], A. Andreazza[69a,69b], V. Andrei[61a], C.R. Anelli[176], S. Angelidakis[9], A. Angerami[39], A.V. Anisenkov[122b,122a], A. Annovi[72a], C. Antel[54], M.T. Anthony[149], E. Antipov[129], M. Antonelli[51], D.J.A. Antrim[171], F. Anulli[73a], M. Aoki[82], J.A. Aparisi Pozo[174], M.A. Aparo[156], L. Aperio Bella[46], N. Aranzabal[36], V. Araujo Ferraz[81a], R. Araujo Pereira[81b], C. Arcangeletti[51], A.T.H. Arce[49], F.A. Arduh[89], J-F. Arguin[110], S. Argyropoulos[52], J.-H. Arling[46], A.J. Armbruster[36], A. Armstrong[171], O. Arnaez[167], H. Arnold[120], Z.P. Arrubarrena Tame[114], G. Artoni[134], K. Asai[126], S. Asai[163], T. Asawatavonvanich[165], N. Asbah[59], E.M. Asimakopoulou[172], L. Asquith[156], J. Assahsah[35e], K. Assamagan[29], R. Astalos[28a], R.J. Atkin[33a], M. Atkinson[173], N.B. Atlay[19], H. Atmani[65], K. Augsten[141], V.A. Austrup[182], G. Avolio[36], M.K. Ayoub[15a], G. Azuelos[110,am], H. Bachacou[144], K. Bachas[162], M. Backes[134], F. Backman[45a,45b], P. Bagnaia[73a,73b], M. Bahmani[85], H. Bahrasemani[152], A.J. Bailey[174], V.R. Bailey[173], J.T. Baines[143], C. Bakalis[10], O.K. Baker[183], P.J. Bakker[120], E. Bakos[16], D. Bakshi Gupta[8], S. Balaji[157], E.M. Baldin[122b,122a], P. Balek[180], F. Balli[144], W.K. Balunas[134], J. Balz[100], E. Banas[85], M. Bandieramonte[138], A. Bandyopadhyay[24], Sw. Banerjee[181,i], L. Barak[161], W.M. Barbe[38], E.L. Barberio[105], D. Barberis[55b,55a], M. Barbero[102], G. Barbour[95], T. Barillari[115], M-S. Barisits[36], J. Barkeloo[131], T. Barklow[153], R. Barnea[160], B.M. Barnett[143], R.M. Barnett[18], Z. Barnovska-Blenessy[60a], A. Baroncelli[60a], G. Barone[29], A.J. Barr[134], L. Barranco Navarro[45a,45b], F. Barreiro[99], J. Barreiro Guimarães da Costa[15a], U. Barron[161], S. Barsov[137], F. Bartels[61a], R. Bartoldus[153], G. Bartolini[102], A.E. Barton[90], P. Bartos[28a], A. Basalaev[46], A. Basan[100], A. Bassalat[65,aj], M.J. Basso[167], R.L. Bates[57], S. Batlamous[35f], J.R. Batley[32], B. Batool[151], M. Battaglia[145], M. Bauce[73a,73b], F. Bauer[144,*], K.T. Bauer[171], H.S. Bawa[31], J.B. Beacham[49], T. Beau[135], P.H. Beauchemin[170], F. Becherer[52], P. Bechtle[24], H.C. Beck[53], H.P. Beck[20,p], K. Becker[178], C. Becot[46], A. Beddall[12d], A.J. Beddall[12a], V.A. Bednyakov[80], M. Bedognetti[120], C.P. Bee[155], T.A. Beermann[182], M. Begalli[81b], M. Begel[29], A. Behera[155], J.K. Behr[46], F. Beisiegel[24], M. Belfkir[5], A.S. Bell[95], G. Bella[161], L. Bellagamba[23b], A. Bellerive[34], P. Bellos[9], K. Beloborodov[122b,122a], K. Belotskiy[112], N.L. Belyaev[112], D. Benchekroun[35a], N. Benekos[10], Y. Benhammou[161], D.P. Benjamin[6], M. Benoit[54], J.R. Bensinger[26], S. Bentvelsen[120], L. Beresford[134], M. Beretta[51], D. Berge[19], E. Bergeaas Kuutmann[172], N. Berger[5], B. Bergmann[141], L.J. Bergsten[26], J. Beringer[18], S. Berlendis[7], G. Bernardi[135], C. Bernius[153], F.U. Bernlochner[24], T. Berry[94], P. Berta[100], C. Bertella[15a], A. Berthold[48], I.A. Bertram[90], O. Bessidskaia Bylund[182], N. Besson[144], A. Bethani[101], S. Bethke[115], A. Betti[42], A.J. Bevan[93], J. Beyer[115],

JHEP04(2021)174

D.S. Bhattacharya[177], P. Bhattarai[26], V.S. Bhopatkar[6], R. Bi[138], R.M. Bianchi[138], O. Biebel[114], D. Biedermann[19], R. Bielski[36], K. Bierwagen[100], N.V. Biesuz[72a,72b], M. Biglietti[75a], T.R.V. Billoud[110], M. Bindi[53], A. Bingul[12d], C. Bini[73a,73b], S. Biondi[23b,23a], C.J. Birch-sykes[101], M. Birman[180], T. Bisanz[36], J.P. Biswal[3], D. Biswas[181,i], A. Bitadze[101], C. Bittrich[48], K. Bjørke[133], T. Blazek[28a], I. Bloch[46], C. Blocker[26], A. Blue[57], U. Blumenschein[93], G.J. Bobbink[120], V.S. Bobrovnikov[122b,122a], S.S. Bocchetta[97], D. Bogavac[14], A.G. Bogdanchikov[122b,122a], C. Bohm[45a], V. Boisvert[94], P. Bokan[53], T. Bold[84a], A.E. Bolz[61b], M. Bomben[135], M. Bona[93], J.S. Bonilla[131], M. Boonekamp[144], C.D. Booth[94], H.M. Borecka-Bielska[91], L.S. Borgna[95], A. Borisov[123], G. Borissov[90], J. Bortfeldt[36], D. Bortoletto[134], D. Boscherini[23b], M. Bosman[14], J.D. Bossio Sola[104], K. Bouaouda[35a], J. Boudreau[138], E.V. Bouhova-Thacker[90], D. Boumediene[38], S.K. Boutle[57], A. Boveia[127], J. Boyd[36], D. Boye[33c], I.R. Boyko[80], A.J. Bozson[94], J. Bracinik[21], N. Brahimi[60d,60c], G. Brandt[182], O. Brandt[32], F. Braren[46], B. Brau[103], J.E. Brau[131], W.D. Breaden Madden[57], K. Brendlinger[46], L. Brenner[46], R. Brenner[172], S. Bressler[180], B. Brickwedde[100], D.L. Briglin[21], D. Britton[57], D. Britzger[115], I. Brock[24], R. Brock[107], G. Brooijmans[39], W.K. Brooks[146d], E. Brost[29], P.A. Bruckman de Renstrom[85], B. Brüers[46], D. Bruncko[28b], A. Bruni[23b], G. Bruni[23b], L.S. Bruni[120], S. Bruno[74a,74b], M. Bruschi[23b], N. Bruscino[73a,73b], L. Bryngemark[153], T. Buanes[17], Q. Buat[36], P. Buchholz[151], A.G. Buckley[57], I.A. Budagov[80], M.K. Bugge[133], F. Bührer[52], O. Bulekov[112], B.A. Bullard[59], T.J. Burch[121], S. Burdin[91], C.D. Burgard[120], A.M. Burger[129], B. Burghgrave[8], J.T.P. Burr[46], C.D. Burton[11], J.C. Burzynski[103], V. Büscher[100], E. Buschmann[53], P.J. Bussey[57], J.M. Butler[25], C.M. Buttar[57], J.M. Butterworth[95], P. Butti[36], W. Buttinger[36], C.J. Buxo Vazquez[107], A. Buzatu[158], A.R. Buzykaev[122b,122a], G. Cabras[23b,23a], S. Cabrera Urbán[174], D. Caforio[56], H. Cai[138], V.M.M. Cairo[153], O. Cakir[4a], N. Calace[36], P. Calafiura[18], G. Calderini[135], P. Calfayan[66], G. Callea[57], L.P. Caloba[81b], A. Caltabiano[74a,74b], S. Calvente Lopez[99], D. Calvet[38], S. Calvet[38], T.P. Calvet[102], M. Calvetti[72a,72b], R. Camacho Toro[135], S. Camarda[36], D. Camarero Munoz[99], P. Camarri[74a,74b], M.T. Camerlingo[75a,75b], D. Cameron[133], C. Camincher[36], S. Campana[36], M. Campanelli[95], A. Camplani[40], V. Canale[70a,70b], A. Canesse[104], M. Cano Bret[78], J. Cantero[129], T. Cao[161], Y. Cao[173], M.D.M. Capeans Garrido[36], M. Capua[41b,41a], R. Cardarelli[74a], F. Cardillo[149], G. Carducci[41b,41a], I. Carli[142], T. Carli[36], G. Carlino[70a], B.T. Carlson[138], E.M. Carlson[176,168a], L. Carminati[69a,69b], R.M.D. Carney[153], S. Caron[119], E. Carquin[146d], S. Carrá[46], G. Carratta[23b,23a], J.W.S. Carter[167], T.M. Carter[50], M.P. Casado[14,f], A.F. Casha[167], F.L. Castillo[174], L. Castillo Garcia[14], V. Castillo Gimenez[174], N.F. Castro[139a,139e], A. Catinaccio[36], J.R. Catmore[133], A. Cattai[36], V. Cavaliere[29], E. Cavallaro[14], V. Cavasinni[72a,72b], E. Celebi[12b], F. Celli[134], K. Cerny[130], A.S. Cerqueira[81a], A. Cerri[156], L. Cerrito[74a,74b], F. Cerutti[18], A. Cervelli[23b,23a], S.A. Cetin[12b], Z. Chadi[35a], D. Chakraborty[121], J. Chan[181], W.S. Chan[120], W.Y. Chan[91], J.D. Chapman[32], B. Chargeishvili[159b], D.G. Charlton[21], T.P. Charman[93], C.C. Chau[34], S. Che[127], S. Chekanov[6], S.V. Chekulaev[168a], G.A. Chelkov[80,ah], B. Chen[79], C. Chen[60a], C.H. Chen[79], H. Chen[29], J. Chen[60a], J. Chen[39], J. Chen[26], S. Chen[136], S.J. Chen[15c], X. Chen[15b], Y. Chen[60a], Y-H. Chen[46], H.C. Cheng[63a], H.J. Cheng[15a], A. Cheplakov[80], E. Cheremushkina[123], R. Cherkaoui El Moursli[35f], E. Cheu[7], K. Cheung[64], T.J.A. Chevalérias[144], L. Chevalier[144], V. Chiarella[51], G. Chiarelli[72a], G. Chiodini[68a], A.S. Chisholm[21], A. Chitan[27b], I. Chiu[163], Y.H. Chiu[176], M.V. Chizhov[80], K. Choi[11], A.R. Chomont[73a,73b], S. Chouridou[162], Y.S. Chow[120], L.D. Christopher[33e], M.C. Chu[63a], X. Chu[15a,15d], J. Chudoba[140], J.J. Chwastowski[85], L. Chytka[130], D. Cieri[115], K.M. Ciesla[85], D. Cinca[47], V. Cindro[92], I.A. Cioară[27b], A. Ciocio[18], F. Cirotto[70a,70b], Z.H. Citron[180,j], M. Citterio[69a], D.A. Ciubotaru[27b], B.M. Ciungu[167], A. Clark[54], M.R. Clark[39], P.J. Clark[50], S.E. Clawson[101], C. Clement[45a,45b], Y. Coadou[102], M. Cobal[67a,67c], A. Coccaro[55b], J. Cochran[79], R. Coelho Lopes De Sa[103], H. Cohen[161], A.E.C. Coimbra[36], B. Cole[39], A.P. Colijn[120], J. Collot[58],

JHEP04(2021)174

P. Conde Muiño[139a,139h], S.H. Connell[33c], I.A. Connelly[57], S. Constantinescu[27b], F. Conventi[70a,an], A.M. Cooper-Sarkar[134], F. Cormier[175], K.J.R. Cormier[167], L.D. Corpe[95], M. Corradi[73a,73b], E.E. Corrigan[97], F. Corriveau[104,ab], M.J. Costa[174], F. Costanza[5], D. Costanzo[149], G. Cowan[94], J.W. Cowley[32], J. Crane[101], K. Cranmer[125], R.A. Creager[136], S. Crépé-Renaudin[58], F. Crescioli[135], M. Cristinziani[24], V. Croft[170], G. Crosetti[41b,41a], A. Cueto[5], T. Cuhadar Donszelmann[171], H. Cui[15a,15d], A.R. Cukierman[153], W.R. Cunningham[57], S. Czekierda[85], P. Czodrowski[36], M.M. Czurylo[61b], M.J. Da Cunha Sargedas De Sousa[60b], J.V. Da Fonseca Pinto[81b], C. Da Via[101], W. Dabrowski[84a], F. Dachs[36], T. Dado[28a], S. Dahbi[33e], T. Dai[106], C. Dallapiccola[103], M. Dam[40], G. D'amen[29], V. D'Amico[75a,75b], J. Damp[100], J.R. Dandoy[136], M.F. Daneri[30], M. Danninger[152], V. Dao[36], G. Darbo[55b], O. Dartsi[5], A. Dattagupta[131], T. Daubney[46], S. D'Auria[69a,69b], C. David[168b], T. Davidek[142], D.R. Davis[49], I. Dawson[149], K. De[8], R. De Asmundis[70a], M. De Beurs[120], S. De Castro[23b,23a], N. De Groot[119], P. de Jong[120], H. De la Torre[107], A. De Maria[15c], D. De Pedis[73a], A. De Salvo[73a], U. De Sanctis[74a,74b], M. De Santis[74a,74b], A. De Santo[156], J.B. De Vivie De Regie[65], C. Debenedetti[145], D.V. Dedovich[80], A.M. Deiana[42], J. Del Peso[99], Y. Delabat Diaz[46], D. Delgove[65], F. Deliot[144], C.M. Delitzsch[7], M. Della Pietra[70a,70b], D. Della Volpe[54], A. Dell'Acqua[36], L. Dell'Asta[74a,74b], M. Delmastro[5], C. Delporte[65], P.A. Delsart[58], D.A. DeMarco[167], S. Demers[183], M. Demichev[80], G. Demontigny[110], S.P. Denisov[123], L. D'Eramo[121], D. Derendarz[85], J.E. Derkaoui[35e], F. Derue[135], P. Dervan[91], K. Desch[24], K. Dette[167], C. Deutsch[24], M.R. Devesa[30], P.O. Deviveiros[36], F.A. Di Bello[73a,73b], A. Di Ciaccio[74a,74b], L. Di Ciaccio[5], W.K. Di Clemente[136], C. Di Donato[70a,70b], A. Di Girolamo[36], G. Di Gregorio[72a,72b], B. Di Micco[75a,75b], R. Di Nardo[75a,75b], K.F. Di Petrillo[59], R. Di Sipio[167], C. Diaconu[102], F.A. Dias[40], T. Dias Do Vale[139a], M.A. Diaz[146a], F.G. Diaz Capriles[24], J. Dickinson[18], E.B. Diehl[106], J. Dietrich[19], S. Díez Cornell[46], A. Dimitrievska[18], W. Ding[15b], J. Dingfelder[24], S.J. Dittmeier[61b], F. Dittus[36], F. Djama[102], T. Djobava[159b], J.I. Djuvsland[17], M.A.B. Do Vale[147], M. Dobre[27b], D. Dodsworth[26], C. Doglioni[97], J. Dolejsi[142], Z. Dolezal[142], M. Donadelli[81c], B. Dong[60c], J. Donini[38], A. D'onofrio[15c], M. D'Onofrio[91], J. Dopke[143], A. Doria[70a], M.T. Dova[89], A.T. Doyle[57], E. Drechsler[152], E. Dreyer[152], T. Dreyer[53], A.S. Drobac[170], D. Du[60b], T.A. du Pree[120], Y. Duan[60d], F. Dubinin[111], M. Dubovsky[28a], A. Dubreuil[54], E. Duchovni[180], G. Duckeck[114], O.A. Ducu[27b], D. Duda[115], A. Dudarev[36], A.C. Dudder[100], E.M. Duffield[18], M. D'uffizi[101], L. Duflot[65], M. Dührssen[36], C. Dülsen[182], M. Dumancic[180], A.E. Dumitriu[27b], A.K. Duncan[57], M. Dunford[61a], A. Duperrin[102], H. Duran Yildiz[4a], M. Düren[56], A. Durglishvili[159b], D. Duschinger[48], B. Dutta[46], D. Duvnjak[1], G.I. Dyckes[136], M. Dyndal[36], S. Dysch[101], B.S. Dziedzic[85], M.G. Eggleston[49], T. Eifert[8], G. Eigen[17], K. Einsweiler[18], T. Ekelof[172], H. El Jarrari[35f], V. Ellajosyula[172], M. Ellert[172], F. Ellinghaus[182], A.A. Elliot[93], N. Ellis[36], J. Elmsheuser[29], M. Elsing[36], D. Emeliyanov[143], A. Emerman[39], Y. Enari[163], M.B. Epland[49], J. Erdmann[47], A. Ereditato[20], P.A. Erland[85], M. Errenst[36], M. Escalier[65], C. Escobar[174], O. Estrada Pastor[174], E. Etzion[161], H. Evans[66], M.O. Evans[156], A. Ezhilov[137], F. Fabbri[57], L. Fabbri[23b,23a], V. Fabiani[119], G. Facini[178], R.M. Faisca Rodrigues Pereira[139a], R.M. Fakhrutdinov[123], S. Falciano[73a], P.J. Falke[24], S. Falke[36], J. Faltova[142], Y. Fang[15a], Y. Fang[15a], G. Fanourakis[44], M. Fanti[69a,69b], M. Faraj[67a,67c,q], A. Farbin[8], A. Farilla[75a], E.M. Farina[71a,71b], T. Farooque[107], S.M. Farrington[50], P. Farthouat[36], F. Fassi[35f], P. Fassnacht[36], D. Fassouliotis[9], M. Faucci Giannelli[50], W.J. Fawcett[32], L. Fayard[65], O.L. Fedin[137,o], W. Fedorko[175], A. Fehr[20], M. Feickert[173], L. Feligioni[102], A. Fell[149], C. Feng[60b], M. Feng[49], M.J. Fenton[171], A.B. Fenyuk[123], S.W. Ferguson[43], J. Ferrando[46], A. Ferrante[173], A. Ferrari[172], P. Ferrari[120], R. Ferrari[71a], D.E. Ferreira de Lima[61b], A. Ferrer[174], D. Ferrere[54], C. Ferretti[106], F. Fiedler[100], A. Filipčič[92], F. Filthaut[119], K.D. Finelli[25], M.C.N. Fiolhais[139a,139c,a], L. Fiorini[174], F. Fischer[114], J. Fischer[100], W.C. Fisher[107], T. Fitschen[21], I. Fleck[151], P. Fleischmann[106], T. Flick[182], B.M. Flierl[114], L. Flores[136],

JHEP04(2021)174

L.R. Flores Castillo[63a], F.M. Follega[76a,76b], N. Fomin[17], J.H. Foo[167], G.T. Forcolin[76a,76b], B.C. Forland[66], A. Formica[144], F.A. Förster[14], A.C. Forti[101], E. Fortin[102], M.G. Foti[134], D. Fournier[65], H. Fox[90], P. Francavilla[72a,72b], S. Francescato[73a,73b], M. Franchini[23b,23a], S. Franchino[61a], D. Francis[36], L. Franco[5], L. Franconi[20], M. Franklin[59], G. Frattari[73a,73b], A.N. Fray[93], P.M. Freeman[21], B. Freund[110], W.S. Freund[81b], E.M. Freundlich[47], D.C. Frizzell[128], D. Froidevaux[36], J.A. Frost[134], M. Fujimoto[126], C. Fukunaga[164], E. Fullana Torregrosa[174], T. Fusayasu[116], J. Fuster[174], A. Gabrielli[23b,23a], A. Gabrielli[36], S. Gadatsch[54], P. Gadow[115], G. Gagliardi[55b,55a], L.G. Gagnon[110], G.E. Gallardo[134], E.J. Gallas[134], B.J. Gallop[143], G. Galster[40], R. Gamboa Goni[93], K.K. Gan[127], S. Ganguly[180], J. Gao[60a], Y. Gao[50], Y.S. Gao[31,l], F.M. Garay Walls[146a], C. García[174], J.E. García Navarro[174], J.A. García Pascual[15a], C. Garcia-Argos[52], M. Garcia-Sciveres[18], R.W. Gardner[37], N. Garelli[153], S. Gargiulo[52], C.A. Garner[167], V. Garonne[133], S.J. Gasiorowski[148], P. Gaspar[81b], A. Gaudiello[55b,55a], G. Gaudio[71a], I.L. Gavrilenko[111], A. Gavrilyuk[124], C. Gay[175], G. Gaycken[46], E.N. Gazis[10], A.A. Geanta[27b], C.M. Gee[145], C.N.P. Gee[143], J. Geisen[97], M. Geisen[100], C. Gemme[55b], M.H. Genest[58], C. Geng[106], S. Gentile[73a,73b], S. George[94], T. Geralis[44], L.O. Gerlach[53], P. Gessinger-Befurt[100], G. Gessner[47], S. Ghasemi[151], M. Ghasemi Bostanabad[176], M. Ghneimat[151], A. Ghosh[65], A. Ghosh[78], B. Giacobbe[23b], S. Giagu[73a,73b], N. Giangiacomi[23b,23a], P. Giannetti[72a], A. Giannini[70a,70b], G. Giannini[14], S.M. Gibson[94], M. Gignac[145], D.T. Gil[84b], D. Gillberg[34], G. Gilles[182], D.M. Gingrich[3,am], M.P. Giordani[67a,67c], P.F. Giraud[144], G. Giugliarelli[67a,67c], D. Giugni[69a], F. Giuli[74a,74b], S. Gkaitatzis[162], I. Gkialas[9,g], E.L. Gkougkousis[14], P. Gkountoumis[10], L.K. Gladilin[113], C. Glasman[99], J. Glatzer[14], P.C.F. Glaysher[46], A. Glazov[46], G.R. Gledhill[131], I. Gnesi[41b,b], M. Goblirsch-Kolb[26], D. Godin[110], S. Goldfarb[105], T. Golling[54], D. Golubkov[123], A. Gomes[139a,139b], R. Goncalves Gama[53], R. Gonçalo[139a,139c], G. Gonella[131], L. Gonella[21], A. Gongadze[80], F. Gonnella[21], J.L. Gonski[39], S. González de la Hoz[174], S. Gonzalez Fernandez[14], C. Gonzalez Renteria[18], R. Gonzalez Suarez[172], S. Gonzalez-Sevilla[54], G.R. Gonzalvo Rodriguez[174], L. Goossens[36], N.A. Gorasia[21], P.A. Gorbounov[124], H.A. Gordon[29], B. Gorini[36], E. Gorini[68a,68b], A. Gorišek[92], A.T. Goshaw[49], M.I. Gostkin[80], C.A. Gottardo[119], M. Gouighri[35b], A.G. Goussiou[148], N. Govender[33c], C. Goy[5], I. Grabowska-Bold[84a], E.C. Graham[91], J. Gramling[171], E. Gramstad[133], S. Grancagnolo[19], M. Grandi[156], V. Gratchev[137], P.M. Gravila[27f], F.G. Gravili[68a,68b], C. Gray[57], H.M. Gray[18], C. Grefe[24], K. Gregersen[97], I.M. Gregor[46], P. Grenier[153], K. Grevtsov[46], C. Grieco[14], N.A. Grieser[128], A.A. Grillo[145], K. Grimm[31,k], S. Grinstein[14,w], J.-F. Grivaz[65], S. Groh[100], E. Gross[180], J. Grosse-Knetter[53], Z.J. Grout[95], C. Grud[106], A. Grummer[118], J.C. Grundy[134], L. Guan[106], W. Guan[181], C. Gubbels[175], J. Guenther[36], A. Guerguichon[65], J.G.R. Guerrero Rojas[174], F. Guescini[115], D. Guest[171], R. Gugel[100], T. Guillemin[5], S. Guindon[36], U. Gul[57], J. Guo[60c], W. Guo[106], Y. Guo[60a], Z. Guo[102], R. Gupta[46], S. Gurbuz[12c], G. Gustavino[128], M. Guth[52], P. Gutierrez[128], C. Gutschow[95], C. Guyot[144], C. Gwenlan[134], C.B. Gwilliam[91], E.S. Haaland[133], A. Haas[125], C. Haber[18], H.K. Hadavand[8], A. Hadef[60a], M. Haleem[177], J. Haley[129], J.J. Hall[149], G. Halladjian[107], G.D. Hallewell[102], K. Hamano[176], H. Hamdaoui[35f], M. Hamer[24], G.N. Hamity[50], K. Han[60a,v], L. Han[60a], S. Han[18], Y.F. Han[167], K. Hanagaki[82,t], M. Hance[145], D.M. Handl[114], M.D. Hank[37], R. Hankache[135], E. Hansen[97], J.B. Hansen[40], J.D. Hansen[40], M.C. Hansen[24], P.H. Hansen[40], E.C. Hanson[101], K. Hara[169], T. Harenberg[182], S. Harkusha[108], P.F. Harrison[178], N.M. Hartman[153], N.M. Hartmann[114], Y. Hasegawa[150], A. Hasib[50], S. Hassani[144], S. Haug[20], R. Hauser[107], L.B. Havener[39], M. Havranek[141], C.M. Hawkes[21], R.J. Hawkings[36], S. Hayashida[117], D. Hayden[107], C. Hayes[106], R.L. Hayes[175], C.P. Hays[134], J.M. Hays[93], H.S. Hayward[91], S.J. Haywood[143], F. He[60a], M.P. Heath[50], V. Hedberg[97], S. Heer[24], A.L. Heggelund[133], C. Heidegger[52], K.K. Heidegger[52], W.D. Heidorn[79], J. Heilman[34], S. Heim[46], T. Heim[18], B. Heinemann[46,ak], J.G. Heinlein[136], J.J. Heinrich[131], L. Heinrich[36], J. Hejbal[140], L. Helary[61b],

JHEP04(2021)174

A. Held[125], S. Hellesund[133], C.M. Helling[145], S. Hellman[45a,45b], C. Helsens[36], R.C.W. Henderson[90], Y. Heng[181], L. Henkelmann[32], A.M. Henriques Correia[36], H. Herde[26], Y. Hernández Jiménez[33e], H. Herr[100], M.G. Herrmann[114], T. Herrmann[48], G. Herten[52], R. Hertenberger[114], L. Hervas[36], T.C. Herwig[136], G.G. Hesketh[95], N.P. Hessey[168a], H. Hibi[83], A. Higashida[163], S. Higashino[82], E. Higón-Rodriguez[174], K. Hildebrand[37], J.C. Hill[32], K.K. Hill[29], K.H. Hiller[46], S.J. Hillier[21], M. Hils[48], I. Hinchliffe[18], F. Hinterkeuser[24], M. Hirose[132], S. Hirose[52], D. Hirschbuehl[182], B. Hiti[92], O. Hladik[140], D.R. Hlaluku[33e], J. Hobbs[155], N. Hod[180], M.C. Hodgkinson[149], A. Hoecker[36], D. Hohn[52], D. Hohov[65], T. Holm[24], T.R. Holmes[37], M. Holzbock[114], L.B.A.H. Hommels[32], T.M. Hong[138], J.C. Honig[52], A. Hönle[115], B.H. Hooberman[173], W.H. Hopkins[6], Y. Horii[117], P. Horn[48], L.A. Horyn[37], S. Hou[158], A. Hoummada[35a], J. Howarth[57], J. Hoya[89], M. Hrabovsky[130], J. Hrdinka[77], J. Hrivnac[65], A. Hrynevich[109], T. Hryn'ova[5], P.J. Hsu[64], S.-C. Hsu[148], Q. Hu[29], S. Hu[60c], Y.F. Hu[15a,15d,ao], D.P. Huang[95], Y. Huang[60a], Y. Huang[15a], Z. Hubacek[141], F. Hubaut[102], M. Huebner[24], F. Huegging[24], T.B. Huffman[134], M. Huhtinen[36], R. Hulsken[58], R.F.H. Hunter[34], P. Huo[155], N. Huseynov[80,ac], J. Huston[107], J. Huth[59], R. Hyneman[106], S. Hyrych[28a], G. Iacobucci[54], G. Iakovidis[29], I. Ibragimov[151], L. Iconomidou-Fayard[65], P. Iengo[36], R. Ignazzi[40], O. Igonkina[120,y,*], R. Iguchi[163], T. Iizawa[54], Y. Ikegami[82], M. Ikeno[82], D. Iliadis[162], N. Ilic[119,167,ab], F. Iltzsche[48], H. Imam[35a], G. Introzzi[71a,71b], M. Iodice[75a], K. Iordanidou[168a], V. Ippolito[73a,73b], M.F. Isacson[172], M. Ishino[163], W. Islam[129], C. Issever[19,46], S. Istin[160], F. Ito[169], J.M. Iturbe Ponce[63a], R. Iuppa[76a,76b], A. Ivina[180], H. Iwasaki[82], J.M. Izen[43], V. Izzo[70a], P. Jacka[140], P. Jackson[1], R.M. Jacobs[46], B.P. Jaeger[152], V. Jain[2], G. Jäkel[182], K.B. Jakobi[100], K. Jakobs[52], T. Jakoubek[180], J. Jamieson[57], K.W. Janas[84a], R. Jansky[54], M. Janus[53], P.A. Janus[84a], G. Jarlskog[97], A.E. Jaspan[91], N. Javadov[80,ac], T. Javůrek[36], M. Javurkova[103], F. Jeanneau[144], L. Jeanty[131], J. Jejelava[159a], P. Jenni[52,c], N. Jeong[46], S. Jézéquel[5], H. Ji[181], J. Jia[155], H. Jiang[79], Y. Jiang[60a], Z. Jiang[153], S. Jiggins[52], F.A. Jimenez Morales[38], J. Jimenez Pena[115], S. Jin[15c], A. Jinaru[27b], O. Jinnouchi[165], H. Jivan[33e], P. Johansson[149], K.A. Johns[7], C.A. Johnson[66], R.W.L. Jones[90], S.D. Jones[156], T.J. Jones[91], J. Jongmanns[61a], J. Jovicevic[36], X. Ju[18], J.J. Junggeburth[115], A. Juste Rozas[14,w], A. Kaczmarska[85], M. Kado[73a,73b], H. Kagan[127], M. Kagan[153], A. Kahn[39], C. Kahra[100], T. Kaji[179], E. Kajomovitz[160], C.W. Kalderon[29], A. Kaluza[100], A. Kamenshchikov[123], M. Kaneda[163], N.J. Kang[145], S. Kang[79], Y. Kano[117], J. Kanzaki[82], L.S. Kaplan[181], D. Kar[33e], K. Karava[134], M.J. Kareem[168b], I. Karkanias[162], S.N. Karpov[80], Z.M. Karpova[80], V. Kartvelishvili[90], A.N. Karyukhin[123], A. Kastanas[45a,45b], C. Kato[60d,60c], J. Katzy[46], K. Kawade[150], K. Kawagoe[88], T. Kawaguchi[117], T. Kawamoto[144], G. Kawamura[53], E.F. Kay[176], S. Kazakos[14], V.F. Kazanin[122b,122a], R. Keeler[176], R. Kehoe[42], J.S. Keller[34], E. Kellermann[97], D. Kelsey[156], J.J. Kempster[21], J. Kendrick[21], K.E. Kennedy[39], O. Kepka[140], S. Kersten[182], B.P. Kerševan[92], S. Ketabchi Haghighat[167], M. Khader[173], F. Khalil-Zada[13], M. Khandoga[144], A. Khanov[129], A.G. Kharlamov[122b,122a], T. Kharlamova[122b,122a], E.E. Khoda[175], A. Khodinov[166], T.J. Khoo[54], G. Khoriauli[177], E. Khramov[80], J. Khubua[159b], S. Kido[83], M. Kiehn[54], C.R. Kilby[94], E. Kim[165], Y.K. Kim[37], N. Kimura[95], B.T. King[91,*], A. Kirchhoff[53], D. Kirchmeier[48], J. Kirk[143], A.E. Kiryunin[115], T. Kishimoto[163], D.P. Kisliuk[167], V. Kitali[46], C. Kitsaki[10], O. Kivernyk[24], T. Klapdor-Kleingrothaus[52], M. Klassen[61a], C. Klein[34], M.H. Klein[106], M. Klein[91], U. Klein[91], K. Kleinknecht[100], P. Klimek[121], A. Klimentov[29], T. Klingl[24], T. Klioutchnikova[36], F.F. Klitzner[114], P. Kluit[120], S. Kluth[115], E. Kneringer[77], E.B.F.G. Knoops[102], A. Knue[52], D. Kobayashi[88], T. Kobayashi[163], M. Kobel[48], M. Kocian[153], T. Kodama[163], P. Kodys[142], D.M. Koeck[156], P.T. Koenig[24], T. Koffas[34], N.M. Köhler[36], M. Kolb[144], I. Koletsou[5], T. Komarek[130], T. Kondo[82], K. Köneke[52], A.X.Y. Kong[1], A.C. König[119], T. Kono[126], V. Konstantinides[95], N. Konstantinidis[95], B. Konya[97], R. Kopeliansky[66], S. Koperny[84a], K. Korcyl[85], K. Kordas[162], G. Koren[161], A. Korn[95], I. Korolkov[14], E.V. Korolkova[149],

JHEP04(2021)174

N. Korotkova[113], O. Kortner[115], S. Kortner[115], V.V. Kostyukhin[149,166], A. Kotsokechagia[65], A. Kotwal[49], A. Koulouris[10], A. Kourkoumeli-Charalampidi[71a,71b], C. Kourkoumelis[9], E. Kourlitis[6], V. Kouskoura[29], R. Kowalewski[176], W. Kozanecki[101], A.S. Kozhin[123], V.A. Kramarenko[113], G. Kramberger[92], D. Krasnopevtsev[60a], M.W. Krasny[135], A. Krasznahorkay[36], D. Krauss[115], J.A. Kremer[100], J. Kretzschmar[91], P. Krieger[167], F. Krieter[114], A. Krishnan[61b], K. Krizka[18], K. Kroeninger[47], H. Kroha[115], J. Kroll[140], J. Kroll[136], K.S. Krowpman[107], U. Kruchonak[80], H. Krüger[24], N. Krumnack[79], M.C. Kruse[49], J.A. Krzysiak[85], O. Kuchinskaia[166], S. Kuday[4b], D. Kuechler[46], J.T. Kuechler[46], S. Kuehn[36], A. Kugel[61a], T. Kuhl[46], V. Kukhtin[80], Y. Kulchitsky[108,af], S. Kuleshov[146b], Y.P. Kulinich[173], M. Kuna[58], T. Kunigo[86], A. Kupco[140], T. Kupfer[47], O. Kuprash[52], H. Kurashige[83], L.L. Kurchaninov[168a], Y.A. Kurochkin[108], A. Kurova[112], M.G. Kurth[15a,15d], E.S. Kuwertz[36], M. Kuze[165], A.K. Kvam[148], J. Kvita[130], T. Kwan[104], F. La Ruffa[41b,41a], C. Lacasta[174], F. Lacava[73a,73b], D.P.J. Lack[101], H. Lacker[19], D. Lacour[135], E. Ladygin[80], R. Lafaye[5], B. Laforge[135], T. Lagouri[146b], S. Lai[53], I.K. Lakomiec[84a], J.E. Lambert[128], S. Lammers[66], W. Lampl[7], C. Lampoudis[162], E. Lançon[29], U. Landgraf[52], M.P.J. Landon[93], M.C. Lanfermann[54], V.S. Lang[52], J.C. Lange[53], R.J. Langenberg[103], A.J. Lankford[171], F. Lanni[29], K. Lantzsch[24], A. Lanza[71a], A. Lapertosa[55b,55a], S. Laplace[135], J.F. Laporte[144], T. Lari[69a], F. Lasagni Manghi[23b,23a], M. Lassnig[36], T.S. Lau[63a], A. Laudrain[65], A. Laurier[34], M. Lavorgna[70a,70b], S.D. Lawlor[94], M. Lazzaroni[69a,69b], B. Le[101], E. Le Guirriec[102], A. Lebedev[79], M. LeBlanc[7], T. LeCompte[6], F. Ledroit-Guillon[58], A.C.A. Lee[95], C.A. Lee[29], G.R. Lee[17], L. Lee[59], S.C. Lee[158], S. Lee[79], B. Lefebvre[168a], H.P. Lefebvre[94], M. Lefebvre[176], C. Leggett[18], K. Lehmann[152], N. Lehmann[20], G. Lehmann Miotto[36], W.A. Leight[46], A. Leisos[162,u], M.A.L. Leite[81c], C.E. Leitgeb[114], R. Leitner[142], D. Lellouch[180,*], K.J.C. Leney[42], T. Lenz[24], S. Leone[72a], C. Leonidopoulos[50], A. Leopold[135], C. Leroy[110], R. Les[167], C.G. Lester[32], M. Levchenko[137], J. Levêque[5], D. Levin[106], L.J. Levinson[180], D.J. Lewis[21], B. Li[15b], B. Li[106], C-Q. Li[60a], F. Li[60c], H. Li[60a], H. Li[60b], J. Li[60c], K. Li[148], L. Li[60c], M. Li[15a,15d], Q. Li[15a,15d], Q.Y. Li[60a], S. Li[60d,60c], X. Li[46], Y. Li[46], Z. Li[60b], Z. Li[134], Z. Li[104], Z. Liang[15a], M. Liberatore[46], B. Liberti[74a], A. Liblong[167], K. Lie[63c], S. Lim[29], C.Y. Lin[32], K. Lin[107], R.A. Linck[66], R.E. Lindley[7], J.H. Lindon[21], A. Linss[46], A.L. Lionti[54], E. Lipeles[136], A. Lipniacka[17], T.M. Liss[173,al], A. Lister[175], J.D. Little[8], B. Liu[79], B.X. Liu[6], H.B. Liu[29], J.B. Liu[60a], J.K.K. Liu[37], K. Liu[60d,60c], M. Liu[60a], P. Liu[15a], Y. Liu[46], Y. Liu[15a,15d], Y.L. Liu[106], Y.W. Liu[60a], M. Livan[71a,71b], A. Lleres[58], J. Llorente Merino[152], S.L. Lloyd[93], C.Y. Lo[63b], E.M. Lobodzinska[46], P. Loch[7], S. Loffredo[74a,74b], T. Lohse[19], K. Lohwasser[149], M. Lokajicek[140], J.D. Long[173], R.E. Long[90], L. Longo[36], K.A. Looper[127], I. Lopez Paz[101], A. Lopez Solis[149], J. Lorenz[114], N. Lorenzo Martinez[5], A.M. Lory[114], P.J. Lösel[114], A. Lösle[52], X. Lou[46], X. Lou[15a], A. Lounis[65], J. Love[6], P.A. Love[90], J.J. Lozano Bahilo[174], M. Lu[60a], Y.J. Lu[64], H.J. Lubatti[148], C. Luci[73a,73b], F.L. Lucio Alves[15c], A. Lucotte[58], F. Luehring[66], I. Luise[135], L. Luminari[73a], B. Lund-Jensen[154], M.S. Lutz[161], D. Lynn[29], H. Lyons[91], R. Lysak[140], E. Lytken[97], F. Lyu[15a], V. Lyubushkin[80], T. Lyubushkina[80], H. Ma[29], L.L. Ma[60b], Y. Ma[95], D.M. Mac Donell[176], G. Maccarrone[51], A. Macchiolo[115], C.M. Macdonald[149], J.C. MacDonald[149], J. Machado Miguens[136], D. Madaffari[174], R. Madar[38], W.F. Mader[48], M. Madugoda Ralalage Don[129], N. Madysa[48], J. Maeda[83], T. Maeno[29], M. Maerker[48], V. Magerl[52], N. Magini[79], J. Magro[67a,67c,q], D.J. Mahon[39], C. Maidantchik[81b], T. Maier[114], A. Maio[139a,139b,139d], K. Maj[84a], O. Majersky[28a], S. Majewski[131], Y. Makida[82], N. Makovec[65], B. Malaescu[135], Pa. Malecki[85], V.P. Maleev[137], F. Malek[58], U. Mallik[78], D. Malon[6], C. Malone[32], S. Maltezos[10], S. Malyukov[80], J. Mamuzic[174], G. Mancini[70a,70b], I. Mandić[92], L. Manhaes de Andrade Filho[81a], I.M. Maniatis[162], J. Manjarres Ramos[48], K.H. Mankinen[97], A. Mann[114], A. Manousos[77], B. Mansoulie[144], I. Manthos[162], S. Manzoni[120], A. Marantis[162], G. Marceca[30], L. Marchese[134], G. Marchiori[135], M. Marcisovsky[140], L. Marcoccia[74a,74b], C. Marcon[97], C.A. Marin Tobon[36], M. Marjanovic[128],

JHEP04(2021)174

Z. Marshall[18], M.U.F. Martensson[172], S. Marti-Garcia[174], C.B. Martin[127], T.A. Martin[178], V.J. Martin[50], B. Martin dit Latour[17], L. Martinelli[75a,75b], M. Martinez[14,w], P. Martinez Agullo[174], V.I. Martinez Outschoorn[103], S. Martin-Haugh[143], V.S. Martoiu[27b], A.C. Martyniuk[95], A. Marzin[36], S.R. Maschek[115], L. Masetti[100], T. Mashimo[163], R. Mashinistov[111], J. Masik[101], A.L. Maslennikov[122b,122a], L. Massa[23b,23a], P. Massarotti[70a,70b], P. Mastrandrea[72a,72b], A. Mastroberardino[41b,41a], T. Masubuchi[163], D. Matakias[29], A. Matic[114], N. Matsuzawa[163], P. Mättig[24], J. Maurer[27b], B. Maček[92], D.A. Maximov[122b,122a], R. Mazini[158], I. Maznas[162], S.M. Mazza[145], J.P. Mc Gowan[104], S.P. Mc Kee[106], T.G. McCarthy[115], W.P. McCormack[18], E.F. McDonald[105], J.A. Mcfayden[36], G. Mchedlidze[159b], M.A. McKay[42], K.D. McLean[176], S.J. McMahon[143], P.C. McNamara[105], C.J. McNicol[178], R.A. McPherson[176,ab], J.E. Mdhluli[33e], Z.A. Meadows[103], S. Meehan[36], T. Megy[38], S. Mehlhase[114], A. Mehta[91], B. Meirose[43], D. Melini[160], B.R. Mellado Garcia[33e], J.D. Mellenthin[53], M. Melo[28a], F. Meloni[46], A. Melzer[24], E.D. Mendes Gouveia[139a,139e], L. Meng[36], X.T. Meng[106], S. Menke[115], E. Meoni[41b,41a], S. Mergelmeyer[19], S.A.M. Merkt[138], C. Merlassino[134], P. Mermod[54], L. Merola[70a,70b], C. Meroni[69a], G. Merz[106], O. Meshkov[113,111], J.K.R. Meshreki[151], J. Metcalfe[6], A.S. Mete[6], C. Meyer[66], J-P. Meyer[144], F. Miano[156], M. Michetti[19], R.P. Middleton[143], L. Mijović[50], G. Mikenberg[180], M. Mikestikova[140], M. Mikuž[92], H. Mildner[149], M. Milesi[105], A. Milic[167], C.D. Milke[42], D.W. Miller[37], A. Milov[180], D.A. Milstead[45a,45b], R.A. Mina[153], A.A. Minaenko[123], I.A. Minashvili[159b], A.I. Mincer[125], B. Mindur[84a], M. Mineev[80], Y. Minegishi[163], L.M. Mir[14], M. Mironova[134], A. Mirto[68a,68b], K.P. Mistry[136], T. Mitani[179], J. Mitrevski[114], V.A. Mitsou[174], M. Mittal[60c], O. Miu[167], A. Miucci[20], P.S. Miyagawa[93], A. Mizukami[82], J.U. Mjörnmark[97], T. Mkrtchyan[61a], M. Mlynarikova[142], T. Moa[45a,45b], S. Mobius[53], K. Mochizuki[110], P. Mogg[114], S. Mohapatra[39], R. Moles-Valls[24], K. Mönig[46], E. Monnier[102], A. Montalbano[152], J. Montejo Berlingen[36], M. Montella[95], F. Monticelli[89], S. Monzani[69a], N. Morange[65], D. Moreno[22a], M. Moreno Llácer[174], C. Moreno Martinez[14], P. Morettini[55b], M. Morgenstern[160], S. Morgenstern[48], D. Mori[152], M. Morii[59], M. Morinaga[179], V. Morisbak[133], A.K. Morley[36], G. Mornacchi[36], A.P. Morris[95], L. Morvaj[155], P. Moschovakos[36], B. Moser[120], M. Mosidze[159b], T. Moskalets[144], H.J. Moss[149], J. Moss[31,m], E.J.W. Moyse[103], S. Muanza[102], J. Mueller[138], R.S.P. Mueller[114], D. Muenstermann[90], G.A. Mullier[97], D.P. Mungo[69a,69b], J.L. Munoz Martinez[14], F.J. Munoz Sanchez[101], P. Murin[28b], W.J. Murray[178,143], A. Murrone[69a,69b], J.M. Muse[128], M. Muškinja[18], C. Mwewa[33a], A.G. Myagkov[123,ah], A.A. Myers[138], J. Myers[131], M. Myska[141], B.P. Nachman[18], O. Nackenhorst[47], A.Nag Nag[48], K. Nagai[134], K. Nagano[82], Y. Nagasaka[62], J.L. Nagle[29], E. Nagy[102], A.M. Nairz[36], Y. Nakahama[117], K. Nakamura[82], T. Nakamura[163], H. Nanjo[132], F. Napolitano[61a], R.F. Naranjo Garcia[46], R. Narayan[42], I. Naryshkin[137], T. Naumann[46], G. Navarro[22a], P.Y. Nechaeva[111], F. Nechansky[46], T.J. Neep[21], A. Negri[71a,71b], M. Negrini[23b], C. Nellist[119], C. Nelson[104], M.E. Nelson[45a,45b], S. Nemecek[140], M. Nessi[36,e], M.S. Neubauer[173], F. Neuhaus[100], M. Neumann[182], R. Newhouse[175], P.R. Newman[21], C.W. Ng[138], Y.S. Ng[19], Y.W.Y. Ng[171], B. Ngair[35f], H.D.N. Nguyen[102], T. Nguyen Manh[110], E. Nibigira[38], R.B. Nickerson[134], R. Nicolaidou[144], D.S. Nielsen[40], J. Nielsen[145], M. Niemeyer[53], N. Nikiforou[11], V. Nikolaenko[123,ah], I. Nikolic-Audit[135], K. Nikolopoulos[21], P. Nilsson[29], H.R. Nindhito[54], Y. Ninomiya[82], A. Nisati[73a], N. Nishu[60c], R. Nisius[115], I. Nitsche[47], T. Nitta[179], T. Nobe[163], D.L. Noel[32], Y. Noguchi[86], I. Nomidis[135], M.A. Nomura[29], M. Nordberg[36], J. Novak[92], T. Novak[92], O. Novgorodova[48], R. Novotny[141], L. Nozka[130], K. Ntekas[171], E. Nurse[95], F.G. Oakham[34,am], H. Oberlack[115], J. Ocariz[135], A. Ochi[83], I. Ochoa[39], J.P. Ochoa-Ricoux[146a], K. O'Connor[26], S. Oda[88], S. Odaka[82], S. Oerdek[53], A. Ogrodnik[84a], A. Oh[101], S.H. Oh[49], C.C. Ohm[154], H. Oide[165], M.L. Ojeda[167], H. Okawa[169], Y. Okazaki[86], M.W. O'Keefe[91], Y. Okumura[163], T. Okuyama[82], A. Olariu[27b], L.F. Oleiro Seabra[139a], S.A. Olivares Pino[146a], D. Oliveira Damazio[29], J.L. Oliver[1], M.J.R. Olsson[171], A. Olszewski[85], J. Olszowska[85],

JHEP04(2021)174

D.C. O'Neil[152], A.P. O'neill[134], A. Onofre[139a,139e], P.U.E. Onyisi[11], H. Oppen[133], R.G. Oreamuno Madriz[121], M.J. Oreglia[37], G.E. Orellana[89], D. Orestano[75a,75b], N. Orlando[14], R.S. Orr[167], V. O'Shea[57], R. Ospanov[60a], G. Otero y Garzon[30], H. Otono[88], P.S. Ott[61a], G.J. Ottino[18], M. Ouchrif[35e], J. Ouellette[29], F. Ould-Saada[133], A. Ouraou[144,*], Q. Ouyang[15a], M. Owen[57], R.E. Owen[21], V.E. Ozcan[12c], N. Ozturk[8], J. Pacalt[130], H.A. Pacey[32], K. Pachal[49], A. Pacheco Pages[14], C. Padilla Aranda[14], S. Pagan Griso[18], G. Palacino[66], S. Palazzo[50], S. Palestini[36], M. Palka[84b], D. Pallin[38], P. Palni[84a], C.E. Pandini[54], J.G. Panduro Vazquez[94], P. Pani[46], G. Panizzo[67a,67c], L. Paolozzi[54], C. Papadatos[110], K. Papageorgiou[9,g], S. Parajuli[42], A. Paramonov[6], C. Paraskevopoulos[10], D. Paredes Hernandez[63b], S.R. Paredes Saenz[134], B. Parida[180], T.H. Park[167], A.J. Parker[31], M.A. Parker[32], F. Parodi[55b,55a], E.W. Parrish[121], J.A. Parsons[39], U. Parzefall[52], L. Pascual Dominguez[135], V.R. Pascuzzi[18], J.M.P. Pasner[145], F. Pasquali[120], E. Pasqualucci[73a], S. Passaggio[55b], F. Pastore[94], P. Pasuwan[45a,45b], S. Pataraia[100], J.R. Pater[101], A. Pathak[181,i], J. Patton[91], T. Pauly[36], J. Pearkes[153], B. Pearson[115], M. Pedersen[133], L. Pedraza Diaz[119], R. Pedro[139a], T. Peiffer[53], S.V. Peleganchuk[122b,122a], O. Penc[140], H. Peng[60a], B.S. Peralva[81a], M.M. Perego[65], A.P. Pereira Peixoto[139a], L. Pereira Sanchez[45a,45b], D.V. Perepelitsa[29], E. Perez Codina[168a], F. Peri[19], L. Perini[69a,69b], H. Pernegger[36], S. Perrella[139a], A. Perrevoort[120], K. Peters[46], R.F.Y. Peters[101], B.A. Petersen[36], T.C. Petersen[40], E. Petit[102], A. Petridis[1], C. Petridou[162], F. Petrucci[75a,75b], M. Pettee[183], N.E. Pettersson[103], K. Petukhova[142], A. Peyaud[144], R. Pezoa[146d], L. Pezzotti[71a,71b], T. Pham[105], F.H. Phillips[107], P.W. Phillips[143], M.W. Phipps[173], G. Piacquadio[155], E. Pianori[18], A. Picazio[103], R.H. Pickles[101], R. Piegaia[30], D. Pietreanu[27b], J.E. Pilcher[37], A.D. Pilkington[101], M. Pinamonti[67a,67c], J.L. Pinfold[3], C. Pitman Donaldson[95], M. Pitt[161], L. Pizzimento[74a,74b], M.-A. Pleier[29], V. Pleskot[142], E. Plotnikova[80], P. Podberezko[122b,122a], R. Poettgen[97], R. Poggi[54], L. Poggioli[135], I. Pogrebnyak[107], D. Pohl[24], I. Pokharel[53], G. Polesello[71a], A. Poley[152], A. Policicchio[73a,73b], R. Polifka[142], A. Polini[23b], C.S. Pollard[46], V. Polychronakos[29], D. Ponomarenko[112], L. Pontecorvo[36], S. Popa[27a], G.A. Popeneciu[27d], L. Portales[5], D.M. Portillo Quintero[58], S. Pospisil[141], K. Potamianos[46], I.N. Potrap[80], C.J. Potter[32], H. Potti[11], T. Poulsen[97], J. Poveda[174], T.D. Powell[149], G. Pownall[46], M.E. Pozo Astigarraga[36], P. Pralavorio[102], S. Prell[79], D. Price[101], M. Primavera[68a], M.L. Proffitt[148], N. Proklova[112], K. Prokofiev[63c], F. Prokoshin[80], S. Protopopescu[29], J. Proudfoot[6], M. Przybycien[84a], D. Pudzha[137], A. Puri[173], P. Puzo[65], D. Pyatiizbyantseva[112], J. Qian[106], Y. Qin[101], A. Quadt[53], M. Queitsch-Maitland[36], A. Qureshi[1], M. Racko[28a], F. Ragusa[69a,69b], G. Rahal[98], J.A. Raine[54], S. Rajagopalan[29], A. Ramirez Morales[93], K. Ran[15a,15d], T. Rashid[65], D.M. Rauch[46], F. Rauscher[114], S. Rave[100], B. Ravina[149], I. Ravinovich[180], J.H. Rawling[101], M. Raymond[36], A.L. Read[133], N.P. Readioff[58], M. Reale[68a,68b], D.M. Rebuzzi[71a,71b], G. Redlinger[29], K. Reeves[43], J. Reichert[136], D. Reikher[161], A. Reiss[100], A. Rej[151], C. Rembser[36], A. Renardi[46], M. Renda[27b], M.B. Rendel[115], S. Resconi[69a], E.D. Resseguie[18], S. Rettie[95], B. Reynolds[127], E. Reynolds[21], O.L. Rezanova[122b,122a], P. Reznicek[142], E. Ricci[76a,76b], R. Richter[115], S. Richter[46], E. Richter-Was[84b], M. Ridel[135], P. Rieck[115], O. Rifki[46], M. Rijssenbeek[155], A. Rimoldi[71a,71b], M. Rimoldi[46], L. Rinaldi[23b], T.T. Rinn[173], G. Ripellino[154], I. Riu[14], P. Rivadeneira[46], J.C. Rivera Vergara[176], F. Rizatdinova[129], E. Rizvi[93], C. Rizzi[36], S.H. Robertson[104,ab], M. Robin[46], D. Robinson[32], C.M. Robles Gajardo[146d], M. Robles Manzano[100], A. Robson[57], A. Rocchi[74a,74b], E. Rocco[100], C. Roda[72a,72b], S. Rodriguez Bosca[174], A.M. Rodríguez Vera[168b], S. Roe[36], J. Roggel[182], O. Røhne[133], R. Röhrig[115], R.A. Rojas[146d], B. Roland[52], C.P.A. Roland[66], J. Roloff[29], A. Romaniouk[112], M. Romano[23b,23a], N. Rompotis[91], M. Ronzani[125], L. Roos[135], S. Rosati[73a], G. Rosin[103], B.J. Rosser[136], E. Rossi[46], E. Rossi[75a,75b], E. Rossi[70a,70b], L.P. Rossi[55b], L. Rossini[69a,69b], R. Rosten[14], M. Rotaru[27b], B. Rottler[52], D. Rousseau[65], G. Rovelli[71a,71b], A. Roy[11], D. Roy[33e], A. Rozanov[102], Y. Rozen[160], X. Ruan[33e], F. Rühr[52],

JHEP04(2021)174

A. Ruiz-Martinez[174], A. Rummler[36], Z. Rurikova[52], N.A. Rusakovich[80], H.L. Russell[104], L. Rustige[38,47], J.P. Rutherfoord[7], E.M. Rüttinger[149], M. Rybar[39], G. Rybkin[65], E.B. Rye[133], A. Ryzhov[123], J.A. Sabater Iglesias[46], P. Sabatini[53], S. Sacerdoti[65], H.F-W. Sadrozinski[145], R. Sadykov[80], F. Safai Tehrani[73a], B. Safarzadeh Samani[156], M. Safdari[153], P. Saha[121], S. Saha[104], M. Sahinsoy[115], A. Sahu[182], M. Saimpert[36], M. Saito[163], T. Saito[163], H. Sakamoto[163], D. Salamani[54], G. Salamanna[75a,75b], A. Salnikov[153], J. Salt[174], A. Salvador Salas[14], D. Salvatore[41b,41a], F. Salvatore[156], A. Salvucci[63a,63b,63c], A. Salzburger[36], J. Samarati[36], D. Sammel[52], D. Sampsonidis[162], D. Sampsonidou[162], J. Sánchez[174], A. Sanchez Pineda[67a,36,67c], H. Sandaker[133], C.O. Sander[46], I.G. Sanderswood[90], M. Sandhoff[182], C. Sandoval[22a], D.P.C. Sankey[143], M. Sannino[55b,55a], Y. Sano[117], A. Sansoni[51], C. Santoni[38], H. Santos[139a,139b], S.N. Santpur[18], A. Santra[174], A. Sapronov[80], J.G. Saraiva[139a,139d], O. Sasaki[82], K. Sato[169], F. Sauerburger[52], E. Sauvan[5], P. Savard[167,am], R. Sawada[163], C. Sawyer[143], L. Sawyer[96,ag], I. Sayago Galvan[174], C. Sbarra[23b], A. Sbrizzi[67a,67c], T. Scanlon[95], J. Schaarschmidt[148], P. Schacht[115], D. Schaefer[37], L. Schaefer[136], S. Schaepe[36], U. Schäfer[100], A.C. Schaffer[65], D. Schaile[114], R.D. Schamberger[155], E. Schanet[114], N. Scharmberg[101], V.A. Schegelsky[137], D. Scheirich[142], F. Schenck[19], M. Schernau[171], C. Schiavi[55b,55a], L.K. Schildgen[24], Z.M. Schillaci[26], E.J. Schioppa[68a,68b], M. Schioppa[41b,41a], K.E. Schleicher[52], S. Schlenker[36], K.R. Schmidt-Sommerfeld[115], K. Schmieden[36], C. Schmitt[100], S. Schmitt[46], J.C. Schmoeckel[46], L. Schoeffel[144], A. Schoening[61b], P.G. Scholer[52], E. Schopf[134], M. Schott[100], J.F.P. Schouwenberg[119], J. Schovancova[36], S. Schramm[54], F. Schroeder[182], A. Schulte[100], H-C. Schultz-Coulon[61a], M. Schumacher[52], B.A. Schumm[145], Ph. Schune[144], A. Schwartzman[153], T.A. Schwarz[106], Ph. Schwemling[144], R. Schwienhorst[107], A. Sciandra[145], G. Sciolla[26], M. Scodeggio[46], M. Scornajenghi[41b,41a], F. Scuri[72a], F. Scutti[105], L.M. Scyboz[115], C.D. Sebastiani[91], P. Seema[19], S.C. Seidel[118], A. Seiden[145], B.D. Seidlitz[29], T. Seiss[37], C. Seitz[46], J.M. Seixas[81b], G. Sekhniaidze[70a], S.J. Sekula[42], N. Semprini-Cesari[23b,23a], S. Sen[49], C. Serfon[29], L. Serin[65], L. Serkin[67a,67b], M. Sessa[60a], H. Severini[128], S. Sevova[153], F. Sforza[55b,55a], A. Sfyrla[54], E. Shabalina[53], J.D. Shahinian[145], N.W. Shaikh[45a,45b], D. Shaked Renous[180], L.Y. Shan[15a], M. Shapiro[18], A. Sharma[134], A.S. Sharma[1], P.B. Shatalov[124], K. Shaw[156], S.M. Shaw[101], M. Shehade[180], Y. Shen[128], A.D. Sherman[25], P. Sherwood[95], L. Shi[95], S. Shimizu[82], C.O. Shimmin[183], Y. Shimogama[179], M. Shimojima[116], I.P.J. Shipsey[134], S. Shirabe[165], M. Shiyakova[80,z], J. Shlomi[180], A. Shmeleva[111], M.J. Shochet[37], J. Shojaii[105], D.R. Shope[128], S. Shrestha[127], E.M. Shrif[33e], E. Shulga[180], P. Sicho[140], A.M. Sickles[173], E. Sideras Haddad[33e], O. Sidiropoulou[36], A. Sidoti[23b,23a], F. Siegert[48], Dj. Sijacki[16], M.Jr. Silva[181], M.V. Silva Oliveira[36], S.B. Silverstein[45a], S. Simion[65], R. Simoniello[100], C.J. Simpson-allsop[21], S. Simsek[12b], P. Sinervo[167], V. Sinetckii[113], S. Singh[152], M. Sioli[23b,23a], I. Siral[131], S.Yu. Sivoklokov[113], J. Sjölin[45a,45b], A. Skaf[53], E. Skorda[97], P. Skubic[128], M. Slawinska[85], K. Sliwa[170], R. Slovak[142], V. Smakhtin[180], B.H. Smart[143], J. Smiesko[28b], N. Smirnov[112], S.Yu. Smirnov[112], Y. Smirnov[112], L.N. Smirnova[113,r], O. Smirnova[97], H.A. Smith[134], M. Smizanska[90], K. Smolek[141], A. Smykiewicz[85], A.A. Snesarev[111], H.L. Snoek[120], I.M. Snyder[131], S. Snyder[29], R. Sobie[176,ab], A. Soffer[161], A. Søgaard[50], F. Sohns[53], C.A. Solans Sanchez[36], E.Yu. Soldatov[112], U. Soldevila[174], A.A. Solodkov[123], A. Soloshenko[80], O.V. Solovyanov[123], V. Solovyev[137], P. Sommer[149], H. Son[170], W. Song[143], W.Y. Song[168b], A. Sopczak[141], A.L. Sopio[95], F. Sopkova[28b], S. Sottocornola[71a,71b], R. Soualah[67a,67c], A.M. Soukharev[122b,122a], D. South[46], S. Spagnolo[68a,68b], M. Spalla[115], M. Spangenberg[178], F. Spanò[94], D. Sperlich[52], T.M. Spieker[61a], G. Spigo[36], M. Spina[156], D.P. Spiteri[57], M. Spousta[142], A. Stabile[69a,69b], B.L. Stamas[121], R. Stamen[61a], M. Stamenkovic[120], E. Stanecka[85], B. Stanislaus[134], M.M. Stanitzki[46], M. Stankaityte[134], B. Stapf[120], E.A. Starchenko[123], G.H. Stark[145], J. Stark[58], P. Staroba[140], P. Starovoitov[61a], S. Stärz[104], R. Staszewski[85], G. Stavropoulos[44], M. Stegler[46], P. Steinberg[29], A.L. Steinhebel[131], B. Stelzer[152],

JHEP04(2021)174

H.J. Stelzer[138], O. Stelzer-Chilton[168a], H. Stenzel[56], T.J. Stevenson[156], G.A. Stewart[36], M.C. Stockton[36], G. Stoicea[27b], M. Stolarski[139a], S. Stonjek[115], A. Straessner[48], J. Strandberg[154], S. Strandberg[45a,45b], M. Strauss[128], T. Strebler[102], P. Strizenec[28b], R. Ströhmer[177], D.M. Strom[131], R. Stroynowski[42], A. Strubig[50], S.A. Stucci[29], B. Stugu[17], J. Stupak[128], N.A. Styles[46], D. Su[153], W. Su[60c,148], S. Suchek[61a], V.V. Sulin[111], M.J. Sullivan[91], D.M.S. Sultan[54], S. Sultansoy[4c], T. Sumida[86], S. Sun[106], X. Sun[101], K. Suruliz[156], C.J.E. Suster[157], M.R. Sutton[156], S. Suzuki[82], M. Svatos[140], M. Swiatlowski[168a], S.P. Swift[2], T. Swirski[177], A. Sydorenko[100], I. Sykora[28a], M. Sykora[142], T. Sykora[142], D. Ta[100], K. Tackmann[46,x], J. Taenzer[161], A. Taffard[171], R. Tafirout[168a], H. Takai[29], R. Takashima[87], K. Takeda[83], T. Takeshita[150], E.P. Takeva[50], Y. Takubo[82], M. Talby[102], A.A. Talyshev[122b,122a], K.C. Tam[63b], N.M. Tamir[161], J. Tanaka[163], R. Tanaka[65], S. Tapia Araya[173], S. Tapprogge[100], A. Tarek Abouelfadl Mohamed[107], S. Tarem[160], K. Tariq[60b], G. Tarna[27b,d], G.F. Tartarelli[69a], P. Tas[142], M. Tasevsky[140], T. Tashiro[86], E. Tassi[41b,41a], A. Tavares Delgado[139a], Y. Tayalati[35f], A.J. Taylor[50], G.N. Taylor[105], W. Taylor[168b], H. Teagle[91], A.S. Tee[90], R. Teixeira De Lima[153], P. Teixeira-Dias[94], H. Ten Kate[36], J.J. Teoh[120], S. Terada[82], K. Terashi[163], J. Terron[99], S. Terzo[14], M. Testa[51], R.J. Teuscher[167,ab], S.J. Thais[183], N. Themistokleous[50], T. Theveneaux-Pelzer[46], F. Thiele[40], D.W. Thomas[94], J.O. Thomas[42], J.P. Thomas[21], E.A. Thompson[46], P.D. Thompson[21], E. Thomson[136], E.J. Thorpe[93], R.E. Ticse Torres[53], V.O. Tikhomirov[111,ai], Yu.A. Tikhonov[122b,122a], S. Timoshenko[112], P. Tipton[183], S. Tisserant[102], K. Todome[23b,23a], S. Todorova-Nova[142], S. Todt[48], J. Tojo[88], S. Tokár[28a], K. Tokushuku[82], E. Tolley[127], R. Tombs[32], K.G. Tomiwa[33e], M. Tomoto[117], L. Tompkins[153], P. Tornambe[103], E. Torrence[131], H. Torres[48], E. Torró Pastor[148], C. Tosciri[134], J. Toth[102,aa], D.R. Tovey[149], A. Traeet[17], C.J. Treado[125], T. Trefzger[177], F. Tresoldi[156], A. Tricoli[29], I.M. Trigger[168a], S. Trincaz-Duvoid[135], D.A. Trischuk[175], W. Trischuk[167], B. Trocmé[58], A. Trofymov[65], C. Troncon[69a], F. Trovato[156], L. Truong[33c], M. Trzebinski[85], A. Trzupek[85], F. Tsai[46], J.C-L. Tseng[134], P.V. Tsiareshka[108,af], A. Tsirigotis[162,u], V. Tsiskaridze[155], E.G. Tskhadadze[159a], M. Tsopoulou[162], I.I. Tsukerman[124], V. Tsulaia[18], S. Tsuno[82], D. Tsybychev[155], Y. Tu[63b], A. Tudorache[27b], V. Tudorache[27b], T.T. Tulbure[27a], A.N. Tuna[59], S. Turchikhin[80], D. Turgeman[180], I. Turk Cakir[4b,s], R.J. Turner[21], R. Turra[69a], P.M. Tuts[39], S. Tzamarias[162], E. Tzovara[100], K. Uchida[163], F. Ukegawa[169], G. Unal[36], A. Undrus[29], G. Unel[171], F.C. Ungaro[105], Y. Unno[82], K. Uno[163], J. Urban[28b], P. Urquijo[105], G. Usai[8], Z. Uysal[12d], V. Vacek[141], B. Vachon[104], K.O.H. Vadla[133], T. Vafeiadis[36], A. Vaidya[95], C. Valderanis[114], E. Valdes Santurio[45a,45b], M. Valente[54], S. Valentinetti[23b,23a], A. Valero[174], L. Valéry[46], R.A. Vallance[21], A. Vallier[36], J.A. Valls Ferrer[174], T.R. Van Daalen[14], P. Van Gemmeren[6], I. Van Vulpen[120], M. Vanadia[74a,74b], W. Vandelli[36], M. Vandenbroucke[144], E.R. Vandewall[129], A. Vaniachine[166], D. Vannicola[73a,73b], R. Vari[73a], E.W. Varnes[7], C. Varni[55b,55a], T. Varol[158], D. Varouchas[65], K.E. Varvell[157], M.E. Vasile[27b], G.A. Vasquez[176], F. Vazeille[38], D. Vazquez Furelos[14], T. Vazquez Schroeder[36], J. Veatch[53], V. Vecchio[101], M.J. Veen[120], L.M. Veloce[167], F. Veloso[139a,139c], S. Veneziano[73a], A. Ventura[68a,68b], N. Venturi[36], A. Verbytskyi[115], V. Vercesi[71a], M. Verducci[72a,72b], C.M. Vergel Infante[79], C. Vergis[24], W. Verkerke[120], A.T. Vermeulen[120], J.C. Vermeulen[120], C. Vernieri[153], M.C. Vetterli[152,am], N. Viaux Maira[146d], T. Vickey[149], O.E. Vickey Boeriu[149], G.H.A. Viehhauser[134], L. Vigani[61b], M. Villa[23b,23a], M. Villaplana Perez[3], E.M. Villhauer[50], E. Vilucchi[51], M.G. Vincter[34], G.S. Virdee[21], A. Vishwakarma[50], C. Vittori[23b,23a], I. Vivarelli[156], M. Vogel[182], P. Vokac[141], S.E. von Buddenbrock[33e], E. Von Toerne[24], V. Vorobel[142], K. Vorobev[112], M. Vos[174], J.H. Vossebeld[91], M. Vozak[101], N. Vranjes[16], M. Vranjes Milosavljevic[16], V. Vrba[141,*], M. Vreeswijk[120], R. Vuillermet[36], I. Vukotic[37], S. Wada[169], P. Wagner[24], W. Wagner[182], J. Wagner-Kuhr[114], S. Wahdan[182], H. Wahlberg[89], R. Wakasa[169], V.M. Walbrecht[115], J. Walder[90], R. Walker[114], S.D. Walker[94], W. Walkowiak[151], V. Wallangen[45a,45b], A.M. Wang[59], A.Z. Wang[181],

JHEP04(2021)174

C. Wang[60c], F. Wang[181], H. Wang[18], H. Wang[3], J. Wang[63a], P. Wang[42], Q. Wang[128], R.-J. Wang[100], R. Wang[60a], R. Wang[6], S.M. Wang[158], W.T. Wang[60a], W. Wang[15c], W.X. Wang[60a], Y. Wang[60a], Z. Wang[106], C. Wanotayaroj[46], A. Warburton[104], C.P. Ward[32], D.R. Wardrope[95], N. Warrack[57], A.T. Watson[21], M.F. Watson[21], G. Watts[148], B.M. Waugh[95], A.F. Webb[11], C. Weber[29], M.S. Weber[20], S.A. Weber[34], S.M. Weber[61a], A.R. Weidberg[134], J. Weingarten[47], M. Weirich[100], C. Weiser[52], P.S. Wells[36], T. Wenaus[29], T. Wengler[36], S. Wenig[36], N. Wermes[24], M. Wessels[61a], T.D. Weston[20], K. Whalen[131], N.L. Whallon[148], A.M. Wharton[90], A.S. White[106], A. White[8], M.J. White[1], D. Whiteson[171], B.W. Whitmore[90], W. Wiedenmann[181], C. Wiel[48], M. Wielers[143], N. Wieseotte[100], C. Wiglesworth[40], L.A.M. Wiik-Fuchs[52], H.G. Wilkens[36], L.J. Wilkins[94], H.H. Williams[136], S. Williams[32], S. Willocq[103], P.J. Windischhofer[134], I. Wingerter-Seez[5], E. Winkels[156], F. Winklmeier[131], B.T. Winter[52], M. Wittgen[153], M. Wobisch[96], A. Wolf[100], R. Wölker[134], J. Wollrath[52], M.W. Wolter[85], H. Wolters[139a,139c], V.W.S. Wong[175], N.L. Woods[145], S.D. Worm[46], B.K. Wosiek[85], K.W. Woźniak[85], K. Wraight[57], S.L. Wu[181], X. Wu[54], Y. Wu[60a], J. Wuerzinger[134], T.R. Wyatt[101], B.M. Wynne[50], S. Xella[40], J. Xiang[63c], X. Xiao[106], X. Xie[60a], I. Xiotidis[156], D. Xu[15a], H. Xu[60a], H. Xu[60a], L. Xu[29], T. Xu[144], W. Xu[106], Z. Xu[60b], Z. Xu[153], B. Yabsley[157], S. Yacoob[33a], K. Yajima[132], D.P. Yallup[95], N. Yamaguchi[88], Y. Yamaguchi[165], A. Yamamoto[82], M. Yamatani[163], T. Yamazaki[163], Y. Yamazaki[83], J. Yan[60c], Z. Yan[25], H.J. Yang[60c,60d], H.T. Yang[18], S. Yang[60a], T. Yang[63c], X. Yang[60b,58], Y. Yang[163], Z. Yang[106,60a], W-M. Yao[18], Y.C. Yap[46], Y. Yasu[82], E. Yatsenko[60c,60d], H. Ye[15c], J. Ye[42], S. Ye[29], I. Yeletskikh[80], M.R. Yexley[90], E. Yigitbasi[25], P. Yin[39], K. Yorita[179], K. Yoshihara[79], C.J.S. Young[36], C. Young[153], J. Yu[79], R. Yuan[60b,h], X. Yue[61a], M. Zaazoua[35f], B. Zabinski[85], G. Zacharis[10], E. Zaffaroni[54], J. Zahreddine[135], A.M. Zaitsev[123,ah], T. Zakareishvili[159b], N. Zakharchuk[34], S. Zambito[36], D. Zanzi[36], D.R. Zaripovas[57], S.V. Zeißner[47], C. Zeitnitz[182], G. Zemaityte[134], J.C. Zeng[173], O. Zenin[123], T. Ženiš[28a], D. Zerwas[65], M. Zgubič[134], B. Zhang[15c], D.F. Zhang[15b], G. Zhang[15b], J. Zhang[6], K. Zhang[15a], L. Zhang[15c], L. Zhang[60a], M. Zhang[173], R. Zhang[181], S. Zhang[106], X. Zhang[60c], X. Zhang[60b], Y. Zhang[15a,15d], Z. Zhang[63a], Z. Zhang[65], P. Zhao[49], Z. Zhao[60a], A. Zhemchugov[80], Z. Zheng[106], D. Zhong[173], B. Zhou[106], C. Zhou[181], H. Zhou[7], M.S. Zhou[15a,15d], M. Zhou[155], N. Zhou[60c], Y. Zhou[7], C.G. Zhu[60b], C. Zhu[15a,15d], H.L. Zhu[60a], H. Zhu[15a], J. Zhu[106], Y. Zhu[60a], X. Zhuang[15a], K. Zhukov[111], V. Zhulanov[122b,122a], D. Zieminska[66], N.I. Zimine[80], S. Zimmermann[52,*], Z. Zinonos[115], M. Ziolkowski[151], L. Živković[16], G. Zobernig[181], A. Zoccoli[23b,23a], K. Zoch[53], T.G. Zorbas[149], R. Zou[37], L. Zwalinski[36]

[1] *Department of Physics, University of Adelaide, Adelaide; Australia*
[2] *Physics Department, SUNY Albany, Albany NY; United States of America*
[3] *Department of Physics, University of Alberta, Edmonton AB; Canada*
[4] [(a)] *Department of Physics, Ankara University, Ankara;* [(b)] *Istanbul Aydin University, Application and Research Center for Advanced Studies, Istanbul;* [(c)] *Division of Physics, TOBB University of Economics and Technology, Ankara; Turkey*
[5] *LAPP, Université Grenoble Alpes, Université Savoie Mont Blanc, CNRS/IN2P3, Annecy; France*
[6] *High Energy Physics Division, Argonne National Laboratory, Argonne IL; United States of America*
[7] *Department of Physics, University of Arizona, Tucson AZ; United States of America*
[8] *Department of Physics, University of Texas at Arlington, Arlington TX; United States of America*
[9] *Physics Department, National and Kapodistrian University of Athens, Athens; Greece*
[10] *Physics Department, National Technical University of Athens, Zografou; Greece*
[11] *Department of Physics, University of Texas at Austin, Austin TX; United States of America*
[12] [(a)] *Bahcesehir University, Faculty of Engineering and Natural Sciences, Istanbul;* [(b)] *Istanbul Bilgi University, Faculty of Engineering and Natural Sciences, Istanbul;* [(c)] *Department of Physics, Bogazici University, Istanbul;* [(d)] *Department of Physics Engineering, Gaziantep University, Gaziantep; Turkey*
[13] *Institute of Physics, Azerbaijan Academy of Sciences, Baku; Azerbaijan*

JHEP04(2021)174

[14] Institut de Física d'Altes Energies (IFAE), Barcelona Institute of Science and Technology, Barcelona; Spain
[15] [(a)] Institute of High Energy Physics, Chinese Academy of Sciences, Beijing;[(b)] Physics Department, Tsinghua University, Beijing;[(c)] Department of Physics, Nanjing University, Nanjing;[(d)] University of Chinese Academy of Science (UCAS), Beijing; China
[16] Institute of Physics, University of Belgrade, Belgrade; Serbia
[17] Department for Physics and Technology, University of Bergen, Bergen; Norway
[18] Physics Division, Lawrence Berkeley National Laboratory and University of California, Berkeley CA; United States of America
[19] Institut für Physik, Humboldt Universität zu Berlin, Berlin; Germany
[20] Albert Einstein Center for Fundamental Physics and Laboratory for High Energy Physics, University of Bern, Bern; Switzerland
[21] School of Physics and Astronomy, University of Birmingham, Birmingham; United Kingdom
[22] [(a)] Facultad de Ciencias y Centro de Investigaciónes, Universidad Antonio Nariño, Bogotá;[(b)] Departamento de Física, Universidad Nacional de Colombia, Bogotá, Colombia; Colombia
[23] [(a)] INFN Bologna and Università di Bologna, Dipartimento di Fisica;[(b)] INFN Sezione di Bologna; Italy
[24] Physikalisches Institut, Universität Bonn, Bonn; Germany
[25] Department of Physics, Boston University, Boston MA; United States of America
[26] Department of Physics, Brandeis University, Waltham MA; United States of America
[27] [(a)] Transilvania University of Brasov, Brasov;[(b)] Horia Hulubei National Institute of Physics and Nuclear Engineering, Bucharest;[(c)] Department of Physics, Alexandru Ioan Cuza University of Iasi, Iasi;[(d)] National Institute for Research and Development of Isotopic and Molecular Technologies, Physics Department, Cluj-Napoca;[(e)] University Politehnica Bucharest, Bucharest;[(f)] West University in Timisoara, Timisoara; Romania
[28] [(a)] Faculty of Mathematics, Physics and Informatics, Comenius University, Bratislava;[(b)] Department of Subnuclear Physics, Institute of Experimental Physics of the Slovak Academy of Sciences, Kosice; Slovak Republic
[29] Physics Department, Brookhaven National Laboratory, Upton NY; United States of America
[30] Departamento de Física, Universidad de Buenos Aires, Buenos Aires; Argentina
[31] California State University, CA; United States of America
[32] Cavendish Laboratory, University of Cambridge, Cambridge; United Kingdom
[33] [(a)] Department of Physics, University of Cape Town, Cape Town;[(b)] iThemba Labs, Western Cape;[(c)] Department of Mechanical Engineering Science, University of Johannesburg, Johannesburg;[(d)] University of South Africa, Department of Physics, Pretoria;[(e)] School of Physics, University of the Witwatersrand, Johannesburg; South Africa
[34] Department of Physics, Carleton University, Ottawa ON; Canada
[35] [(a)] Faculté des Sciences Ain Chock, Réseau Universitaire de Physique des Hautes Energies - Université Hassan II, Casablanca;[(b)] Faculté des Sciences, Université Ibn-Tofail, Kénitra;[(c)] Faculté des Sciences Semlalia, Université Cadi Ayyad, LPHEA-Marrakech;[(d)] Moroccan Foundation for Advanced Science Innovation and Research (MAScIR), Rabat;[(e)] LPMR, Faculté des Sciences, Université Mohamed Premier, Oujda;[(f)] Faculté des sciences, Université Mohammed V, Rabat; Morocco
[36] CERN, Geneva; Switzerland
[37] Enrico Fermi Institute, University of Chicago, Chicago IL; United States of America
[38] LPC, Université Clermont Auvergne, CNRS/IN2P3, Clermont-Ferrand; France
[39] Nevis Laboratory, Columbia University, Irvington NY; United States of America
[40] Niels Bohr Institute, University of Copenhagen, Copenhagen; Denmark
[41] [(a)] Dipartimento di Fisica, Università della Calabria, Rende;[(b)] INFN Gruppo Collegato di Cosenza, Laboratori Nazionali di Frascati; Italy
[42] Physics Department, Southern Methodist University, Dallas TX; United States of America
[43] Physics Department, University of Texas at Dallas, Richardson TX; United States of America
[44] National Centre for Scientific Research "Demokritos", Agia Paraskevi; Greece
[45] [(a)] Department of Physics, Stockholm University;[(b)] Oskar Klein Centre, Stockholm; Sweden

JHEP04(2021)174

[46] Deutsches Elektronen-Synchrotron DESY, Hamburg and Zeuthen; Germany
[47] Lehrstuhl für Experimentelle Physik IV, Technische Universität Dortmund, Dortmund; Germany
[48] Institut für Kern- und Teilchenphysik, Technische Universität Dresden, Dresden; Germany
[49] Department of Physics, Duke University, Durham NC; United States of America
[50] SUPA - School of Physics and Astronomy, University of Edinburgh, Edinburgh; United Kingdom
[51] INFN e Laboratori Nazionali di Frascati, Frascati; Italy
[52] Physikalisches Institut, Albert-Ludwigs-Universität Freiburg, Freiburg; Germany
[53] II. Physikalisches Institut, Georg-August-Universität Göttingen, Göttingen; Germany
[54] Département de Physique Nucléaire et Corpusculaire, Université de Genève, Genève; Switzerland
[55] [(a)] Dipartimento di Fisica, Università di Genova, Genova; [(b)] INFN Sezione di Genova; Italy
[56] II. Physikalisches Institut, Justus-Liebig-Universität Giessen, Giessen; Germany
[57] SUPA - School of Physics and Astronomy, University of Glasgow, Glasgow; United Kingdom
[58] LPSC, Université Grenoble Alpes, CNRS/IN2P3, Grenoble INP, Grenoble; France
[59] Laboratory for Particle Physics and Cosmology, Harvard University, Cambridge MA; United States of America
[60] [(a)] Department of Modern Physics and State Key Laboratory of Particle Detection and Electronics, University of Science and Technology of China, Hefei; [(b)] Institute of Frontier and Interdisciplinary Science and Key Laboratory of Particle Physics and Particle Irradiation (MOE), Shandong University, Qingdao; [(c)] School of Physics and Astronomy, Shanghai Jiao Tong University, Key Laboratory for Particle Astrophysics and Cosmology (MOE), SKLPPC, Shanghai; [(d)] Tsung-Dao Lee Institute, Shanghai; China
[61] [(a)] Kirchhoff-Institut für Physik, Ruprecht-Karls-Universität Heidelberg, Heidelberg; [(b)] Physikalisches Institut, Ruprecht-Karls-Universität Heidelberg, Heidelberg; Germany
[62] Faculty of Applied Information Science, Hiroshima Institute of Technology, Hiroshima; Japan
[63] [(a)] Department of Physics, Chinese University of Hong Kong, Shatin, N.T., Hong Kong; [(b)] Department of Physics, University of Hong Kong, Hong Kong; [(c)] Department of Physics and Institute for Advanced Study, Hong Kong University of Science and Technology, Clear Water Bay, Kowloon, Hong Kong; China
[64] Department of Physics, National Tsing Hua University, Hsinchu; Taiwan
[65] IJCLab, Université Paris-Saclay, CNRS/IN2P3, 91405, Orsay; France
[66] Department of Physics, Indiana University, Bloomington IN; United States of America
[67] [(a)] INFN Gruppo Collegato di Udine, Sezione di Trieste, Udine; [(b)] ICTP, Trieste; [(c)] Dipartimento Politecnico di Ingegneria e Architettura, Università di Udine, Udine; Italy
[68] [(a)] INFN Sezione di Lecce; [(b)] Dipartimento di Matematica e Fisica, Università del Salento, Lecce; Italy
[69] [(a)] INFN Sezione di Milano; [(b)] Dipartimento di Fisica, Università di Milano, Milano; Italy
[70] [(a)] INFN Sezione di Napoli; [(b)] Dipartimento di Fisica, Università di Napoli, Napoli; Italy
[71] [(a)] INFN Sezione di Pavia; [(b)] Dipartimento di Fisica, Università di Pavia, Pavia; Italy
[72] [(a)] INFN Sezione di Pisa; [(b)] Dipartimento di Fisica E. Fermi, Università di Pisa, Pisa; Italy
[73] [(a)] INFN Sezione di Roma; [(b)] Dipartimento di Fisica, Sapienza Università di Roma, Roma; Italy
[74] [(a)] INFN Sezione di Roma Tor Vergata; [(b)] Dipartimento di Fisica, Università di Roma Tor Vergata, Roma; Italy
[75] [(a)] INFN Sezione di Roma Tre; [(b)] Dipartimento di Matematica e Fisica, Università Roma Tre, Roma; Italy
[76] [(a)] INFN-TIFPA; [(b)] Università degli Studi di Trento, Trento; Italy
[77] Institut für Astro- und Teilchenphysik, Leopold-Franzens-Universität, Innsbruck; Austria
[78] University of Iowa, Iowa City IA; United States of America
[79] Department of Physics and Astronomy, Iowa State University, Ames IA; United States of America
[80] Joint Institute for Nuclear Research, Dubna; Russia
[81] [(a)] Departamento de Engenharia Elétrica, Universidade Federal de Juiz de Fora (UFJF), Juiz de Fora; [(b)] Universidade Federal do Rio De Janeiro COPPE/EE/IF, Rio de Janeiro; [(c)] Instituto de Física, Universidade de São Paulo, São Paulo; Brazil
[82] KEK, High Energy Accelerator Research Organization, Tsukuba; Japan
[83] Graduate School of Science, Kobe University, Kobe; Japan

JHEP04(2021)174

[84] [(a)] AGH University of Science and Technology, Faculty of Physics and Applied Computer Science, Krakow;[(b)] Marian Smoluchowski Institute of Physics, Jagiellonian University, Krakow; Poland
[85] Institute of Nuclear Physics Polish Academy of Sciences, Krakow; Poland
[86] Faculty of Science, Kyoto University, Kyoto; Japan
[87] Kyoto University of Education, Kyoto; Japan
[88] Research Center for Advanced Particle Physics and Department of Physics, Kyushu University, Fukuoka; Japan
[89] Instituto de Física La Plata, Universidad Nacional de La Plata and CONICET, La Plata; Argentina
[90] Physics Department, Lancaster University, Lancaster; United Kingdom
[91] Oliver Lodge Laboratory, University of Liverpool, Liverpool; United Kingdom
[92] Department of Experimental Particle Physics, Jožef Stefan Institute and Department of Physics, University of Ljubljana, Ljubljana; Slovenia
[93] School of Physics and Astronomy, Queen Mary University of London, London; United Kingdom
[94] Department of Physics, Royal Holloway University of London, Egham; United Kingdom
[95] Department of Physics and Astronomy, University College London, London; United Kingdom
[96] Louisiana Tech University, Ruston LA; United States of America
[97] Fysiska institutionen, Lunds universitet, Lund; Sweden
[98] Centre de Calcul de l'Institut National de Physique Nucléaire et de Physique des Particules (IN2P3), Villeurbanne; France
[99] Departamento de Física Teorica C-15 and CIAFF, Universidad Autónoma de Madrid, Madrid; Spain
[100] Institut für Physik, Universität Mainz, Mainz; Germany
[101] School of Physics and Astronomy, University of Manchester, Manchester; United Kingdom
[102] CPPM, Aix-Marseille Université, CNRS/IN2P3, Marseille; France
[103] Department of Physics, University of Massachusetts, Amherst MA; United States of America
[104] Department of Physics, McGill University, Montreal QC; Canada
[105] School of Physics, University of Melbourne, Victoria; Australia
[106] Department of Physics, University of Michigan, Ann Arbor MI; United States of America
[107] Department of Physics and Astronomy, Michigan State University, East Lansing MI; United States of America
[108] B.I. Stepanov Institute of Physics, National Academy of Sciences of Belarus, Minsk; Belarus
[109] Research Institute for Nuclear Problems of Byelorussian State University, Minsk; Belarus
[110] Group of Particle Physics, University of Montreal, Montreal QC; Canada
[111] P.N. Lebedev Physical Institute of the Russian Academy of Sciences, Moscow; Russia
[112] National Research Nuclear University MEPhI, Moscow; Russia
[113] D.V. Skobeltsyn Institute of Nuclear Physics, M.V. Lomonosov Moscow State University, Moscow; Russia
[114] Fakultät für Physik, Ludwig-Maximilians-Universität München, München; Germany
[115] Max-Planck-Institut für Physik (Werner-Heisenberg-Institut), München; Germany
[116] Nagasaki Institute of Applied Science, Nagasaki; Japan
[117] Graduate School of Science and Kobayashi-Maskawa Institute, Nagoya University, Nagoya; Japan
[118] Department of Physics and Astronomy, University of New Mexico, Albuquerque NM; United States of America
[119] Institute for Mathematics, Astrophysics and Particle Physics, Radboud University/Nikhef, Nijmegen; Netherlands
[120] Nikhef National Institute for Subatomic Physics and University of Amsterdam, Amsterdam; Netherlands
[121] Department of Physics, Northern Illinois University, DeKalb IL; United States of America
[122] [(a)] Budker Institute of Nuclear Physics and NSU, SB RAS, Novosibirsk;[(b)] Novosibirsk State University Novosibirsk; Russia
[123] Institute for High Energy Physics of the National Research Centre Kurchatov Institute, Protvino; Russia
[124] Institute for Theoretical and Experimental Physics named by A.I. Alikhanov of National Research Centre "Kurchatov Institute", Moscow; Russia

JHEP04(2021)174

[125] Department of Physics, New York University, New York NY; United States of America
[126] Ochanomizu University, Otsuka, Bunkyo-ku, Tokyo; Japan
[127] Ohio State University, Columbus OH; United States of America
[128] Homer L. Dodge Department of Physics and Astronomy, University of Oklahoma, Norman OK; United States of America
[129] Department of Physics, Oklahoma State University, Stillwater OK; United States of America
[130] Palacký University, RCPTM, Joint Laboratory of Optics, Olomouc; Czech Republic
[131] Institute for Fundamental Science, University of Oregon, Eugene, OR; United States of America
[132] Graduate School of Science, Osaka University, Osaka; Japan
[133] Department of Physics, University of Oslo, Oslo; Norway
[134] Department of Physics, Oxford University, Oxford; United Kingdom
[135] LPNHE, Sorbonne Université, Université de Paris, CNRS/IN2P3, Paris; France
[136] Department of Physics, University of Pennsylvania, Philadelphia PA; United States of America
[137] Konstantinov Nuclear Physics Institute of National Research Centre "Kurchatov Institute", PNPI, St. Petersburg; Russia
[138] Department of Physics and Astronomy, University of Pittsburgh, Pittsburgh PA; United States of America
[139] [(a)] Laboratório de Instrumentação e Física Experimental de Partículas - LIP, Lisboa;[(b)] Departamento de Física, Faculdade de Ciências, Universidade de Lisboa, Lisboa;[(c)] Departamento de Física, Universidade de Coimbra, Coimbra;[(d)] Centro de Física Nuclear da Universidade de Lisboa, Lisboa;[(e)] Departamento de Física, Universidade do Minho, Braga;[(f)] Departamento de Física Teórica y del Cosmos, Universidad de Granada, Granada (Spain);[(g)] Dep Física and CEFITEC of Faculdade de Ciências e Tecnologia, Universidade Nova de Lisboa, Caparica;[(h)] Instituto Superior Técnico, Universidade de Lisboa, Lisboa; Portugal
[140] Institute of Physics of the Czech Academy of Sciences, Prague; Czech Republic
[141] Czech Technical University in Prague, Prague; Czech Republic
[142] Charles University, Faculty of Mathematics and Physics, Prague; Czech Republic
[143] Particle Physics Department, Rutherford Appleton Laboratory, Didcot; United Kingdom
[144] IRFU, CEA, Université Paris-Saclay, Gif-sur-Yvette; France
[145] Santa Cruz Institute for Particle Physics, University of California Santa Cruz, Santa Cruz CA; United States of America
[146] [(a)] Departamento de Física, Pontificia Universidad Católica de Chile, Santiago;[(b)] Universidad Andres Bello, Department of Physics, Santiago;[(c)] Instituto de Alta Investigación, Universidad de Tarapacá;[(d)] Departamento de Física, Universidad Técnica Federico Santa María, Valparaíso; Chile
[147] Universidade Federal de São João del Rei (UFSJ), São João del Rei; Brazil
[148] Department of Physics, University of Washington, Seattle WA; United States of America
[149] Department of Physics and Astronomy, University of Sheffield, Sheffield; United Kingdom
[150] Department of Physics, Shinshu University, Nagano; Japan
[151] Department Physik, Universität Siegen, Siegen; Germany
[152] Department of Physics, Simon Fraser University, Burnaby BC; Canada
[153] SLAC National Accelerator Laboratory, Stanford CA; United States of America
[154] Physics Department, Royal Institute of Technology, Stockholm; Sweden
[155] Departments of Physics and Astronomy, Stony Brook University, Stony Brook NY; United States of America
[156] Department of Physics and Astronomy, University of Sussex, Brighton; United Kingdom
[157] School of Physics, University of Sydney, Sydney; Australia
[158] Institute of Physics, Academia Sinica, Taipei; Taiwan
[159] [(a)] E. Andronikashvili Institute of Physics, Iv. Javakhishvili Tbilisi State University, Tbilisi;[(b)] High Energy Physics Institute, Tbilisi State University, Tbilisi; Georgia
[160] Department of Physics, Technion, Israel Institute of Technology, Haifa; Israel
[161] Raymond and Beverly Sackler School of Physics and Astronomy, Tel Aviv University, Tel Aviv; Israel
[162] Department of Physics, Aristotle University of Thessaloniki, Thessaloniki; Greece

JHEP04(2021)174

[163] International Center for Elementary Particle Physics and Department of Physics, University of Tokyo, Tokyo; Japan
[164] Graduate School of Science and Technology, Tokyo Metropolitan University, Tokyo; Japan
[165] Department of Physics, Tokyo Institute of Technology, Tokyo; Japan
[166] Tomsk State University, Tomsk; Russia
[167] Department of Physics, University of Toronto, Toronto ON; Canada
[168] [(a)] TRIUMF, Vancouver BC; [(b)] Department of Physics and Astronomy, York University, Toronto ON; Canada
[169] Division of Physics and Tomonaga Center for the History of the Universe, Faculty of Pure and Applied Sciences, University of Tsukuba, Tsukuba; Japan
[170] Department of Physics and Astronomy, Tufts University, Medford MA; United States of America
[171] Department of Physics and Astronomy, University of California Irvine, Irvine CA; United States of America
[172] Department of Physics and Astronomy, University of Uppsala, Uppsala; Sweden
[173] Department of Physics, University of Illinois, Urbana IL; United States of America
[174] Instituto de Física Corpuscular (IFIC), Centro Mixto Universidad de Valencia - CSIC, Valencia; Spain
[175] Department of Physics, University of British Columbia, Vancouver BC; Canada
[176] Department of Physics and Astronomy, University of Victoria, Victoria BC; Canada
[177] Fakultät für Physik und Astronomie, Julius-Maximilians-Universität Würzburg, Würzburg; Germany
[178] Department of Physics, University of Warwick, Coventry; United Kingdom
[179] Waseda University, Tokyo; Japan
[180] Department of Particle Physics and Astrophysics, Weizmann Institute of Science, Rehovot; Israel
[181] Department of Physics, University of Wisconsin, Madison WI; United States of America
[182] Fakultät für Mathematik und Naturwissenschaften, Fachgruppe Physik, Bergische Universität Wuppertal, Wuppertal; Germany
[183] Department of Physics, Yale University, New Haven CT; United States of America

[a] Also at Borough of Manhattan Community College, City University of New York, New York NY; United States of America
[b] Also at Centro Studi e Ricerche Enrico Fermi; Italy
[c] Also at CERN, Geneva; Switzerland
[d] Also at CPPM, Aix-Marseille Université, CNRS/IN2P3, Marseille; France
[e] Also at Département de Physique Nucléaire et Corpusculaire, Université de Genève, Genève; Switzerland
[f] Also at Departament de Fisica de la Universitat Autonoma de Barcelona, Barcelona; Spain
[g] Also at Department of Financial and Management Engineering, University of the Aegean, Chios; Greece
[h] Also at Department of Physics and Astronomy, Michigan State University, East Lansing MI; United States of America
[i] Also at Department of Physics and Astronomy, University of Louisville, Louisville, KY; United States of America
[j] Also at Department of Physics, Ben Gurion University of the Negev, Beer Sheva; Israel
[k] Also at Department of Physics, California State University, East Bay; United States of America
[l] Also at Department of Physics, California State University, Fresno; United States of America
[m] Also at Department of Physics, California State University, Sacramento; United States of America
[n] Also at Department of Physics, King's College London, London; United Kingdom
[o] Also at Department of Physics, St. Petersburg State Polytechnical University, St. Petersburg; Russia
[p] Also at Department of Physics, University of Fribourg, Fribourg; Switzerland
[q] Also at Dipartimento di Matematica, Informatica e Fisica, Università di Udine, Udine; Italy
[r] Also at Faculty of Physics, M.V. Lomonosov Moscow State University, Moscow; Russia
[s] Also at Giresun University, Faculty of Engineering, Giresun; Turkey
[t] Also at Graduate School of Science, Osaka University, Osaka; Japan

JHEP04(2021)174

[u] Also at Hellenic Open University, Patras; Greece
[v] Also at IJCLab, Université Paris-Saclay, CNRS/IN2P3, 91405, Orsay; France
[w] Also at Institucio Catalana de Recerca i Estudis Avancats, ICREA, Barcelona; Spain
[x] Also at Institut für Experimentalphysik, Universität Hamburg, Hamburg; Germany
[y] Also at Institute for Mathematics, Astrophysics and Particle Physics, Radboud University/Nikhef, Nijmegen; Netherlands
[z] Also at Institute for Nuclear Research and Nuclear Energy (INRNE) of the Bulgarian Academy of Sciences, Sofia; Bulgaria
[aa] Also at Institute for Particle and Nuclear Physics, Wigner Research Centre for Physics, Budapest; Hungary
[ab] Also at Institute of Particle Physics (IPP); Canada
[ac] Also at Institute of Physics, Azerbaijan Academy of Sciences, Baku; Azerbaijan
[ad] Also at Instituto de Fisica Teorica, IFT-UAM/CSIC, Madrid; Spain
[ae] Also at Istanbul University, Dept. of Physics, Istanbul; Turkey
[af] Also at Joint Institute for Nuclear Research, Dubna; Russia
[ag] Also at Louisiana Tech University, Ruston LA; United States of America
[ah] Also at Moscow Institute of Physics and Technology State University, Dolgoprudny; Russia
[ai] Also at National Research Nuclear University MEPhI, Moscow; Russia
[aj] Also at Physics Department, An-Najah National University, Nablus; Palestine
[ak] Also at Physikalisches Institut, Albert-Ludwigs-Universität Freiburg, Freiburg; Germany
[al] Also at The City College of New York, New York NY; United States of America
[am] Also at TRIUMF, Vancouver BC; Canada
[an] Also at Università di Napoli Parthenope, Napoli; Italy
[ao] Also at University of Chinese Academy of Sciences (UCAS), Beijing; China
[*] Deceased

JHEP04(2021)174